# MASS SPECTROMETRIC STUDIES OF DISTORTED PORPHYRINS: FRAGMENTATION PATHWAYS AND IONIZATION ENERGIES

By

JAMES ALLEN FERGUSON

A DISSERTATION PRESENTED TO THE GRADUATE SCHOOL
OF THE UNIVERSITY OF FLORIDA IN PARTIAL FULFILLMENT
OF THE REQUIREMENTS FOR THE DEGREE OF
DOCTOR OF PHILOSOPHY

UNIVERSITY OF FLORIDA

1997

For SPTHB

## ACKNOWLEDGMENTS

There are a number of people who gave me assistance, guidance, and support while completing this dissertation; it is my desire to thank them all. The human condition of being less than perfect means that I will inevitably forget someone. If I should inadvertently overlook someone in these acknowledgments, I hope they will forgive me the slight and know that I am truly grateful, if forgetful. There are several individuals who have definitely contributed more assistance than duty, friendship, or relationship require. The words with which I voice my thanks below cannot adequately express my appreciation.

I am most definitely indebted to Professor Richard A. Yost for providing the instrumentation and tools with which to perform this (largely unfunded) research and a group in which independence and excellent science are important. There are several "Post Yosties" and current Yost group members who deserve special mention: Dr. Jodie Johnson for his patience in showing me how to make the TSQ70 work when I first started to be a mass spectrometrist and didn't know one scan function from another, and later for showing me how to make the blasted thing work when I thought I did know, but the instrument was not being cooperative; Dr. Uli Bernier for many of the same reasons and for his perennial optimism and encouragement; Dr. John Laycock for the initial work on the 5-mononitrooctaethylporphyrin which led to this dissertation research; Mr. Scott Quarmby for his help when the electronics of the instrument were acting up; and the whole group, past and present, for their help, encouragement, and friendship throughout my time at UF and for putting up with my idiosyncrasies and attention to details.

Professor J. Martin E. Quirke of Florida International University also deserves both high praise and my deepest gratitude for his help and interest in my work. In an

average week, Martin has enough ideas about how to use mass spectrometry to answer questions about the porphyrins to keep an entire research group busy for at least a year. Whatever questions I had about the porphyrins, academic politics and how to play the game, pushing electrons around to make sense of fragmentations, or life in general, Martin was there with the answer. I am especially appreciative of his weekend trips to Gainesville at his own personal expense to work long hours with me on this research. His concern for my growth as a scientist and as a person have been a great help and support to me and I look forward to continuing our friendship.

I am thankful for the help and encouragement of friends at Holy Trinity Episcopal Church which provided me an outlet for my musical talents in the choir (and paid me to enjoy myself doing what I would have done anyhow). Also, when the church was rebuilt after the fire, for providing a marvelous organ on which to practice and, when the pressure of the academic world was too great, to vent some of my frustration. The people of the Chapel of the Incarnation, especially Dave Francoeur for hiring me and Bonnie Roberts and Nancy Tiederman for being good listeners, also deserve my thanks for their encouragement and support and for giving me both a job as organist and, since August, for providing me with a place to live, rent-free. A simple thank you cannot express the thanks I owe.

The encouragement of my parents, siblings, grandparents, aunts, uncles, and cousins (first, second, and higher) in my pursuit of this degree, no matter how long it has taken, has been uniformly solid. Mom and Dad and my grandparents taught me the value of hard work and persistence. Mom and Dad have always been there to listen, admonish, encourage, and support me in my education and career. My siblings have also helped me get through this work by listening and by e-mail. The love of my entire family has been an ever-present comfort and support no matter what.

Others have helped in too many ways to mention. Please accept my profound gratitude and my thanks.

TABLE OF CONTENTS

ACKNOWLEDGMENTS ..... iii

ABSTRACT ..... vii

1 INTRODUCTION ..... 1
Porphyrins ..... 1
History of Porphyrin Research ..... 3
Porphyrins in Analytical Chemistry ..... 6
Porphyrins in Inorganic, Organic, and Physical Chemistry ..... 7
Porphyrin Biochemistry ..... 10
Porphyrins in Geochemistry ..... 15
Porphyrins in Medicine ..... 18
Porphyrins in Materials Science ..... 19
Distorted Porphyrins ..... 20
Mass Spectrometry ..... 22
Triple Quadrupole Mass Spectrometry ..... 24
Porphyrin Mass Spectrometry ..... 29
Electron Ionization ..... 30
Chemical Ionization ..... 33
Thermospray ..... 34
Electrospray ..... 34
Ionization and Appearance Energies ..... 35
Definitions ..... 35
Methods for Determining Ionization and Appearance Energies ..... 38
Optical Spectroscopy ..... 38
Photoelectron Spectroscopy ..... 38
Ion/Molecule Equilibrium Constant Determinations ..... 39
Photoelectron-Photoion Coincidence ..... 40
Electron Ionization ..... 40
Scope of the Dissertation ..... 42

2 FRAGMENTATION PATHWAYS ..... 44
Introduction ..... 44
Mass Spectrometry of Porphyrins ..... 48
Interpreting Fragmentation Pathways ..... 49
Experimental ..... 55
Samples and Sample Preparation for Analysis ..... 55
MS Operating Conditions ..... 55

Results and Discussion ..... 57
OEP and OEMNP ..... 57
EI-MS ..... 57
EI-MS/MS ..... 63
High Resolution EI-MS ..... 73
Structures and Fragmentation Pathways for Selected Ions ..... 76
Other NitroOEPs ..... 81
EI-MS Spectra ..... 81
Selected EI-MS/MS Spectra and Fragmentation Pathways ..... 85
Surface-Induced Thermal Decomposition ..... 94
Suppression of β-Cleavage of Methyl Groups ..... 98
Conclusions ..... 98

3 IONIZATION ENERGY DETERMINATIONS ..... 101
Background ..... 101
Thermodynamics ..... 101
IE Determination using EI-MS: Problems and Solutions ..... 102
Experimental ..... 109
Samples ..... 109
Sample Preparation ..... 111
MS Operating Conditions ..... 111
Sample Handling ..... 115
Single Compounds ..... 115
Porphyrin Mixtures ..... 115
Internal Standard and Compound Experiments ..... 116
Results and Discussion ..... 116
Single Compound Results ..... 117
Mixed Sample Results ..... 117
Variable Leak Valve Results ..... 119
Conclusions ..... 123

4 CONCLUSIONS AND FUTURE WORK ..... 125
Fragmentation Pathways ..... 126
Ionization/Appearance Energies ..... 127
Future Work ..... 127
Distortion versus Electron Withdrawing Question ..... 128
Other Biologically Active Tetrapyrroles ..... 129
Porphyrin Type Isomers ..... 130
Porphyrin Structural Isomers ..... 132
Additional Experiments to Improve the Reliability of IE Determinations ..... 135

REFERENCES ..... 138

BIOGRAPHICAL SKETCH ..... 150

Abstract of Dissertation Presented to the Graduate School
of the University of Florida in Partial Fulfillment of the
Requirements for the Degree of Doctor of Philosophy

MASS SPECTROMETRIC STUDIES OF DISTORTED PORPHYRINS:
FRAGMENTATION PATHWAYS AND IONIZATION ENERGIES

By

James Allen Ferguson

May, 1997

Chairman: Dr. Richard A. Yost
Major Department: Chemistry

This work describes novel fragmentation pathways for the entire suite of *meso*-nitrosubstituted octaethylporphyrins (OEPs) as determined by various mass spectrometric techniques, as well as determinations of the first ionization energies of divalent metal complexes of OEP and the *meso*-nitrosubstituted OEPs under automated instrument control.

Porphyrin macrocycles which are stable in their ground and ionized states are critical in biological functions. Fragmentation pathways resulting in novel ring scissions of the *meso*-nitroOEPs were elucidated by a combination of electron ionization mass spectrometry (EI-MS), EI-high resolution mass spectrometry (EI-HRMS), collision-induced dissociation (CID) during EI-tandem mass spectrometry (EI-MS/MS), and the use of isotopically labeled compounds. New pathways and plausible explanations for fragmentations previously noted but not explained are presented and results are compared with previous work on 5-mononitroOEP [Laycock *et al.*, **1996**]. Scissions of the mono-,

di-, and trinitroOEP macrocycles resulting in elimination of two pyrrolic rings, unusual in EI-MS of porphyrins, were observed. Increased nitro substitution was seen to increase the likelihood of surface-induced dissociation of nitro groups in the ion source Increased nitro substitution also resulted in decreased β-cleavage, normally observed for substituted porphyrins, and increased tendency toward other fragmentation pathways. These observations indicate a destabilization of these porphyrin macrocycles in the excited (ionized) state.

Three techniques for determining ionization energies using electron ionization on the Finnigan MAT TSQ70 triple quadrupole mass spectrometer are presented and evaluated. The use of a variable leak valve for introduction of a standard of known ionization energy into the ion source simultaneously with the unknown sample produced IEs which agreed well with photoelectron spectroscopy results for divalent metal complexes of OEP. The first IEs of the Ni(II) *meso*-nitroOEPs were found to correlate with the root-mean-square out-of-plane distortions of the macrocycles, indicating that increased distortion of the porphyrins may lead to increased ionization energy. The difficulty in separating the effect of distortion on ionization energies from the effect of the electron withdrawing character of the substituent is also discussed.

Future work, designed to answer many of the questions raised by both the fragmentation and ionization energy research presented here, is presented in the concluding chapter.

# CHAPTER 1

# INTRODUCTION

This dissertation is a report on two aspects of mass spectrometric investigations of distorted porphyrins. The first aspect is the electron ionization (EI) mass spectra of the *meso*-nitrosubstituted octaethylporphyrins (OEPs) and their collision-induced dissociation (CID) fragmentation pathways. The second is the determination of the first ionization energies of metallated OEPs and the *meso*-nitrosubstituted OEPs. The remainder of this chapter is devoted to topics which will provide general background and previous work relevant to the research presented in this dissertation. A brief explanation of what porphyrins are and how they are significant in several fields will be presented followed by a brief introduction to triple quadrupole tandem mass spectrometry and the mass spectrometry of porphyrins. The last section of this chapter (Scope of the Dissertation) will include an overview of the dissertation and put it into perspective with previous work. Background information specific to the topics covered in subsequent chapters will be presented in those chapters.

## Porphyrins

'Why grasse is greene, or why our blood is red are mysteries which none haue reach'd vnto.' This statement was made in 1612 by the Anglican divine John Donne in his 'Second Anniuersarie', subtitled 'Of the Progres of the Soule' [Donne, **1995**]. The questions Donne raised have been answered and the answers are chlorophyll (a porphyrin analog) and hemoglobin, a porphyrin-containing protein, respectively. However, there are still so many unanswered questions about the porphyrins that the field of porphyrin

research has proved fruitful for many scientists. A quick check of recent literature shows approximately five thousand publications every year for the last several years involving some fundamental study of porphyrins or some practical application of them. The word porphyrin comes from the Greek word for purple, πορφυρα, and stems from a purple decomposition product of hemoglobin. The porphyrins are highly conjugated, aromatic, cyclic tetrapyrroles with four one-carbon bridges (the *meso* carbons) linking the four pyrrole subunits. The simplest porphyrin, porphine, along with the IUPAC numbering for porphyrins, is illustrated in Figure 1-1. The carbons in the pyrrolic rings adjacent to the nitrogens are designated to be in the α-position, and the peripheral carbons are in β-pyrrolic positions. The four pyrrolic subunits are sometimes designated by the indicated letters (A-D). The high level of conjugation of the $sp^2$ carbons leads to a planar geometry for the molecule.

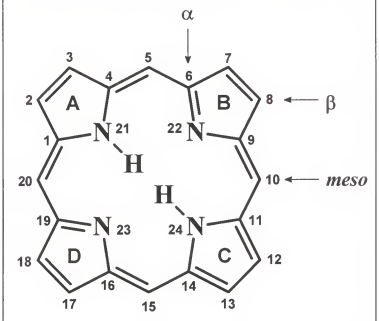


Figure 1-1. Porphine, the simplest porphyrin, showing the IUPAC numbering for porphyrins.

Porphyrins are important in many fields including analytical, inorganic, organic, and physical chemistry, biochemistry, geochemistry, medicine, and materials science. They are the reactive centers of several biologically important molecules including hemoglobin, myoglobin, all of the cytochromes, and the chlorophylls (dihydroporphyrins). Porphyrin analogs such as the corrins and chlorins are important in bacterial systems.

History of Porphyrin Research

What is probably the first instance of porphyrin research was reported in 1815 by Verdeil, who chemically altered chlorophyll from a green to a red pigment [Drabkin, **1978**]. Based on his observations, Verdeil suggested a relationship between chlorophyll and heme. As an early winner of the Nobel Prize in chemistry (1915), Richard Martin Willstätter was recognized for his work on the purification and structural determination of plant pigments, especially the chlorophylls [James, **1993**]. Another Nobel Prize was awarded in 1930 to Hans Fischer, regarded as the "father of modern porphyrin chemistry," for his work on the structures of hemin, an iron(III) porphyrin pigment derived from hemoglobin. Two of the main areas of Fischer's research were the synthesis of pyrroles and methods to assemble the pyrroles, which had been identified as constituents of various porphyrins. In 1926 the first synthesized porphyrin was formed from four pyrroles, using reactions discovered by Fisher. The synthesis of hemin, however, was not completed until 1929. After completing the hemin synthesis, Fisher devoted himself to the synthesis of chlorophyll from its constituent pyrroles but was unable to complete the work before he died. One of Fischer's most important contributions to the field was his three-volume treatise on the synthesis and structure of porphyrins, *Die Chemie des Pyrrols* [Fischer and Orth, **1937a, b**; Fischer and Stern, **1940**].

In the 1930s Alfred Treibs identified vanadyl deoxophylloerythroetioporphyrin (DPEP) as a major metalloporphryrin in petroleums and shales [Treibs, **1934**, **1936**]. He proposed ancient chlorophylls as the source materials for DPEP. This proposal, known as the Treibs' Hypothesis, was the foundation of the field of molecular organic geochemistry. This work and its significance will discussed in more detail in the Geochemistry section of this chapter.

John Kendrew and Max Perutz shared the 1962 Nobel Prize in chemistry for their work on the X-ray crystallographic determination of the structures of the oxygen-binding

proteins hemoglobin and myoglobin, two proteins in which the reactive center of the molecule is a porphyrin [James, **1993**]. The 1964 and 1965 Nobel Prizes for chemistry were awarded for work on vitamin $B_{12}$, like the porphyrins a tetrapyrrole. The 1964 prize went to Dorothy Hodgkin for her work on the X-ray crystallographic determination of the structures of vitamin $B_{12}$ and penicillin. Robert Woodward, a giant in the field of organic chemistry, won the Nobel Prize in 1965, in part, for his total synthesis of vitamin $B_{12}$.

One of the early texts to provide a review of porphyrin research was *Porphyrins and Metalloporphyrins*, [Falk, **1964**]. The physical and chemical aspects of the porphyrins were reviewed in this important work. Most of the research on porphyrins involved work on their structure, synthesis, or biosynthesis until the middle of the 1970s. Research continues on those important topics, but recent research also includes examination of porphyrin function and mode of action in many important biological systems and development of practical applications of porphyrins. A seven-volume series, edited by D. Dolphin, dealing with the chemistry and biochemistry of the porphyrins, was published in 1978 [Dolphin, **1978**].

The most recent Nobel Prize for work with porphyrins was shared by Robert Huber, Johann Deisenhofer, and Hartmut Michel in 1988. It was awarded for their crystallization and structural elucidation of a porphyrin-containing membrane protein complex from the purple photosynthetic bacterium *Rhodopseudomonas viridis* [Deisenhofer and Michel, **1989**]. A more complete picture of the importance of porphyrins and their applications will be provided in the next several sections of this chapter.

One of the most interesting areas of porphyrin research has been opened up by the recent synthesis of stable isomers of porphine (Figure 1-2) [Sessler, **1994**; Borman, **1995**]. In the light of the existence of these porphyrinoids, J. L. Sessler raised what is probably the most intriguing unanswered question about the porphyrins. He asked "why nature chose porphyrin, as opposed to one of its isomers, as its workhorse tetrapyrrolic macrocycle?" [Borman, **1995**, p. 30] It had previously been assumed that the isomers

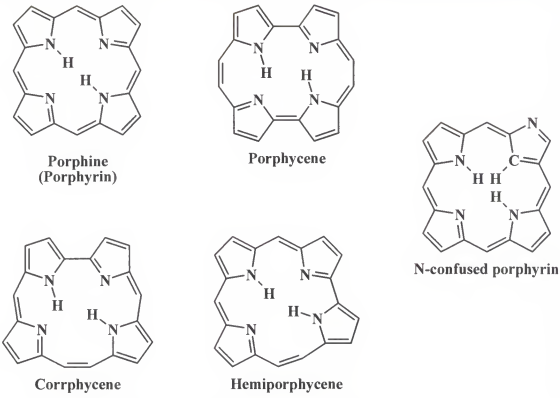


Figure 1-2. Porphine and its recently synthesized isomers.

would not be stable; however, their existence eliminates instability as an answer. Another obvious, but incorrect, answer is that the isomers would be unable to chelate with the biologically important metal cations, *e.g.*, iron, cobalt, nickel, and magnesium. Extensive research by Vogel's group at Cologne [Bernard *et al.*, **1994**; Vogel *et al.*, **1986, 1987**; Waluk *et al.*, **1991**; Vogel, **1996**] has shown that porphycene forms stable complexes with the significant metals and that the other porphyrinoids should as well [Vogel, **1996**]. The first isomer to be synthesized was porphycene [Vogel *et al.*, **1986**]. The other two isomers with the pyrroles in the normal porphyrinoid configuration were synthesized only within the last two years [Sessler *et al.*, **1994**; Callot *et al.*, **1995**]. The N-confused porphyrins, porphyrin isomers with their own unique properties, were first reported in 1994 [Chmielewski *et al.*, **1994**; Furuta *et al.*, **1994**]. These compounds will be discussed in greater detail in Chapter 4.

Porphyrins in Analytical Chemistry

One of the more interesting analytical uses of porphyrins has been reported by Xiao and Meyerhoff [Xiao and Meyerhoff, **1995**]. They reported the normal-phase HPLC separation of fullerenes from $C_{60}$ to $C_{90}$ using a novel stationary phase, the distorted porphyrin, tetraphenylporphyrin zinc(II), covalently attached to a silica support. The significance of distorted porphyrins will be discussed in more detail in a section devoted to the topic later in this chapter.

Porphyrins have been used in ion-selective electrodes (ISE) [Angnes *et al.*, **1996**; Badr *et al.*, **1996**]. In the first paper, dopamine and NADH were detected using chemically modified electrodes. The electrodes were prepared from glassy carbon by depositing films of cobalt(II) *meso*-tetrapyridylporphyrins in which each of the four pyridyl groups was modified with ruthenium-*bis*-2,2′bipyridine chloride. The electrodes were highly selective for the analytes of interest. In the Badr paper, solvent/polymeric membrane ISEs based on either of two Sn(IV) porphyrins were shown to have higher potentiometric anion selectivity toward 2-hydroxybenzhydroxamate, a drug used to prevent the formation of kidney stones, over common interferents including salicylate and other, more lipophilic anions such as thiocyanate, perchlorate, etc.

Porphyrins have also been used to develop several different sensors. Microsensors consisting of several layers of p-type electropolymerized porphyrin films and the cation exchange membrane Nafion® were shown to have potential as detectors for nitric oxide in aqueous solution [Trévin *et al.*, **1996**]. Another porphyrin-based sensor uses tetraphenylporphine dispersed in ethylcellulose for the optochemical detection of hydrochloric acid gas [Tanaka *et al.*, **1996**]. The absorbances of the Soret and Q-bands of the free base porphyrin in the sensor were reversibly affected by sub-ppm levels of HCl. A third sensor uses 5,10,15,20-tetraphenylporphyrinatoiron(III) chloride to amperometrically detect the herbicide Propanil [Priyantha and Weerabahu, **1996**].

Possibly the most intriguing use of porphyrins in analytical chemistry was work done to determine whether the ions formed under electrospray ionization conditions actually give an accurate representation of the equilibrium ion abundances of their precursors in solution, as has commonly been held to date [Chillier *et al.*, **1996**]. Under the conditions employed in this research, the authors found that, although the free base octaethylporphyrin was found in solution predominantly as the doubly charged, diprotonated molecule, the electrospray mass spectrum showed the singly charged, monoprotonated molecule to dominate. Although electrochemistry has been done at the tip of the electrospray needle to create ions [Van Berkel and Zhou, **1995**], in the 1996 paper, the conversion of the doubly protonated porphyrin to the monoprotonated species was determined, through monitoring the fluorescence excitation spectra of the porphyrins in the electrospray plume, to have occurred later in the ion formation process, *i.e.*, during the desolvation of the droplets in the atmospheric pressure/vacuum interface of the mass spectrometer.

Porphyrins in Inorganic, Organic, and Physical Chemistry

In inorganic chemistry, the porphyrins are famous for their chelating ability. They form complexes with all the stable metallic elements in the periodic table. Coordination of a metal ion into the porphyrin alters the physical (*e.g.*, color and solubility), chemical (*e.g.*, redox potentials), and spectroscopic (*e.g.*, $\lambda_{max}$ and absorbtivity) properties of the porphyrin. The reversible metallation reaction in which the free-base porphyrin ($H_2P$) chelates with the metal ion (for example, $M^{2+}$) to form the metalloporphyrins (MP) is illustrated in Figure 1-3. Demetallation, which occurs in the presence of acids, is also illustrated in Figure 1-3 (reverse reaction). When coordinated with certain metals, the porphyrin macrocycle may become either more planar or less so than its free-base analog

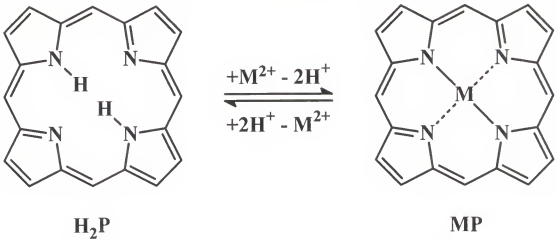


Figure 1-3. Metallation and demetallation reactions of porphyrins with divalent metals.

[Scheidt, **1978**]. The significance of distorted porphyrins will be discussed in greater detail in the appropriate section of this chapter.

Five stability classes, characterized by the ease of demetallation of the metalloporphyrins in the presence of various protic agents, have been have recognized [Falk, **1964**; Buchler, **1975**]. Buchler developed a stability index to relate properties inherent in the metal (electronegativity, valence, and ionic radius) to the stability of the metalloporphyrin complex [Buchler, **1975**, **1978**]. The Buchler stability index ($S_i$) is a simple function of these properties of the metal:

$$S_i = 100\frac{(PE)(V)}{R} \qquad (1\text{-}1$$

where PE is the Pauling electronegativity of the metal, V is the metal's valence, and R is its ionic radius. The higher the value for the stability index, the more difficult it is to demetallate the complex in solution. Correlation of the Buchler stability index with mass spectral properties will be discussed in the mass spectrometry section later in this chapter.

It is interesting to note the first observation of a water-soluble lithium porphyrin, which was reported in July of this year [Richards *et al.*, **1996**]. This was noteworthy in that, although lithium porphyrins had been observed in the past, this was the first case in

which the lithium/porphyrin complex did not demetallate upon addition of water. Development of a stable, water-soluble, lithium porphyrin puts the predictive power of the Buchler stability index, based solely on the properties of the metal, into question.

The importance of the work of Fisher and Woodward to synthetic organic chemistry has already been discussed. The current level of interest in porphyrins can be seen in the approximately 5,000 publications per year on all aspects of porphyrin research which appear in the Chemical Abstracts Selects section for porphyrins. The commercial availability of porphyrins is low and their cost is quite high. As a cost comparison, one gram of hemin, octaethylporphyrin, uroporphyrin-III methyl ester, or porphine, when traded for its equivalent, current (12/3/96) market value in gold would yield approximately 1.1 g, 240 g, 4.3 kg, and 4.8, kg respectively [*The Gainesville Sun*, **1996**; Sigma Chemical Company, **1996**]. Synthetic work today involves the creation of porphyrins with new and unusual substituents such as crown ethers attached to the β-pyrrolic carbons of the macrocycle [Murashima *et al.*, **1996**]. Another approach to porphyrin synthesis is to use biomimetic techniques. Using biomimetic syntheses, Franck and Nonn [Franck and Nonn, **1995**] were able to synthesize novel porphyrins and porphyrinoids more efficiently.

One last organic chemistry aspect of porphyrins is their use as catalysts. Halogenated metalloporphyrins have been used to activate the oxidation of acyclic alkanes by molecular oxygen [Lyons *et al.*, **1995**]. Iron porphyrins have been used as biomimetic catalysts for the oxidation of cyclopenta[*a*]phenanthrenones which are polyaromatic hydrocarbons of biological importance [Harden and Coombs, **1995**]. An iron(0) porphyrin has been reported to be an efficient homogeneous catalyst for the electrochemical reduction of carbon dioxide to carbon monoxide [Bhugun *et al.*, **1994**]. The polymerization of methyl methacrylate was found to be dramatically accelerated by enolate complexation of the methyl methacrylate to an aluminum porphyrin [Kuroki *et al.*, **1991**].

In order to increase their understanding of biochemical processes such as oxygen transport by hemoglobin and myoglobin or photosynthesis, physical chemists have used

porphyrins as models in theoretical calculations because of their relationship to chlorophyll and their presence in many other biochemically important processes (see next section). Magnesium porphine and magnesium pheoporphine have served as useful models for the electronic excited states of chlorophyll, as determined by intermediate neglect of differential overlap (INDO) techniques [Edwards *et al.*, **1982**; Edwards and Zerner, **1983**]. In this work, the authors propose that the initial event of photosynthesis may be the excitation of the visible Q band of the porphyrin, leading to the charge transfer state by movement of the Mg atom out of the plane of the ring and internal conversion. The movement of the Mg atom was hypothesized to result in intermolecular charge transfer followed by relaxation of the Mg atom back into the plane of the macrocycle. The Zerner group has also determined the ground state of $D_{4h}$ iron(II) porphine, the simplest model compound for heme, using similar techniques [Edwards *et al.*, **1986**].

Using the theoretical foundations of porphyrin spectroscopy laid by Gouterman in the 1960s [Gouterman, **1978**], the trends in the optical and redox properties of porphyrins and porphyrin analogs can be taken into account by comparing their highest occupied (HOMO) and lowest unoccupied (LUMO) molecular orbitals. Getting back to John Donne's question about grass and blood (page 1), quantum chemistry gives the less poetic answer that since the gap between the HOMOs and LUMOs of chlorophylls is smaller than that in heme, grass is green and blood is red. Taking this information a step further, Fajer proposed that a better understanding of the *in vivo* functioning and electronic properties of porphyrins could lead to tailoring biomimetic catalysts for *in vitro* use [Fajer, **1991**].

Porphyrin Biochemistry

Porphyrins and other cyclic tetrapyrroles are essential to many biological processes, including oxygen transport (heme group of hemoglobin), electron transport (heme

group of the cytochromes), and photosynthesis (chlorophyll, a magnesium-containing chlorin) [Addison *et al.*, **1977**]. Figure 1-4 illustrates the most important classes of cyclic tetrapyrroles in biochemistry: porphyrins, chlorins and phlorins (dihydroporphyrins), bacteriochlorins (tetrahydroporphyrins), porphyrinogens (hexahydroporphyrins) and corrins.

The porphyrin known as heme is found in many important biomolecules including the hemoglobins, myoglobins, cytochromes, catalases, and peroxidases. The chemical structure of protoheme (a precursor to heme) is illustrated in Figure 1-5a (page 13).

Hemoglobin, the molecule responsible for the red color of our blood, contains four protein-bound hemes. Oxygen is transported as an axial ligand on the iron atoms of the hemes. When one of the heme groups has bound oxygen, the remaining three hemes have an increased affinity for binding oxygen [Marks, **1969**]. Myoglobin, another molecule with protein-bound heme, serves as an emergency storage device for oxygen. One of the axial sites of the heme iron of deoxymyoglobin is occupied by the nitrogen on the side chain of one of the protein's histidine residues while oxygen occupies the axial position on the opposite face of the heme. The myoglobin-bound oxygen is only released during strenuous exercise, when the demand of the muscles for oxygen exceeds the supply available from the blood (from hemoglobin) [Marks, **1969**].

There are three classes of cytochromes, *a*, *b*, and *c*, characterized by their absorption spectra. They are responsible for electron transport processes in the mitochondria and chloroplasts during respiration. The prosthetic group of the cytochromes *b* and cytochromes *c* is heme. In the cytotchromes *c*, the vinyl groups at positions 3 and 8 of the heme are modified by covalent attachment to cystine residues in the protein through sulfide linkages. Reversible redox chemistry in which the iron cycles between the reduced, iron (II), and oxidized, iron (III), states is responsible for the ability of the cytochromes to transport electrons [Lemberg and Barrett, **1973**; Ortiz de Montellano, **1995**].

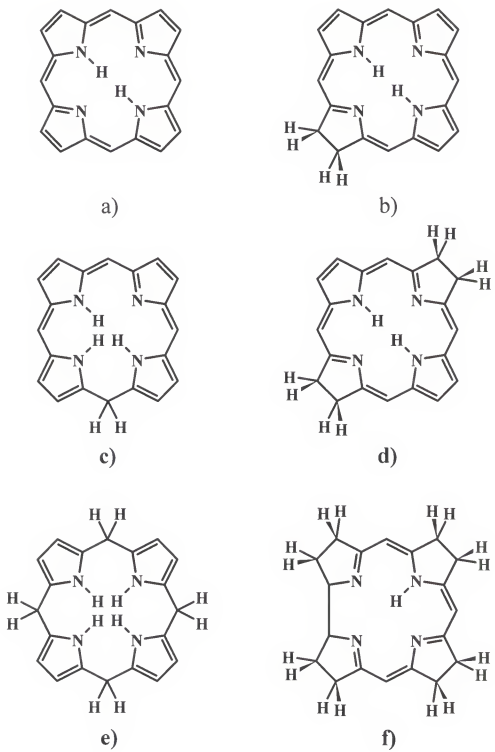


Figure 1-4. Metal-free skeletons of biologically important cyclic tetrapyrroles: a) porphyrins, b) chlorins, c) phlorins, d) bacteriochlorins, e) porphyrinogens, and f) corrins.

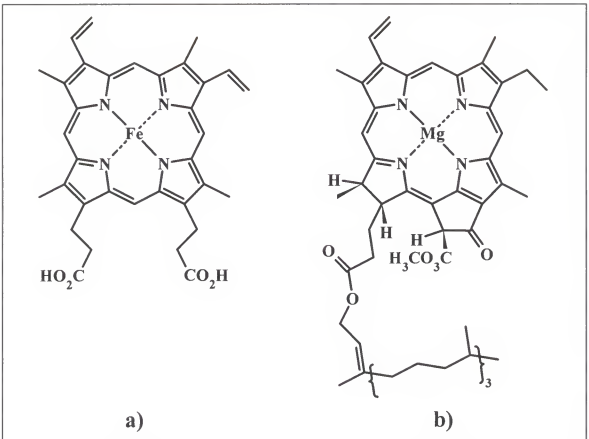


Figure 1-5. Structures for a) protoheme (a heme precursor) and b) chlorophyll *a*.

Metalloporphyrins are also the active sites in many enzymes including the peroxidases and catalases [Marks, **1969**; Williams *et al.*, **1977**]. The peroxidases are the enzymes responsible for catalyzing the oxidation of several organic compound classes and certain inorganic ions, such as iodide, by hydrogen peroxide. Peroxidases are found in all plants, many bacteria, and most animals. The catalases are responsible for catalyzing the decomposition of hydrogen peroxide. The porphyrin in both enzyme classes is heme.

The chlorophyll *a* molecule, which is a chlorin (Figure 1-4b) derivative, is illustrated in Figure 1-5b. Chlorophyll *b*, in which the methyl group on carbon 7 is replaced with CHO, is normally found in approximately one third the abundance of chlorophyll *a* in higher plants. In order to form a chlorin from a porphyrin, one of the double bonds between two β-pyrrolic carbons (usually shown in pyrrolic subunit D) is reduced with the consequential addition of a hydrogen to each carbon. The addition of the two hydrogens

leads to considerable changes in the properties of the molecule. For example, while most porphyrins have a reddish color, the chlorins are mostly greenish. The similarities (five of eight substituents the same) and differences (oxidation of one alkene side chain, cyclization, reduction of one β-pyrrolic bond, and esterification of the second acid with a long-chain isoprenoid) between protoheme, which is the iron(II) complex of protoporphyrin IX, and chlorophyll *a* can be seen by comparing parts a and b of Figure 1-5. The chlorophylls are the molecules by which the process of photosynthesis, conversion of the sun's energy into chemical potential energy, occurs.

The phlorins (Figure 1-4c), like the chlorins, are also dihydroporphyrins, but with the two extra hydrogens added to one of the meso-carbons and one pyrrolic nitrogen rather than across the bond between a pair of β-pyrrolic carbons. While the phlorins are important to chemists, they have no apparent biological significance. Iron complexes of the oxophlorins (Figure 1-6), however, are believed to be intermediates in the catabolism of waste hemes into bile pigments.

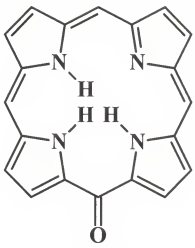


Figure 1-6. Oxophlorin skeleton.

The bacteriochlorin skeleton (Figure 1-4d) is found in the bacteriochlorophylls. These molecules serve as the light-harvesting antennules of photosynthetic bacteria [Tronrud *et al.*, **1986**; Deisenhofer and Michel, **1989**]. The bacteria funnel photons into a reaction center complex in which separation of positively and negatively charged ions across a membrane creates a voltage gradient. The electrical potential energy thus stored is the fuel for the bacterium's biochemical processes [Feher *et al.*, **1989**; Norris and Schiffer, **1990**].

The porphyrinogens (Figure 1-4e) are hexahydroporphyrin precursors in many biochemical syntheses of hemes and chlorophylls. Since there is no conjugation between the pyrrole subunits, the porphyrinogens are colorless.

The best known natural product with a corrin skeleton (Figure 1-4f) is vitamin $B_{12}$, an essential nutrient. Vitamin $B_{12}$ is present in coenzymes responsible for a number of biochemical functions including the oxidation of fatty acids and the synthesis of DNA [Addison *et al.*, **1977**; Smith, **1984**].

Porphyrins in Geochemistry

In the previous section, the biochemical roles of porphyrins and porphyrin-like compounds were shown to be widespread. Their ubiquity and the inherent stability of the porphyrin macrocycle, stemming from its aromaticity, make the porphyrins extremely important in geochemistry. The discovery of porphyrins in oil, for example, was one of the cornerstones of the proof of oil's biological origins. Alfred Treibs [Treibs, **1934**, **1936**] proposed that the origin of the geoporphyrins was ancient chlorophylls. This proposal and the reaction scheme (Figure 1-7) by which the diagenesis was supposed to have occurred have become known as the Treibs' Hypothesis. The compounds in the series have been characterized by both UV-Vis spectroscopy [Stern and Wenderlein, **1936**] and mass spectrometry [Baker *et al.*, **1968**; Baker and Smith, **1973**].

In the Treibs' Hypothesis, the initial reactions of demetallation, saponification, and decarbomethoxlyation of the chlorophyll *a* molecule occur at the water/sediment interface under very little external pressure or temperature stress. The remainder of the reactions in the series occur as the sediments become compacted and the thermal and pressure stresses increase. The reaction order is not fixed and can vary with the environment.

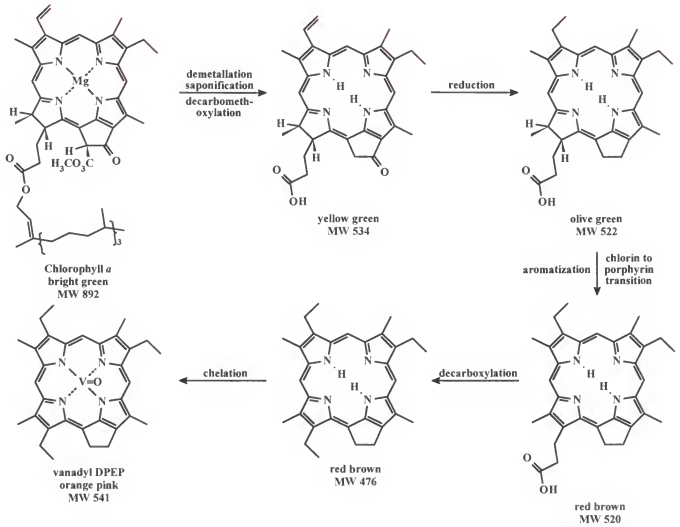


Figure 1-7. Treibs' scheme for the diagenesis of porphyrins [adapted from Treibs, **1934**, **1936**].

The geoporphyrins generated in the diagenesis process, as mentioned above, are present in all petroleum deposits, but generally constitute only a small fraction of the total carbon in the deposits. A variety of classes of porphyrins is found in petroleums. These porphyrin classes are characterized by differing peripheral substituents (β-pyrrolic substituents are the most prevalent; *meso*-substitutions are, for the most part, found only when there are isocyclic rings). Their durability combined with their pervasive presence in petroleums make the geoporphyrins important biomarkers [Eglinton and Calvin, **1967**].

Biomarkers can be defined as compounds having a basic carbon skeleton which remains unchanged during geological deposition and throughout the processes of diagenesis. Because the basic carbon skeleton remains intact, biomarkers permit determination of the source of organic materials; for this reason they are also sometimes known as chemical fossils [Bonnett *et al.*, **1991**]. The structural complexity and number of skeletal types of the geoporphyrins allows fingerprinting of samples for oil-oil or oil-source rock correlations [Corwin, **1960**; Chicarelli *et al.*, **1987**; Filby and Van Berkel, **1987**; Ocampo *et al.*, **1987**].

One of the most active areas of geoporphyrin research at the present time is clarification of the diagenesis processes under which biological precursors are transformed into geoporphyrins. In fact, the total synthesis of various geoporphyrin skeletal types is an ongoing area of interest for the organic geochemist [Bauder *et al.*, **1992**]. One area under debate is the origin of geoporphyrins which contain extended isocyclic rings of up to seven carbons. The existence of these compounds cannot be explained satisfactorily by the processes in the Treibs' Hypothesis [Bonnett *et al.*, **1991**]. Likewise, the discovery in this laboratory, through tandem mass spectrometric analysis, of high carbon-number geoporphyrins which cannot be generated by degradative processes [Johnson *et al.*, **1986**] puts Treibs' scheme further into question. The use of tandem mass spectrometry (MS/MS) for the characterization of geoporphyrins has been one of the fruitful areas of research in the Yost research group [Britton, **1985**; Quirke *et al.*, **1988, 1989**; Beato,

**1989**; Beato *et al.*, **1989a**, **b**]. Most recently MS/MS has been used to characterize several types of cycloalkanoporphyrins (CAPs) and the fragmentation pathways of 5-nitro-octaethylporphyrin [Laycock, **1994**; Laycock *et al.*, **1995**, **1996**].

Porphyrins in Medicine

The biochemical importance of the porphyrins was discussed above. They are important compounds in medicine as well. For instance, products of porphyrin catabolism are important markers for liver diseases. Changes in porphyrin metabolism have been monitored as biomarkers for mercury exposure and toxicity [Woods, **1996**]. Many of the porphyrin-related diseases involve photosensitivity and most medical uses of porphyrins include photoirradiation because of the light-absorbing and catalytic properties of the porphyrins.

There are many disorders in which abnormal porphyrin synthesis and metabolism are implicated. The best known of these disorders are the porphyrias, in which reactions catalyzed by the photoactivity of the porphyrins under the skin have been implicated [Blum, **1941**; Downey, **1996**]. The porphyrias are a complex group of metabolic diseases defined by the lack of a specific enzyme. One of the more potent forms of porphyria is believed to have been responsible for the periodic mental instability of King George III of Great Britain [Macalpine and Hunter, **1969**; Bennett, **1995**]. The porphyrias are congenital, and are passed on by autosomal dominant genes, but show various levels of expression. As more and more enzymes are discovered, and testing for their presence (made possible by advances in analytical chemistry) becomes more common, greater numbers of porphyric diseases are becoming known. For instance, it is highly likely that many of the recently publicized fatigue syndromes are due to some form of porphyria [Downey, **1992**, **1994**].

The photochemistry of the porphyrins is also used in medicine to kill bacteria and cancer cells. Photoinactivation of bacteria has potential uses in sterilization and treatment of disease. Cationic *meso*-substituted porphyrins and cationic water-soluble zinc phthalocyanines have been reported to be efficient photoinactivators of both Gram-positive and Gram-negative bacteria [Merchat *et al.*, **1996**; Minnock *et al.*, **1996**].

In a branch of medicine known as photodynamic therapy, the photochemical properties of porphyrins are used for the treatment of various cancers [Gomer, **1990**; Nauta *et al.* **1996**; Schuitmaker *et al.*, **1996**]. Much research has gone into the development of new photosensitizers [*e.g.*, Pasternak *et al.*, **1983**; Le Nouën *et al.*, **1989**; Zenkevich *et al.*, **1996**]. Although considerable research has gone into the chemistry and modes of action of the photodynamic therapy agents [*e.g.*, Orenstein *et al.*, **1996**], there is still much to be learned about this medical technique. The photosensitizing reactions of photofrin, the most commonly used photodynamic therapy agent, with model compounds were investigated in this laboratory using tandem mass spectrometry and on-line and off-line photoreaction chambers and thermospray ionization to detect the products [Laycock, **1994**].

Porphyrins in Materials Science

In the field of optical disk storage media, porphyrins have been employed as dyes for shorter wavelength recording and show promise for use in ultrahigh density recording [Seto *et al.*, **1996**]. Another information storage usage is the formation of charge-trapping porphyrin films on indium tin oxide (ITO) and /$SiO_2$/Si [Liu *et al.*, **1996**]. In this work, tiny capacitors are formed as sandwiches of zinc *octakis* (β-octyloxyethyl) porphyrin (ZnOOEP) between layers of ITO or in an ITO/ZnOOEP/$SiO_2$/Si configuration. A small amount of charge (similar to conventional capacitors) could be stored when the cells were kept in the dark. However, when the photoconductive ZnOOEP was irra-

diated, the charge stored was three orders of magnitude higher. The stored charge could not be removed under short-circuit conditions in the dark, making these sandwiches potential candidates for information storage devices.

Porphyrins have also demonstrated potential utility in the area of molecular electronics. In one application, green photons were transmitted along a porphyrin chain with greater than 80% efficiency. The photons exited from the other end of the "photonic wire" in the red portion of the spectrum [Wagner and Lindsey, **1994**]. More recent work has shown that the transmission of photons through the "wire" can be switched on and off by altering the redox state of a switching porphyrins attached to the chain [Wagner *et al.*, **1996**].

Various molecular wires, designed to conduct electricity and consisting of rigid fused porphyrin oligomers, have been reported [Crossley and Burn, **1991**] and recently have been made long enough (110 Å) for nanoelectrode spanning [Reimers *et al.*, **1996**]. Nanofabrication of photoelectronic devices on a molecular scale has also been reported [Shimidzu, *et al.*, **1995**]. Using electropolymerized one- and two-dimensional porphyrins polymers connected by oligothienyl molecular wires, layered diodes and a microscopic polymer junction chip having photovoltage and photocurrent applications were constructed. A sandwich of the polymer with polybiothiophene showed electric rectifying in the dark.

Distorted Porphyrins

The porphyrins in many biological systems are distorted from planarity by their environments. For example, the heme unit in cytochrome *c* is substantially distorted owing to covalent linkages between the heme periphery and cysteine residues in the protein [Anderson *et al.*, **1993**; Hobbs *et al.*, **1994**]. The heme is essentially planar when not in the protein. Recent work on dodecasubstituted porphyrins (*i.e.*, having substituents

on all eight β-pyrrolic carbons and all four *meso,* bridge, carbons) indicated that such porphyrins are distorted from planarity and that the non-planarity of the molecules produces significant modification of the molecular properties. For example, 2,3,7,8,12,13, 17,18-octaethyl-5,10,15,20-tetraphenylporphinato Zn(II), a distorted porphyrin, absorbs light at longer wavelengths than more planar porphyrins and is easier to oxidize; these properties are useful in explaining why photosynthetic reaction centers such as Factor 430 contain non-planar tetrapyrroles [Barkigia *et al.*, **1990**]. The full significance of the non-planarity of the porphyrins has yet to be ascertained. Non-planar distortions in synthetic porphyrins may be used to model the naturally occurring distortions such as those seen in cytochrome *c*. Shelnutt and coworkers have suggested that information about non-planar distortions may be useful in tailoring biomimetic catalysts with specific function and catalytic selectivity [Sparks *et al.*, **1993**]. For example, certain iron, ruthenium, and other metallated porphyrins can catalyze the oxidation of alkanes [Belova *et al.*, **1987**; Wayland and Del Rossi, **1984**; de Poorter *et al.*, **1985**].

When porphyrins (even those without bulky substituents crowded around the macrocycle to cause distortion) contain a metal with a small ionic radius such as nickel (0.69 Å), they have been shown to interconvert between planar and non-planar conformers [Meyer, **1972**; Cullen and Meyer, **1974**; Brennan *et al.*, **1988**]. For example, Ni(II)octaethylporphyrin (NiOEP) has three distinct crystalline forms, two planar forms (the A and B triclinic forms) and one non-planar (tetragonal) form. Resonance Raman spectrometry has been used to determine that these conformers exist in equilibrium in non-coordinating solvents such as carbon disulfide and methylene chloride [Alden *et al.*, **1989**, **1990**].

Two processes can be used to shift the equilibrium conformation of a porphyrin from planar to non-planar: crowding of substituents (steric effects) around the macrocycle and contraction of the porphyrin core, which can be achieved by chelating different metals. The non-planarity induced by either process can be used to model the naturally occurring distortions found in heme proteins. X-ray crystallographic data have shown

that the distortions affect not only the shape of the macrocycle, but also the interactions between the pyrrolic nitrogens and the chelated metal which sits in the central cavity [Hobbs *et al.*, **1994**]. These structural changes affect chemical processes such as the binding and release of axial ligands bound to the central metal and the redox properties of the metal. The distortions produced by attaching one to four nitro groups to the *meso* carbons of OEP are illustrated by the energy-optimized structures generated by the molecular modeling program POLYGRAF which are shown in Figure 1-8. The modeling utilized force fields based on potential energy functions and force constants from normal coordinate analysis of Ni(II)OEP [Li *et al.*, **1990**].

## Mass Spectrometry

The origins of mass spectrometry (MS) can be traced back to the discovery by Goldstein [Goldstein, **1886**] of "positive rays" in a low-pressure electrical discharge [Duckworth *et al.*, **1986**]. Using a perforated cathode, Goldstein noted visible rays which he named *kanalstrahlen* passing through the holes (canals) into the space behind the cathode. A few years later, the existence of the electron was established by J. J. Thomson [Thomson, **1897**] in his famous cathode ray experiments. At about the same time Thomson reported the electron, Wien experimented with Goldsteins' "canal rays" and found they could be deflected by magnetic and electric fields [Wien, **1898**, **1902**]. The deflection of the rays showed them to be composed of positive particles with much lower charge-to-mass ratios (specific charge) than the electron. Thomson later turned to the examination of positive rays and conducted investigations using a positive ray parabola apparatus [Thomson, **1912a**, **b**]. These experiments presented strong evidence for the existence of two forms of neon, the most common form having an atomic weight of 20 and a much less abundant isotope with an atomic weight of 22. Although the concept of isotopes had been developed by Soddy to explain why certain radioactive atoms had

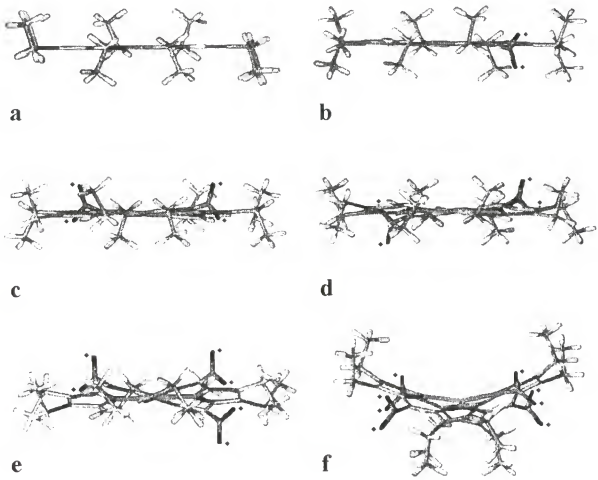


Figure 1-8. Energy-optimized structures for Ni(II) derivatives of octaethylporphyrin a) NiOEP, b) 5-mononitrooctaethylporphyrin (NiOEMNP), c) 5,10-dinitrooctaethylporphyrin (NiOE5,10DNP), d) 5,15-dinitrooctaethylporphyrin (NiOE5,15DNP), e) 5,10,15-trinitrooctaethylporphyrin (NiOEtriNP), and f) 5,10,15,20-tetranitrooctaethylporphyrin (NIOETNP) [adapted from Hobbs *et al.*, **1994**]. Note: the nitro group oxygen atoms are indicated by diamonds.

identical chemical properties, this was the first evidence for the existence of isotopes of non-radioactive elements.

The man most widely credited with the development of the mass spectrometer, Francis William Aston, had been Thomson's research student at Cambridge University and assisted him in his experiments with neon. Thomson encouraged him to further investigate stable isotopes. Aston's first attempts at enriching the $^{22}Ne$ isotope using fractionating techniques did not achieve success. In order to improve on this lackluster performance, he developed an instrument to analyze and focus positive rays which he coined a "mass spectrograph" [Aston, **1919**]. Aston won the Nobel prize in chemistry in 1922 for his contributions to analytical chemistry and his study of atomic structure. However, it is his work on the mass spectrograph for which he is best known [James, **1993**]. Since Aston's initial work, several types of mass spectrometer have been developed. In analytical chemistry, magnetic sector, quadrupole, time-of-flight, and ion cyclotron resonance instruments are the mass spectrometers most commonly used.

Triple Quadrupole Mass Spectrometry

The ionization energy and fragmentation pathway determinations presented in this dissertation were performed on a triple quadrupole mass spectrometer (TQMS), (Figure 1-9). As illustrated in Figure 1-9, the modified Finnigan MAT TSQ70 instrument employed in these studies has an octopole in place of the second quadrupole for improved ion transmission through the collision cell. Although most commercial instruments employ a hexapole or octopole collision cell, the term triple quadrupole mass spectrometer (TQMS), is still commonly used. The instrument consists of an ion source, a quadrupole mass filter (Q1), an RF-only octopole in a collision cell into which gas can be introduced (Q2), a second quadrupole mass filter (Q3), and a conversion dynode and electron multiplier which serve as the detector. Operation of a quadrupole or an octopole

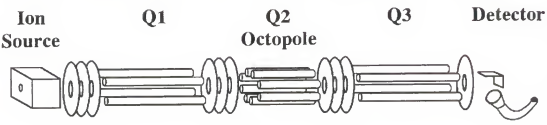


Figure 1-9. Block diagram of the TSQ70 triple quadrupole mass spectrometer.

in the RF-only mode allows ions of nearly every mass-to-charge (m/z) ratio to pass through. Operation of a quadrupole with appropriate levels of RF and DC voltages allows passage of ions of only a single m/z, hence the term mass filter. Ion focusing lenses are placed between the various parts of the instrument to improve the transmission of the ion beam. Because the instrument has two independent mass analyzers, two separate stages of mass analysis (MS/MS) are possible [Yost and Enke, **1979**; Yost and Fetterolf, **1983**]. The second stage of mass analysis provides several advantages, including reduction of chemical noise (resulting in lower limits of detection) and minimal or no sample clean-up or chromatographic separation required (resulting in a lowered need for sample to compensate for the inevitable losses from those processes) [Johnson and Yost, **1985**].

Although a TQMS can be operated in the MS/MS mode, it also functions well as a single-stage mass filter (MS mode) by setting either the first or the third quadrupole in the RF-only mode and scanning the other quadrupole. Scan modes available in the MS mode of operation are illustrated in Figure 1-10. For applications in which one or more selected ions rather than a range of masses are monitored, the selected ion monitoring mode, using either Q1 or Q3 (as illustrated) for mass selection, provides a higher signal-to-noise ratio by allowing a longer integration time for the selected ion(s).

In the MS/MS (tandem MS) mode of operation, additional scan modes are possible. The three MS/MS scan modes which were used in this research are illustrated in Figure 1-11. All three of the MS/MS modes discussed are useful for structure determina-

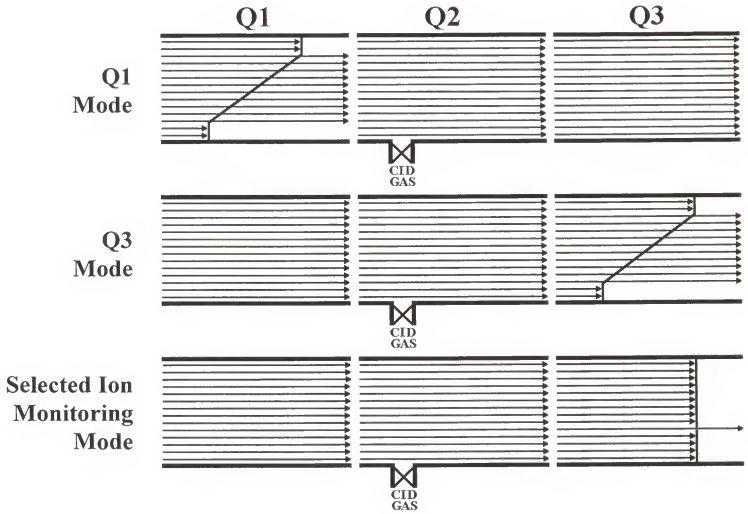


Figure 1-10. Scan modes possible with a single stage of MS. In the Q1 mode, for example, Q1 is scanned from low to high m/z, while Q2 and Q3 are operated in the RF-only mode, passing the ions from Q1 to the detector after Q3.

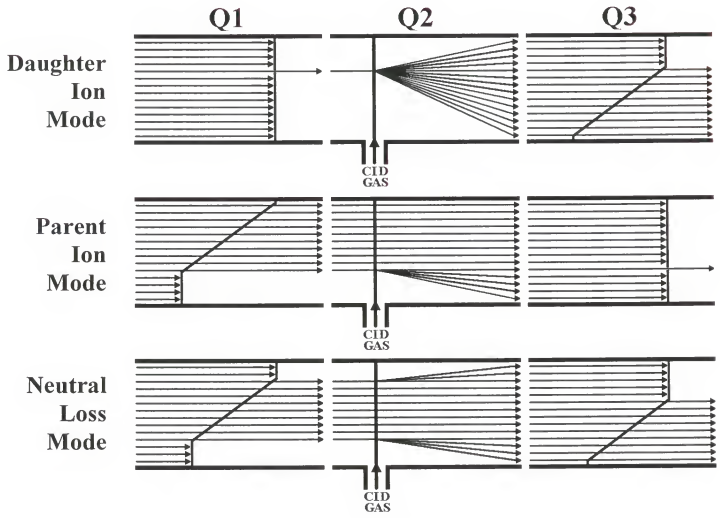


Figure 1-11. Scan modes possible with two stages of MS (MS/MS).

tion and determining the reaction pathways of ions (fragmentation pathways). For instance, GC/MS/MS has been used to determine the compounds emanating from human skin which are attractive to mosquitoes [Bernier, **1995**].

In the daughter ion mode, Q1 is used to mass select an ion of a given m/z (the parent ion) which then passes into the collision cell (Q2) which has been pressurized with an inert target gas (helium, nitrogen, and argon are commonly used at pressures between 1 and 3 mtorr). The collision cell is maintained at a voltage offset relative to the ion source to give the ions kinetic (collision) energy for collision with the gas. The collisions impart internal energy to the parent ion and, if enough energy is transferred, the ion fragments. This process is known as collision-induced dissociation (CID). The resulting fragment (daughter) ions are passed through Q2, which is operated in RF-only mode, and are mass analyzed in the Q3. A daughter ion spectrum therefore contains the fragment (daughter) ions produced by CID of the chosen parent ion.

In the parent ion mode, Q1 is scanned, passing ions (parents) with a range of m/z values into Q2 to undergo CID. Q3 is used to mass select one fragment (daughter) ion of a given m/z. Those parent ions which fragment to form the given daughter ion constitute a parent ion spectrum.

In the neutral loss mode, those parent ions which lose a given m/z value (*e.g.*; loss of 18 mass units owing to loss of water from singly charged ions) to form a daughter ion comprise the neutral loss spectrum. In order to generate this spectrum, Q1 and Q3 are scanned simultaneously so that Q1 passes ions which are 18 mass units higher than those passing Q3.

One final mode of MS/MS, not used in this dissertation research, is the selected reaction monitoring mode (Figure 1-12). In this mode, the TQMS is set so that only one selected parent ion is allowed to react and one selected daughter ion at a time is detected. In this mode, the chemical noise is reduced to the point where trace compounds can be detected in complex matrices [Johnson and Yost, **1985**; Johnson *et al.*, **1986**]. Any of the

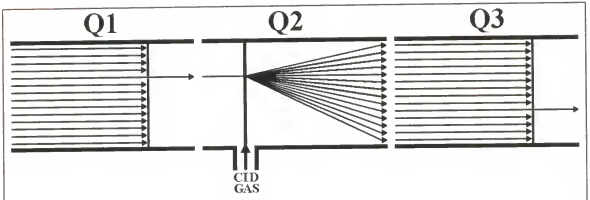


Figure 1-12. The selected reaction monitoring mode (MS/MS operation).

MS/MS modes can also be used to monitor ion/molecule reactions by replacing the inert gas in the collision cell with a reactive one. An application of this was modeling solution-phase reactions between DNA and carcinogens (reactive electrophiles) by reacting model nucleophiles (DNA base or nucleotide ions mass selected in Q1) with electrophilic gases in Q2 and scanning Q3 to detect the adduct ions which formed [Freeman *et al.*, **1990**; Annachino, **1993**].

Porphyrin Mass Spectrometry

The classic studies involving porphyrin characterization using mass spectrometry were performed in the 1960s and 70s [Baker, **1966**; Baker *et al.*, **1967**; Clezy *et al.*, **1974**]. In the Baker papers, structural data for many petroporphyrins were obtained using a combination of high resolution MS and chromatographic separation techniques. The Clezy paper discusses the mass spectrometry of the *meso*-substituted porphyrins. An excellent review of the early work on the EI-MS of porphyrins emphasized the fragmentation behavior of alkyl-substituted porphyrins [Budzikiewicz *et al.*, **1985**]. In this paper, the α- and β-cleavage patterns were shown to be the most commonly observed fragmentations. When referring to cleavages, the α and β terms indicated cleavages which occur α and β to the ring (*i.e.*, cleavage of the entire substituent or cleavage removed from the ring by one bond), and should not be confused with the α- and β-pyrrolic carbons of the

porphyrin macrocycle. Another, commonly encountered term, used interchangeably with β-cleavage, is benzylic cleavage. Both α- and β-cleavages produce neutral alkyl radicals with the charge remaining on the remainder of the porphyrin macrocycle.

Electron Ionization

The electron ionization (EI) mass spectrometric behavior typical of most biological and geochemical porphyrins can be seen in the mass spectrum of the model compound 2,3,7,8,12,13,17,18-octaethylporphyrin. The 70 eV EI mass spectrum of OEP is shown in Figure 1-13. The most important feature to note in the spectrum is that the porphyrin macrocycle remains intact. Again, this is theorized to be due to the resonance stabilization possible in such a highly conjugated system [Jackson *et al.*, **1965**]. Other important features of the spectrum are the presence of relatively abundant doubly charged ions, the β-cleavages, and to a much smaller extent, α-cleavages of the ethyl substituents (Figure 1-14). The β-cleavage of a methyl group from the ethyl substituents of OEP was first reported in 1968 [Seibl, **1968**]. The β-cleavage pattern has been found to be the dominant mode of fragmentation for the alkyl-substituted porphyrins no matter what the alkyl chain length [Britton, **1985**; Johnson *et al.*, **1986**]. This phenomenon has been utilized extensively for determining the nature of the peripheral substituents on porphyrins.

The doubly charged ions, which are not commonly seen in EI-MS, are prevalent in the MS of porphyrins because the high level of conjugation of the macrocycle allows the molecule to easily retain multiple charges [Jackson *et al.*, **1965**]. Nuclear magnetic resonance studies have shown that the charges are separated by localization at two of the pyrrolic nitrogens in the molecular core [Chakraborty *et al.*, **1982**]. The β-cleavage pattern, which was seen to predominate in the singly charged portion of the spectrum, occurs to a greater extent in the doubly charged region. The incidence of *a*-cleavage in this region is also enhanced [Beato *et al.*, **1989b**].

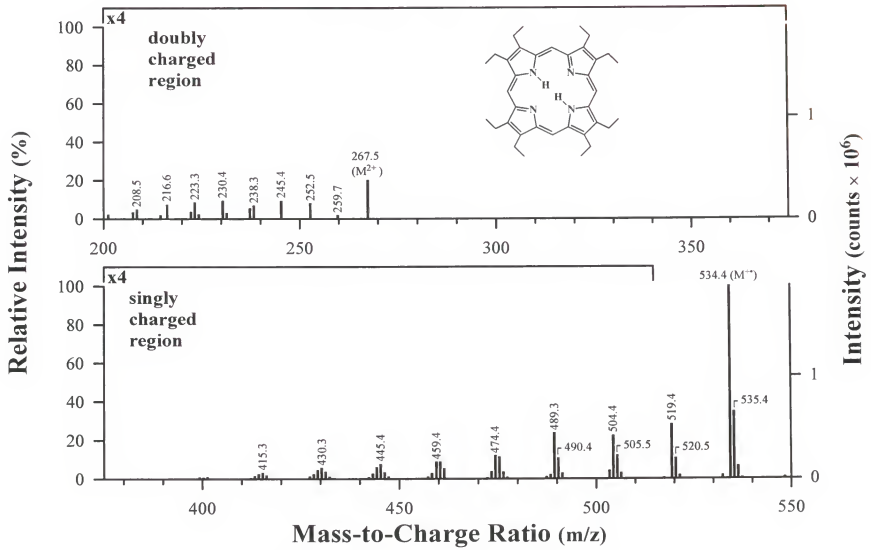


Figure 1-13. EI (70 eV) mass spectrum of OEP.

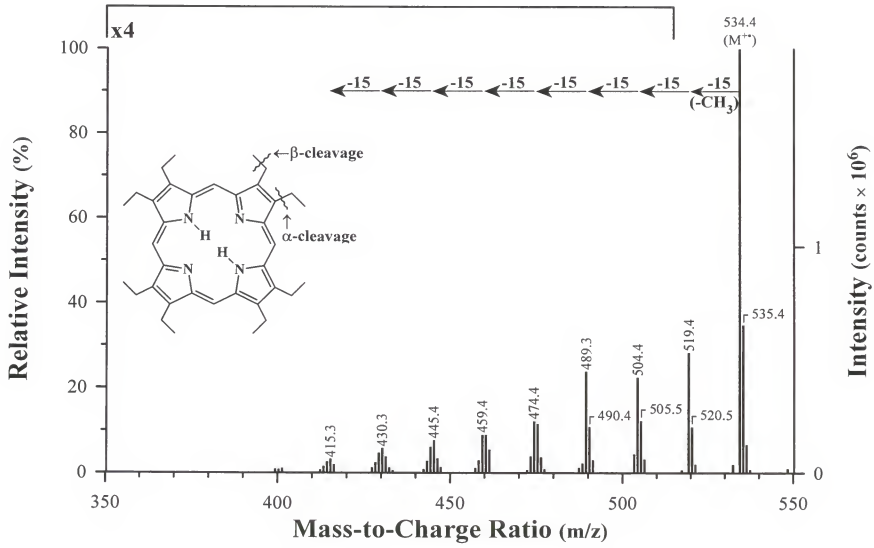


Figure 1-14. Partial EI mass spectrum of OEP showing repeated β-cleavage in the singly charged region only.

When the porphyrin contains a chelated metal ion, the fragmentation pathway and relative abundances of the fragment ions are both altered significantly. The relative abundances of the ions in the doubly charged portion of the mass spectrum was found to correlate well with a modified Buchler stability index ($S_i$) for the metal. The relative abundances of the ions in the singly charged region, however were relatively unchanged. [Beato *et al.*, **1989b**].

Chemical Ionization

Chemical ionization (CI) mass spectrometry is a "soft" ionization technique which produces predominantly molecular ions and provides information complementary to that from EI-MS. CI-MS using methane as the reagent gas has been utilized for determining their molecular weights of porphyrins [Eglinton *et al.*, **1979**]. A new fragmentation pathway was observed when the CI reagent gas was hydrogen or ammonia, and to a lesser extent with methane, [Beato *et al.*, **1991**]. The presence of mono-, di-, and tripyrrolic fragments indicated that macrocycle scission had occurred. The porphyrins under study were introduced into the mass spectrometer from the direct exposure probe (DEP) heated to relatively high temperatures. (The DEP temperature in those experiments was ramped from ambient to 1350 °C at 600 °C/min). A small fraction (estimated at $1/10^4$) of the porphyrin molecules coming off the probe was ionized and found its way into the mass spectrometer relatively quickly. However, the majority of the molecules remained un-ionized and some deposited onto the cooler (relative to the probe) metal surface of the ion volume of the mass spectrometer where they could undergo a surface-induced reduction to porphyrinogens. As the temperature of the DEP increased, radiative heating of the ion volume led to volatilization of the porphyrinogen compounds and their subsequent ionization, fragmentation, and mass analysis. The porphyrinogens are hexahydroporphyrins (Figure 1-4e) in which the bridge carbons are $sp^3$ hybridized, short circuiting the conjugation between the pyrrolic subunits (*vide supra*). The acid-labile porphyrinogens readily

fragmented, yielding pyrrolic sequence and individual pyrrole composition information [Shaw *et al.*, **1981**; Van Berkel *et al.*, **1989a**, **b**; Beato *et al.*, **1991**].

Thermospray

Thermospray (TSP) ionization was the first practical interface for liquid chromatography (LC) and mass spectrometry. Like CI, it is a "soft" ionization technique Both polar and involatile compounds can be analyzed using TSP [Vestal, **1984**] which also permits higher sample flow rates into the ionizer than previous techniques had allowed. An exhaustive review of TSP-LC/MS was published by Arpino in 1992 [Arpino, **1992**].

The photosensitizing reactions of the porphyrins were discussed in the "Porphyrins in Medicine" section of this dissertation. The high flow rates allowed by the TSP interface minimize the dead time the sample spends traversing the plumbing connections between the reaction cell and the mass spectrometer. The shorter dead times allow the study of rapid photochemical reactions. The reactions of several photoreactive porphyrins with tryptophan (TRP, an amino acid known to be highly reactive toward photosensitizers) have been monitored using both on-line and off-line photochemistry/TSP-MS [Laycock, **1994**]. The conversion of TRP to photoproducts was found to increase 50-fold by the addition of hematoporphyrin to the mixture.

Electrospray

The latest "soft" ionization technique used to study porphyrins is electrospray ionization (ESI). Like thermospray, it is an important interface between solution phase chemistry and the gas-phase mass spectrometer [Kebarle and Tang, **1993**]. In addition to the advantages of thermospray, ESI can be used to analyze thermally labile compounds which might decompose in the high heat required for thermospray.

In ESI, a plume of ion-containing droplets (the spray) is generated by a high voltage gradient between a needle, through which the solution passes, and the inlet to the mass spectrometer. Because it is still a relatively new ionization technique, the mecha-

nism for ion formation and transport into the mass spectrometer is not fully characterized. In order to study the complex procedures involved, the behavior of porphyrin ions in the ESI process was monitored using optical spectroscopy of the porphyrin ions (in solution and in the electrospray plume) and mass spectrometry to detect the ions which made it through the interface [Chillier *et al.*, **1996**]. Metal-free (free-base) OEP was studied because the UV-Vis spectra of the $OEP^+$ and $OEP^{2+}$ ions are significantly different, and solutions containing exclusively one or the other ion can be made by adjusting the solvent conditions appropriately. When solutions of the dication were sprayed, the fluorescence spectra of the droplets produced indicated that the dication was the chromophore in the droplets. In contrast, no matter what the skimmer-nozzle voltage setting, the predominant ion in the mass spectrum was the monocation. The predominance of monocations in the mass spectrum indicated that the dications had been converted to monocations at some time during their desolvation between the needle and the mass filter. The electrospray ionization process is still poorly understood. The observed change in ion charge state during desolvation complicates the debate over how and when ions form in electrospray.

## Ionization and Appearance Energies

### Definitions

The adiabatic ionization energy ($IE_a$) of an cation ($AB^{+\bullet}$) is the energy required to remove an electron from the neutral molecule (AB) and produce the ion [Lias *et al.*, **1988**]:

$$AB \xrightarrow{IE_a} AB^{+\bullet} + e^- \qquad (1\text{-}2$$

The adiabatic appearance energy ($AE_a$) of a fragment ion is defined as the energy required to ionize the neutral molecule and impart sufficient excess internal energy into the

ion thus formed to lead to the unimolecular fragmentation of the ion into the fragment ion of interest ( $A^+$ ) and an additional neutral fragment ( $B^\bullet$ ) which is typically a radical:

$$AB \xrightarrow{AE_a} A^+ + B^\bullet + e^- \quad (1\text{-}3$$

In thermodynamic terms, the gas-phase enthalpy change of ionization ( $\Delta H_I$ ) is related to the heat of formation of the ion at a given temperature ( $\Delta H_f(M^+)_T$ ) and the heat of formation of the neutral precursor at that temperature ( $\Delta H^\circ_f(M)_T$ ) and the adiabatic ionization energy as shown here:

$$\Delta H_f(M^+)_T = \Delta H^\circ_f(M)_T + \Delta H_I \quad (1\text{-}4$$

The question of how to relate $\Delta H_I$ to $IE_a$ can be answered in two ways. The rigorously correct relationship between them at absolute zero is:

$$IE_a - \Delta H_f e = \Delta H_I \quad (1\text{-}5$$

where $\Delta H_f e$ represents the energy imparted to the electron in the ionization process. Which of the alternatives is chosen depends on whether one is a thermodynamicist or an ion chemist or ion physicist (mass spectrometrist). The thermodynamicists' convention, known as the "thermal electron convention", treats the electron as a standard chemical element and carries the $\Delta H_f e$ term through all calculations. The mass spectrometrists' convention, also known as the "stationary electron convention" or the "ion convention", treats the electron as a subatomic particle. These two conventions are in agreement only at absolute zero. Ionization energy values in compilations using the ion convention vary by 1.481 kcal/mol, 6.197 kJ/mol or 0.06422 eV/molecule from the values found in standard compilations such as the JANAF tables [Chase *et al.*, **1985**] or the NBS Tables of Chemical Thermodynamic Properties [Wagman *et al.*, **1982**]. IE values under the ion convention values are lower for positive ions and higher for negative ions. Because the research presented here was performed on a mass spectrometer, the ion convention will be used throughout this dissertation.

Even though (according to the ion convention) we can ignore the $\Delta H_f e$ term, we still cannot assume that $\Delta H_I$ and $IE_a$ are equal. The adiabatic ionization energy of a

molecule is properly defined as the energy difference between the lowest vibronic level of the electronic ground state of the molecule and the lowest vibronic level of the electronic ground state of the ion. These levels are only attainable at absolute zero. Correction terms must be added for the heat capacities of the neutral molecule (A) and the ion (B).

$$\Delta H_1 = IE_a + B - A \tag{1-6}$$

We now have a rigorously correct relationship between the gas-phase enthalpy change of ionization ($\Delta H_1$) and the adiabatic ionization energy $IE_a$. Analysis of the integrated heat capacities of the molecule (M) and the molecular ion ($M^+$) for several molecules [Lias and Ausloos, **1978**] indicated that: 1) for most molecules, the difference between the rotational and vibrational heat capacities of M and $M^+$ is negligible, 2) over the temperature range of 300–400K, the differences between degenerate energy levels of multiplet ground states of M and $M^+$ do not exceed 0.009 eV, and 3) the only significant contribution to a difference between the heat capacities of M and $M^+$ arises in those cases where the frequency of a vibrational mode is significantly shifted. The vibrational contribution to the heat capacities can be ignored in most instances. For example, when ethylene is ionized, the C-C stretch is shifted from 1620 to 1230 $cm^{-1}$ and the twisting mode about the bond (from which an electron was removed in the ionization process) is shifted from 1027 to 430 $cm^{-1}$. Even with such significant changes in the vibrational frequencies, the predicted increase in the measured ionization energy at 298K over the $IE_a$ value is only 0.0069 eV. This value is much smaller than could be measured by most instruments used in determining IEs and can safely be ignored. With this information, we can finally set $\Delta H_1$ and $IE_a$ equal and, subject to the limitations mentioned, write:

$$\Delta H_f(M^+)_T = \Delta H_f^\circ(M)_T + IE_a \tag{1-7}$$

Similar arguments can be applied to appearance energy determinations.

Methods for Determining Ionization and Appearance Energies

Although many methods have been developed for the determination of ionization and appearance energies[Lias *et al.*, **1988**], only a few selected methods will be discussed here .

Optical Spectroscopy

One of the oldest techniques for determining ionization energies involves identification of a Rydberg series in the atomic or molecular spectrum. The present advanced state of optical monochromator technology allows highly accurate wavelength (energy) determinations. This technique is most easily applied to atoms and small molecules which have simple spectra [Moore, **1970**]. The increase in the complexity of the optical spectra of large molecules with their greater number of possible vibrational and rotational levels renders this method much less useful for such molecules [Rosenstock, **1976**, Rosenstock *et al.*, **1977**].

Photoelectron Spectroscopy

In photoelectron spectroscopy [Brundle and Baker, **1977**; Rabalais, **1977**], the ionization process is initiated by means of a photon of known energy and the kinetic energy of the resulting electrons is measured:

$$M + h\nu \rightarrow M^{+\bullet} + e^{-} \qquad (1\text{-}8$$

The ejected electrons have a distribution of energies dependent on the amount of internal energy retained in the ion ( $M^{+\bullet}$ ). The binding energy of the electron ( I ) is a function of the photon energy ( $h\nu$ ), the internal energy (vibrational and rotational) of the ion ( $E^{\bullet}_{V,R}$ ), and the kinetic energy of the ejected electron ( $KE_e$ ):

$$I = h\nu - KE_e - E^{\bullet}_{V,R} \qquad (1\text{-}9$$

The abundances of the $KE_e$ s are mapped, producing the photoelectron spectrum. The shapes of these maps provide information on the different energy states of $M^{+\bullet}$ and the Franck-Condon probabilities for transitions between M and $M^{+\bullet}$.

Ion/Molecule Equilibrium Constant Determinations

In this technique an ion/molecule equilibrium:

$$A^+ + B \leftrightharpoons C^+ + D \qquad (1\text{-}10$$

is maintained in a high pressure mass spectrometer [Kebarle, **1977**], flow tube [Ferguson, **1972**], or ion cyclotron resonance spectrometer [Moylan and Brauman, **1983**]. The neutral reactants are kept in great abundance relative to the ionic reactants, maintaining the [D]/[B] ratio essentially constant throughout the reaction. The relative abundances of $A^+$ and $C^+$ are monitored and the equilibrium constant is determined after a large number of collisions:

$$K_{eq} = \frac{[C^+][D]}{[A^+][B]} \qquad (1\text{-}11$$

From a single measurement of the $K_{eq}$, the Gibbs free energy change ( $\Delta G$ ) of reaction 1-10 can be calculated:

$$\Delta G = -RT ln K_{eq} = \Delta H - T\Delta S \qquad (1\text{-}12$$

In common practice, only one measurement is made and the entropy contribution is estimated by the use of statistical mechanical models.

The charge-transfer reactions employed in this technique are used to form "thermochemical ladders" based on the relative ionization energies of the reactants [Lias and Ausloos, **1978**]. In order to determine the ionization energy of a compound, standards of known ionization energies bracketing the unknown are used. While the technique is less quantitative (it is dependent on the availability of reactive standards with known ionization energies near that of the compound of interest) than the others already discussed, it is important for molecules which undergo a large change in geometry upon ionization. Such molecules have very slow onsets of ionization and are therefore not amenable to threshold techniques such as photoelectron-photoion coincidence and electron ionization (which will be discussed in more detail in the next two sections).

Photoelectron-Photoion Coincidence

The most powerful threshold technique, in which the onset of ionization is detected as a function of the energy of the ionizing agent, is photoelectron-photoion coincidence (PEPICO) [Dannacher, **1984**]. In order to ionize the molecule, photons with energies in excess of the ionization energy strike the neutral molecule, forming a positive ion and ejecting an electron:

$$M + h\nu \rightarrow M^{+\bullet} + e^{-} \qquad (1\text{-}13$$

In PEPICO, the electrons ejected during the ionization process with "zero" kinetic energy are matched with their corresponding positive ions. The relative probabilities for forming various daughter ions from parent ions ($M^{+\bullet}$) which have excess internal energy and undergo unimolecular dissociation (breakdown curves) can also be generated using this technique. PEPICO provides highly accurate ionization energy and breakdown curve information, which, however, can be more rapidly obtained using electron ionization (described in the next section). Additionally, by detecting the ions and electrons at different times, PEPICO can provide time-dependence information for the dissociation process. The interpretation of the data requires modeling of the dissociation process by statistical mechanics using quasi-equilibrium theory or RRKM theory [Rosenstock *et al.*, **1952**; Rosenstock and Krauss, **1963**].

In spite of its great strengths, PEPICO is not widely employed. This is probably due to the expensive and delicate instrumentation required, the complexity of the data analysis, the large amount of time required to set-up and conduct the experiments, and the need for an expert operator and interpreter of the data [Dannacher, **1984**].

Electron Ionization

The ionization process for electron ionization (EI) is similar to the one used in PEPICO, except that electrons strike the neutral molecule rather than photons:

$$M + e^{-} \rightarrow M^{+\bullet} + 2e^{-} \qquad (1\text{-}14$$

The electrons striking the neutral molecules have a known energy which is varied over a range including the ionization energy of the ion. Provision of an ionizing medium of known energy is easily accomplished in optical spectroscopy, where a monochromator gives precise control of the photon wavelength and, therefore, energy. In electron ionization, however, the production of monoenergetic electrons is quite difficult [Field and Franklin, **1957**]. The electron generating (EI) filament of the mass spectrometer produces ions with a Maxwellian distribution of energies. Several attempts have been made at making monoenergetic or "monochromatic" electron beams [Clarke, **1954**; Marmet and Kerwin, **1960**; Maeda *et al.*, **1968**; Rosenstock, **1976**]. Others have sought ways to work around the problems of data interpretation caused by the non-monoenergetic electron beam.

The non-monoenergetic nature of the electron beam and the presence of electrical fields in the ion source both have an effect on the shape of the ionization efficiency curve (Figure 1-15). The ideal behavior, when there are no electrical fields within the ionization volume to affect the electron energies and the electron beam entering the ion volume is monoenergetic, is illustrated by curve ④ of Figure 1-15. There is no ion current for the argon ion until its ionization energy of 15.76 eV is reached. At electron energies above the ionization energy, the ion current or ionization efficiency increases linearly. Unfortunately, this behavior is not seen in real experimental data unless scrupulous attention is paid to electron energy and fringing field details. When the trouble is taken to ensure the electron beam is monoenergetic, but fringing fields (normally from the ion optics lenses used to accelerate the ions into the mass analyzer, see Figure 1-9) are not eliminated, the ionization efficiency curve resembles curve ③ of Figure 1-15. When the electron beam is non-monoenergetic and/or fringing fields affect the electron energies, curves ① and ② result. The details of how this affects data interpretation will be discussed in detail in Chapter 3, Ionization Energy Determinations.

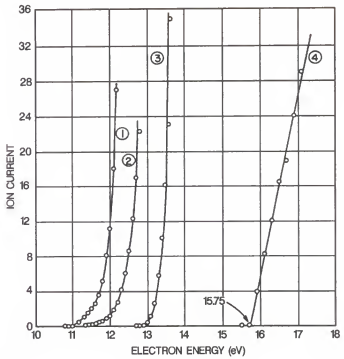


Figure 1-15. The effects of a non-monoenergetic electron beam and electrical fields in the ion volume on the ionization efficiency curves of argon [adapted from Fox *et al.*, **1951**].

## Scope of the Dissertation

The remainder of this dissertation deals with two aspects of distorted porphyrins as studied by mass spectrometry. The EI mass spectra of the *meso*-nitrosubstituted octaethylporphyrins (OEPs) and selected collision-induced dissociation (CID) fragmentation pathways of the mononitro, dinitro, and trinitroOEPs are presented in Chapter 2. Chapter 3 deals with the determination of the first ionization energies of metallated OEPs and the *meso*-nitrosubstituted OEPs. The final chapter, Chapter 4, includes conclusions based on the data presented in Chapters 2 and 3 and outlines areas for future work

In Chapter 2, the EI-MS, EI-MS/MS, and EI-high resolution MS (EI-HRMS) analyses of the free base *meso*-nitroOEPs (all isomers, see Figure 1-8) are presented. In order to put the new data into perspective, the previous work on 5-mononitroOEP

(OEMNP), done by Dr. John Laycock is first presented. Additional fragmentations of OEMNP, discovered during the research presented here are also presented. Explanations for fragmentations previously noted but not explained are also presented.

Having discussed OEMNP, the EI-MS spectra of the remainder of the *meso*-nitroOEPs are then presented. Using EI-MS/MS and EI-HRMS, the fragmentation patterns leading to several of the fragments of the dinitro- and trinitroOEPs are discussed. The effects of greater substitution on opening new fragmentation pathways and suppression of others, along with the additional complication introduced by surface-induced thermal decomposition on the ion volume, are also discussed.

Determination of the first ionization energies of selected divalent metal ion complexes of OEP and the Ni(II) derivatives of the entire suite of *meso*-nitroOEPs is the subject of Chapter 3. Several techniques for determining the ionization energies using EI data obtained with the TSQ70 are presented. The results from determinations of the first ionization energies of selected divalent metal complexes of OEP are compared with results from photoelectron spectroscopy. The results of determinations on the Ni(II) *meso*-nitroOEPs are plotted versus the root-mean-square out-of-plane distortions of the macrocycles. The difficulty in separating the effect of distortion on ionization energies from the effect of the electron withdrawing character of the substituent is also discussed.

Chapter 4 includes a summary of the work presented; proposals for future work, designed to answer many of the questions raised by both the fragmentation and ionization energy research presented here, are also discussed.

CHAPTER 2

# FRAGMENTATION PATHWAYS

## Introduction

Although there are many possible ionization modes in mass spectrometry (MS), the oldest one, electron ionization (EI), is still the most commonly employed. The continued popularity of EI is due, in large part, to its provision of more structural information than is available from any other ionization technique. The ready availability of libraries of reference spectra of pure compounds and library search routines for correlating unknown and reference spectra allow easy matching of an unknown spectrum with a reference spectrum [Watson, **1985**]. Although some libraries contain spectra generated using other ionization modes (predominantly CI), these libraries, for the most part, contain EI spectra. To date, correlation of collision-induced dissociation (CID) tandem mass spectrometric (MS/MS) data has not proven practical [Dawson and Douglas, **1983**]. Several criteria for matching spectra from instruments of differing design have been tried but none have proven useful. The lack of correlation between MS/MS spectra obtained on different instruments may be due to parent and daughter ion losses owing to scattering which is dependent on instrument design. For example, instruments whose collision cells employ an octopole will have a better ion throughput than those with a quadrupole.

The EI ionization process involves bombarding neutral molecules with electrons (with *ca.* 70 eV of kinetic energy in common practice). These electrons are generated by a hot rhenium filament which is resistively heated to the point at which it emits electrons. The ionization takes place in a low pressure (typically $10^{-4}$ to $10^{-7}$ torr) ion volume to minimize ion-molecule collisions (reactions). The ion source region of the TSQ70 mass

spectrometer, the instrument employed in the research presented here, is illustrated in Figure 2-1. The electrons generated at the filament enter the ion volume through a small collimating slot (not visible in the figure) in its top side. They then travel through the neutral molecules and exit the ion volume through a larger slot in its bottom (not visible) and are stopped at the collector. The electron beam is collimated by the slots and by a magnetic field, generated by two small permanent magnets, which constrains the electrons to a helical path of small diameter.

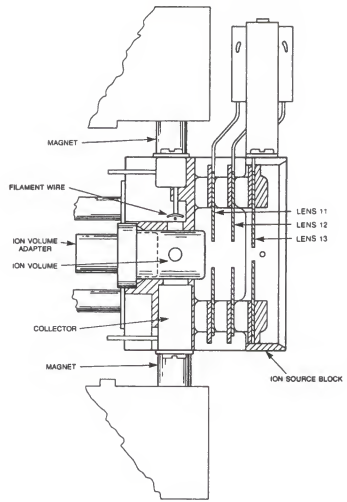


Figure 2-1. The ion source region of the TSQ70 mass spectrometer [Finnigan MAT, **1984**].

For most organic molecules the ionization efficiency increases exponentially between *ca.* 10 eV and 20 eV and then levels off (Figure 2-2). Region A of the figure is the threshold region in which molecular ions are the majority of the ions produced. In region B the number of fragments and their relative abundances increases. Region C is the region in which most EI-MS is performed. The indicated leveling off of the ionization efficiency is one of the reasons most reference spectra are collected at 70 eV. At that level, any perturbations in the electron energy will have a negligible effect on the ionization efficiency. The second reason is that the fragmentation pathways of the molecular ions produced at 70 eV are reproducible [Biemann, **1962**].

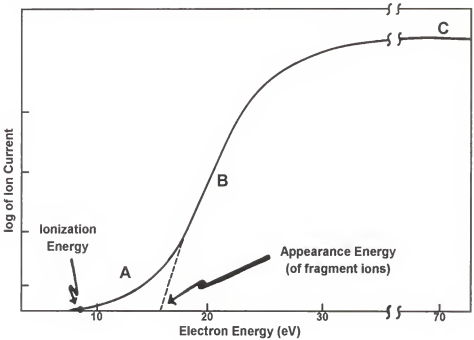


Figure 2-2. Ion production as a function of the energy (eV) of the ionizing electrons [adapted from Watson, **1985**].

The ionization process can be written:

$$M + e^- \rightarrow M^{+\bullet} + 2e^- \qquad (2\text{-}1$$

Many of the molecular ions ( $M^{+\bullet}$ ) produced in EI are generally unstable for two reasons: 1) they have excess internal energy because the electrons striking the neutral molecules have kinetic energies more than sufficient to ionize the molecule and a portion of the excess energy is imparted to the ion during the collision process; and 2) the molecular ion is an odd-electron ion having an unpaired electron [McLafferty, **1963**]. Since the pressure is kept low in the ion source, ion-molecule collisions cannot occur rapidly enough to collisionally cool these "hot" ions which then undergo unimolecular decompositions or fragmentation. These fragmentations often produce more stable even-electron ions by elimination of free radicals.

Because molecular ions generated by the EI process tend to fragment, the relative abundance of the molecular ion to the total of all the ions (total ion current, TIC) is often low. A list of relative abundances for selected compounds is found in Table 2-1. The compounds which tend to produce stable molecular ions under EI are those with polycyclic structures, especially those that are also aromatic. Some molecules, especially those which are highly conjugated like the porphyrins, also form stable doubly charged ions ( $M^{2+}$ ).

Table 2-1. Relative abundance of the Molecular ions in EI mass spectra of selected compounds [adapted from Biemann, **1962**].

| Compound | Relative Abundance (% TIC) |
|---|---|
| Naphthalene | 44.3 |
| Quinoline | 39.6 |
| *n*-Butylbenzene | 8.26 |
| Diamyl sulfide | 3.70 |
| *n*-Decane | 1.41 |
| Myrcene | 1.00 |
| *n*-Decylamine | 0.5 |
| Diamyl ether | 0.33 |
| 3-Nonanol | 0.05 |
| *n*-Decanol | 0.002 |

Mass Spectrometry of Porphyrins

As discussed in Chapter 1, the EI-MS behavior of most biological and geochemical porphyrins is characterized by 1) relatively high relative abundances for the molecular ions, 2) high abundance of doubly charged ions, 3) fragmentation pathways dominated by β-cleavage, and 4) α-cleavage (to a much smaller extent then β-cleavage) of their alkyl substituents. The most important feature to note in their spectra is that the porphyrin macrocycles remain intact. This behavior is theorized to be due to the resonance stabilization possible in such highly conjugated systems [Jackson *et al.*, **1965**]. The β-cleavage pattern has been found to be the dominant mode of fragmentation for alkyl-substituted porphyrins no matter what the alkyl chain length [Britton, **1985**; Johnson *et al.*, **1986**]. This phenomenon has been utilized extensively for determining the nature of the peripheral substituents on porphyrins.

Chelation of a metal ion by the porphyrin significantly changes both the fragmentation pathway and relative abundances of the fragment ions. Previous research done in the Yost group has shown that the relative abundances of the ions in the doubly charged portion of the mass spectrum correlate well with the modified Buchler stability index ($S_i$) of the metal. The relative abundances of the ions in the singly charged region, however were relatively unchanged. [Beato *et al.*, **1989b**].

It has been suggested that *meso* substituents have little effect on the fragmentation pathways [Budzikiewicz *et al.*, **1985**]; however, studies on cycloalkano-porphyrins and 5-nitrooctaethylporphyrin (OEMNP) [Laycock *et al.*, **1995**, **1996**] indicate that unusual fragmentations can occur for both porphyrin classes. Examination of the EI mass spectrum of OEMNP showed, for the first time, scission of the porphyrin macrocyclic ring under EI conditions. Ring scission had been observed previously under CI conditions [Beato *et al.*, **1991**]; however, these scissions were determined to involve surface-induced thermal decomposition of the porphyrin ring on the hot metal surfaces of the ion volume

in the source region of the mass spectrometer. The ring scission fragmentations of *meso*-substituted porphyrins discussed in the 1996 Laycock paper occurred in the gas-phase.

The novel fragmentation pathway leading to ring scission in OEMNP [Laycock *et al.*, **1996**] led to the investigation of the fragmentation behavior of the entire suite of meso-nitrosubstituted octaethylporphyrins (Figure 2-3) reported here. Investigation of novel EI fragmentation pathways using EI-MS and EI-MS/MS is of fundamental interest in that the data may correlate with other characteristic spectroscopic properties of the molecules such as their absorption and emission spectra.

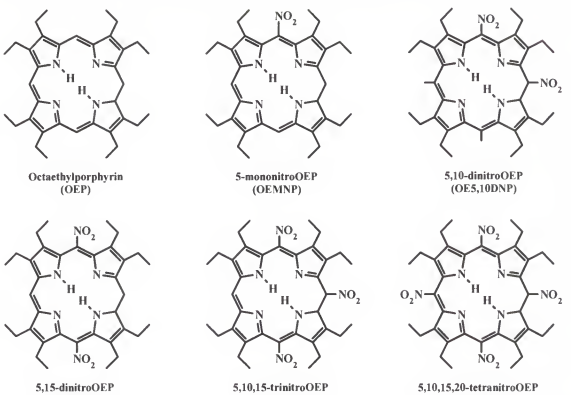


Figure 2-3. Octaethylporphyrin, its *meso*-nitro derivatives, and their abbreviations.

Interpreting Fragmentation Pathways

The fragmentations which occur in the source region of the mass spectrometer are typically unimolecular. This is ensured by maintaining a low pressure, which minimizes

the chance of ion-molecule reactions, within the ion source in EI-MS. The ions produced by EI have a wide range of internal energies dependent on a large number of factors including the energy distribution of the bombarding electrons. Ions which receive only an amount of energy sufficient for ionization will have very little excess internal (vibrational and rotational) energy and will be detected as the molecular ion ($M^{+\bullet}$). The ions into which excess internal energy has been deposited can decompose unimolecularly to fragment ions which, if they still have enough internal energy, may then further decompose before detection.

For positive ions, the relative abundances of the fragment ions from a given ion can be affected by several factors. The most abundant peaks, in general, are those which arise from fragmentations which produce the most stable ionic and/or neutral products. The four basic rules for determining the relative abundances of fragment ions resulting from a given precursor ion (precursor ions may be molecular ions or fragment ions produced from the molecular ion which still have sufficient internal energy to fragment again) include: 1) the more stable the fragment ion (owing to *e.g.*, electron sharing or resonance stabilization) the more abundant it will be, 2) Stevenson's Rule [Stevenson, **1951**] which states that the fragment ion with the lower appearance energy will be preferred, 3) in precursors with more than one alkyl substituent, the ion resulting from loss of the largest alkyl group (which is an exception to Stevenson's Rule) will be the most abundant, and 4) the ion which is generated when the most stable neutral fragment is produced will be more abundant than the others [McLafferty, **1980**]. Steric effects may also play a role. The physical chemistry behind these reasons can be understood by considering substituent effects which are explained in the next several paragraphs.

A study of substituent effects involves answering the question: given two ions which are identical except for one substituent, what effect will the substitution have? From this point of view the basic considerations for relative fragment ion abundance are: 1) the internal energy distributions of the precursor ions, 2) the stability of the fragment

ion, 3) the strengths of all the bonds cleft or formed in the process, 4) competitive reactions, and 5) subsequent decomposition of the fragment ions [McLafferty, **1968**]. The effects of these factors will be discussed in turn. The terms fragment ion and product ion are used interchangeably throughout. While reading the following discussion on substituent effects, it will be important to keep in mind that the various effects under discussion are being considered in isolation. In the mass spectrometer, any or all of them (and other, unidentified factors) may apply simultaneously.

(1) Internal energy distribution. Under EI-MS conditions, the source region of the mass spectrometer is purposefully kept at a low pressure to minimize ion-molecule reactions, thereby insuring that the molecular ion retains any energy from the ionizing electron which is over and above that required for ionization. When this excess internal energy is sufficient for a fragmentation reaction to occur and the kinetics of the reaction are such that the reaction is complete before mass selection occurs, the resulting product ion is detected. Fragmentation processes which require more energy are, therefore, less likely to occur and their resulting fragment ions will have a lower relative abundance in the mass spectrum.

As an example, consider two *meta*-substituted benzene compounds identical, except for one substituent (Figure 2-4a and b). Changing the substituent *meta* to the methyl group from $NO_2$ to $NH_2$ lowers the ionization energy of the molecule from 9.48 eV to 7.50 eV. If the only effect of changing the substituent were to be a lowering of the energies of the molecular ions (owing to lower ionization energy), then the number of frag-

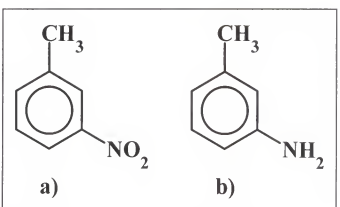

Figure 2-4. 3 nitrotoluene and 3-aminotoluene.

ment ions should increase because the amount of energy converted to internal energy should be larger.

However, when the site where the positive charge on the ion resides is shifted by altering the substituent, the ionization energy effect is confounded by the charge site effect and the same behavior may not occur. For example, when the *para* substituent on the ethylbenzene portion of the two *p*-substituted butyrophenones illustrated in Figure 2-5 is switched from $NO_2$ (a) to $NH_3$ (b), the mostly likely site for charge moves as illustrated [Wachs and McLafferty, **1967**]. Owing to this movement of the charge site, the amino-substituted molecule (b) tends to undergo much less fragmentation at the carbonyl group than is observed in the nitrosubstituted molecule (a).

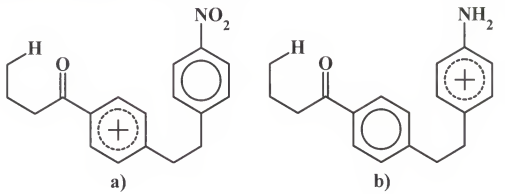


Figure 2-5. Two substituted butyrophenones, illustrating effect of substituent on charge location within the ion.

(2) Fragment ion stabilization. If a given substituent on the precursor ion is retained in the product ion, the internal energy effect is generally offset. The effect of the substituent on the stability of the product ion becomes more important than its effect on the precursor ion. In addition, substituent effects on the stabilization of the free radical (factor 5) are generally much less important than their effect on the resulting ion.

(3) Bond strength. The ion $RPh_aCOPh_b^{+\bullet}$ can decompose by two pathways, illustrated in Figure 2-6. If, all other conditions being equal, the substituent causes an in-

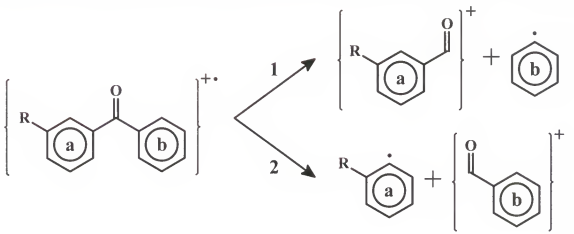


Figure 2-6. Effect of bond strength on fragmentation.

creased electron density (stronger bond) in the bond between phenyl group (a) and the carbonyl carbon over the bond between phenyl group (b) and the carbonyl carbon, then reaction path 1 will be preferred over reaction path 2. If the substituent should lower the electron density in the $Ph_a$ - C bond with respect to the C - $Ph_b$ bond, then the pathway 2 will be favored. Note that this effect can be in competition with effects (1) and (2).

(4) Competitive Reactions. According to quasi-equilibrium theory [Rosenstock and Krauss, **1963**], when a number of fragmentation pathways are possible for an ion with a given internal energy, the relative abundances of the product ions formed will be a function of the kinetic rates of the reactions leading to the product ion. When a substituent affects the relative rates of competing reactions leading to differing fragment ions, then the ion resulting from the reaction with a higher rate of reaction will be more abundant. In other words, the faster the fragmentation reaction, the more abundant the resulting fragment ion.

(5) Subsequent decomposition of product ions. If the substituent is retained by a product ion and the substituent has a destabilizing effect on the product ion, then, unless the rate of decomposition of the fragment is slow enough that the intact fragment reaches

the detector, the substituent will have the effect of lowering the abundance of the product ion.

Internal rearrangements of ions such as the famous McLafferty rearrangement [McLafferty, **1980**] and steric effects must also be considered. That there are at least seven basic factors to consider in explaining a fragmentation pathway, indicates a great deal of caution must be exercised in the interpretation of the data.

While the EI mass spectrum shows the molecular ion and the fragment ions resulting from unimolecular decompositions, the complex relationships between precursor and fragment ions can only be ascertained by using MS/MS. Under CID conditions, selected ions collide with a neutral collision gas in the collision cell. These collisions, because they occur with an non-reactive gas, simply serve to "heat up" the ions by increasing their internal energies. What were termed precursor ions in the single stage MS mode of operation are now termed parent ions in MS/MS. Likewise, fragment or product ions from single stage MS are termed daughter ions in MS/MS. The fragmentation pathway for an ion can be elucidated by monitoring the fragmentation reactions which a given parent ion undergoes (using daughter ion MS/MS scan mode) and the parents which produce a given daughter ion (using parent ion MS/MS scan mode). The neutral loss mode can also be used to provide information about reactions in which neutrals of a specific mass are lost. These scan modes were explained in Chapter 1.

The fragmentation pathways resulting from CID of a given ion have also been used to probe energetics. Several studies of the CID behavior of $M^{+\bullet}$ ion of *n*-butylbenzene [Griffiths *et al.*, **1981**; Dawson and Sun, **1982**; Boyd *et al.*, **1985**] have shown that the ratio of the abundances of m/z 91 and m/z 92 ions is a probe of the energy deposited. Because the fragmentation pathway to the formation of the $91^+$ ion requires more energy, as the deposited energy increases, the $91^+/92^+$ ratio increases. The collision energy is varied by changing the offset voltage between the ion source and second quad-

rupole. Comparison of the daughter spectra at different collision energies gives a picture of the relative bond strengths within the ion.

## Experimental

### Samples and Sample Preparation for Analysis

The entire suite of *meso*-nitrosubstituted octaethylporphrins were prepared by Professor J. M. E. Quirke, of Florida International University, using the methods of Bonnett and Stephenson [Bonnett and Stephenson, **1965**] and Gong and Dolphin [Gong and Dolphin, **1985**]. The synthesis of the mononitro compound involved the electrophilic substitution at the bridge (*meso*) carbons of the porphyrin ring using fuming nitric acid and acetic acid as the nitrating agent. The di- tri- and tetranitro OEPs were formed by nitration of Zn(II)OEP with $NO_2$ in methylene chloride. A mixture of the nitroporphyrins was obtained. The mixture was separated into individual compounds using TLC and the free base porphyrins were obtained by demetallation with either hydrochloric or perchloric acid. Isotopically labeled compounds were prepared using the methods of Callot *et al.*, [Callot *et al.*, **1983**] and nitrated using the method of Bonnett and Stephenson, as above.

All samples were dissolved in reagent grade dichloromethane from Fisher Scientific and deposited as a solution onto the filament of the direct exposure probe (DEP) of the TSQ70. The amount of sample deposited onto the filament ranged between 0.5 µl and 4 µl depending on the analysis being performed.

### MS Operating Conditions

All EI-MS and EI-MS/MS spectra presented here were obtained using a Finnigan MAT TSQ70 triple quadrupole mass spectrometer. The instrument used has been upgraded by inclusion of an octopole collision cell and fitted with a 20 kV conversion dyn-

ode. All spectra were obtained at 70 eV electron energy and 200 μA emission current from the EI filament. The EI spectra were obtained in the Q3MS mode in which Q1 and Q2 were set to pass all ions and Q3 was scanned for mass selection which provided approximately twice the sensitivity of operation in the Q1MS mode. The CID (MS/MS spectra were all obtained, using a variety of scan modes, at 12.5 eV collision energy and 1 mtorr average (usual range of pressures is approximately $\bar{x} \pm 0.1$ mtorr) indicated pressure of argon in the collision cell unless otherwise indicated. Because of the low volatility of the porphyrins, the ion source was maintained at 225°C. Owing to the tendency of these porphyrins toward surface-induced thermal decomposition, the sample introduction was by DEP with the probe ramped from 25 to 625°C at 200 °C per minute. Significantly faster temperature ramping of the DEP caused the samples to volatilize so rapidly that signal averaging was not practical owing to collection of an insufficient number of scans across the thermal desorption peak.

The EI-MS and EI-MS/MS spectra presented here have been generated using the lists of ions and their intensities produced by the TSQ70 and formatted using the program, *Grapher*, version 1.21 for Windows, from Golden Software. Peaks with % relative abundances (%RA) of less than 0.5% were not included in the spectra. Owing to problems with Q1 calibration drift, the masses in some parent ion spectra are corrected for this drift by comparison between Q1MS and Q3MS spectra run immediately before or immediately after the parent ion spectrum was taken and run under conditions matching those of the parent ion spectrum as closely as possible. In the data from EI-MS and EI-MS/MS experiments, the m/z ratios of ions are shown in spectra and reported in tables to 0.1 amu but are rounded to the nearest integer value in the text.

High resolution EI-MS (EI-HRMS)spectra were obtained using a Finnigan MAT 95 high resolution mass spectrometer operated at a resolution of 7000 ($m/\Delta m$). The exact masses of certain fragment ions obtained from EI-HRMS were useful in determining the elemental compositions of some of the daughter ions.

## Results and Discussion

### OEP and OEMNP

The initial studies of OEP and OEMNP were performed by Dr. John D. Laycock of this research group on the Finnigan MAT TSQ45 triple quadrupole mass spectrometer [Laycock, **1994**]. The studies on OEMNP were repeated on the TSQ70 and expanded upon by the author [Laycock *et al.*, **1996**] and in this dissertation. The results from both sets of studies are reported here in order to facilitate comparisons between all of the nitroOEPs.

#### EI-MS

In order to discuss the effects of nitration on fragmentation pathways in the mass spectra of OEP derivatives, the mass spectrum of OEP must first be examined. The singly charged portion of the EI-MS spectrum of OEP is shown in Figure 2-7. This spectrum shows the typical behavior of porphyrins under EI operating conditions: 1) β-cleavage of methyl groups to form $[M-15]^+$, $[M-30]^+$, etc. ions is the predominant mode of fragmentation with minor contributions from α-cleavage (loss of ethyl radicals) and 2) the OEP macrocycle remains intact. This spectrum and the spectra of all the nitroOEPs were taken under operating conditions as close to identical as practically possible. Therefore, any differences between the spectra of the compounds cannot be attributed to the MS conditions under which the spectra were obtained and must be due to differences in the gas-phase chemistries of their ions.

The EI-MS analyses of the nitroOEPs were difficult to perform. For example, the nitro group of OEMNP is prone to surface-induced thermal decomposition resulting in elimination of $NO_2$ and intermolecular hydrogen abstraction from water (omnipresent in the source region of the instrument) [Clezy *et al.*, **1974**] to form OEP (Figure 2-8). Similar thermal decomposition reactions were found to occur for all of the nitroOEPs.

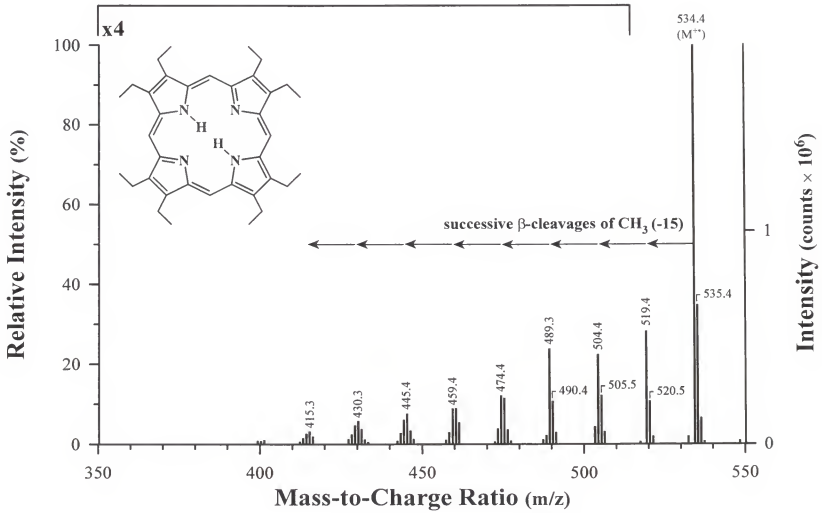


Figure 2-7. Singly charged portion of the EI mass spectrum of octaethylporphyrin (OEP).

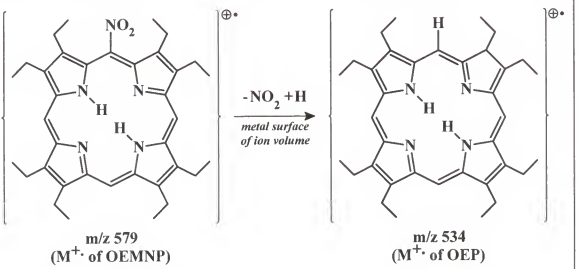


Figure 2-8. Surface-induced thermal decomposition of OEMNP resulting in OEP.

The singly charged portion of the EI mass spectrum of OEMNP is shown in Figure 2-9. It is essentially the same as the spectrum reported by Clezy *et al* **[1974]**. The level of surface-induced thermal decomposition is evident in the comparatively low relative abundance (14%) of the m/z 534 ion (the molecular ion of OEP) which is the surface-induced thermal decomposition product.

The OEMNP spectrum is significantly different from that of OEP. The most abundant fragment ions in the OEMNP spectrum with comments on their proposed origin are listed in Table 2-2. The results from EI-MS taken alone are not sufficient to explain fully the origin of the fragment ions in the spectrum of OEMNP. The fragmentations found in the OEMNP spectra which are not normally found in the mass spectra of porphyrins will be discussed here and in the next two sections.

The first striking difference in fragmentation pathways between OEP and OEMNP is the β-cleavage fragmentation pathway. For OEMNP, the path leading to the $[M-15]^+$ ion at m/z 564 is less favored than the formation of the $[M-17]^+$ (m/z 562) ion. In contrast, the most common fragmentations of OEP by far are due to β-cleavages. The m/z 562 ion is presumed to form by an intramolecular rearrangement (Figure 2-10) with

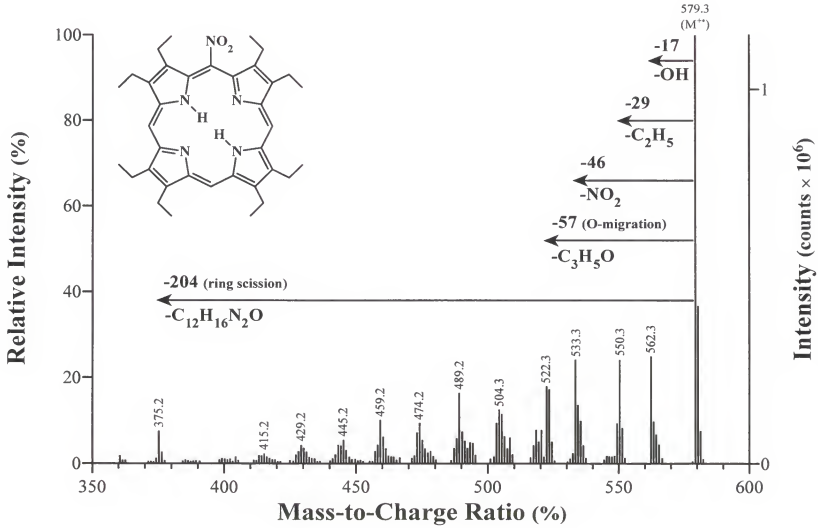


Figure 2-9. Singly charged portion of the EI mass spectrum of 5-nitroOEP (OEMNP).

Table 2-2. Selected ions from the EI-MS spectrum of OEMNP.

| m/z | % Relative-Abundance | Ion Formula | Neutral Loss Formula (radicals) | Comments |
|---|---|---|---|---|
| 580.3 | 36.75 | $C_{35}H_{45}N_5O_2{}^{13}C$ | NA | $^{13}C$ -isomer of the following ion |
| 579.3 | 100.00 | $C_{36}H_{45}N_5O_2$ | NA | Molecular ion ($M^+$) |
| 564.3 | 6.79 | $C_{35}H_{42}N_5O_2$ | $CH_3$ | β-cleavage of methyl group |
| 563.3 | 9.79 | $C_{35}H_{44}N_5O{}^{13}C$ | OH | $^{13}C$ -isomer of the following ion |
| 562.3 | 24.97 | $C_{36}H_{44}N_5O$ | OH | Clezy *et al.*, 1974 |
| 550.3 | 24.17 | $C_{34}H_{40}N_5O_2$ | $C_2H_5$ | α-cleavage of ethyl group |
| 549.3 | 9.39 | $C_{35}H_{43}N_5O$ or $C_{36}H_{45}N_4O$ | $CH_2O$ or NO | cannot distinguish using EI-MS |
| 534.3 | 13.65 | $C_{36}H_{46}N_4$ | $NO_2$ (with addition of H) | OEP, thermal elimination product |
| 533.3 | 24.20 | $C_{36}H_{45}N_4$ | $NO_2$ | Gas-phase loss of nitro group |
| 523.3 | 17.28 | $C_{33}H_{41}N_5O$? | $C_3H_4O$? | Relative abundance is too high to be the $^{13}C$-isomer of the following ion |
| 522.3 | 17.99 | $C_{33}H_{40}N_5O$ | $C_3H_5O$ | Oxygen migration |
| 489.2 | 16.45 | $C_{33}H_{37}N_4$ | $(CH_3)_3$* | β-cleavage from OEP |
| 474.2 | 9.46 | $C_{32}H_{34}N_4$ | $(CH_3)_4$* | β-cleavage from OEP |
| 459.2 | 10.17 | $C_{31}H_{31}N_4$ | $(CH_3)_5$* | β-cleavage from OEP |
| 444.2 | 4.21 | $C_{30}H_{28}N_4$ | $(CH_3)_6$* | β-cleavage from OEP |
| 375.2 | 7.59 | $C_{24}H_{29}N_3O$ | $C_{12}H_{16}N_2O$ | ring scission with loss of one pyrrole |

* Indicates loss from OEP rather than from OEMNP

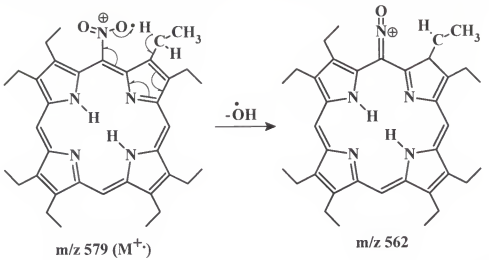


Figure 2-10. Formation of the m/z 562 ion from the molecular (m/z 579) ion of OEMNP according to the scheme proposed by Clezy [Clezy *et al.*, **1974**].

elimination of a hydroxyl group as proposed by Clezy [Clezy *et al.*, **1974**]. The ion at m/z 550 is most likely due to α-cleavage of an ethyl group. Although some α-cleavage is observed in the OEP spectrum, it does not occur to nearly as great an extent as is seen for OEMNP. The α-cleavage seen in the EI-MS spectrum OEP will be discussed further in the EI-MS/MS section which follows. The ion at m/z 549 could be due to loss of $CH_2O$, NO, two successive β-cleavages of $CH_3$, or a combination thereof; the means for determining which loss(s) is(are) responsible will be discussed in the next two sections.

The next significant peak is at m/z 534, arising from surface-induced thermal decomposition and formation of the $M^{+\bullet}$ ion of OEP discussed above (see also Figure 2-8). The peak at m/z 533 is due to the gas-phase unimolecular loss of $NO_2$ group (more discussion in the EI-MS/MS section). The peaks at m/z 523 and 522 will be explained in subsequent sections. The peaks at 489, 474, 459, and 444 are likely due to β-cleavages of methyl groups (losses of m/z 15) from the molecular ion and fragment ions arising from OEP which was formed by surface-induced thermal decomposition (Figure 2-8).

The most significant peak in the spectrum (Figure 2-9) is the one at m/z 375. This ion could not result from simple α- or β-cleavages of alkyl substituents from either

OEMNP or OEP or combinations of the same with loss of NO or $NO_2$ from OEMNP. It, therefore must result from ring scission with resultant loss of a portion of the macrocycle.

In order to ascertain the fragmentation pathways which lead to the formation of these ions, EI-MS/MS and EI-high resolution MS (EI-HRMS) experiments were performed on OEMNP and isotopically labeled OEMNPs containing $^{15}N$ at the nitro group, designated OEMNP-$^{15}NO_2$, $^{15}N$ at all four pyrrolic ring nitrogen positions, designated OEMNP-$(^{15}N_p)_4$, and $^{13}C$ at all four *meso* (bridge) carbon positions, designated OEMNP-$(^{13}C_m)_4$. The isotopically labeled compounds are illustrated in Figure 2-11.

EI-MS/MS

The daughter spectra of the molecular ion of OEP (m/z 534) at two different collision energies are illustrated in Figure 2-12. The 12.5 eV of collision energy employed in the top spectrum (Figure 2-12a) is the collision energy used for all experiments with the nitroOEPs. Again, all spectra were taken under conditions as close to identical as possible to minimize any effect instrument operating conditions might have on the spectra. It is important to note the following features of the spectrum: 1) the ions present in this spectrum arise almost exclusively from β-cleavages, 2) the comparatively high relative abundance of the β-cleavage ion resulting from the loss of one-methyl group (the $[M-15]^+$ intensity which is 89% of the $M^{+\bullet}$ peak intensity), 3) the rapid fall-off in intensities of the daughter ions (the intensity of the $[M-30]^+$ ion is only 11% of the $M^{+\bullet}$ peak intensity while the $[M-45]^+$ ion is only 1% as intense), and 4) the very small amount of α-cleavage (the $[M-29]^+$ intensity is only 3% of the $M^{+\bullet}$ peak intensity). Even at a collision energy of 20.0 eV (Figure 2-12b), only three β-cleavages (m/z 519, 504, and 489) and three α-cleavages (m/z 505, 490, and 475) are observed. Additionally and more importantly, even at the higher collision energy, no cleavage of the macrocycle is apparent.

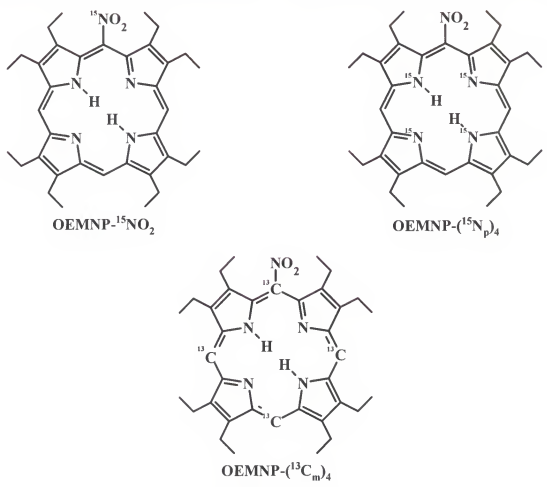


Figure 2-11. Isotopically labeled OEMNPs: a) $^{15}$N-labeled pyrollic nitrogens, b) $^{13}$C-labeled meso-carbons, and c) $^{15}$N-labeled nitro group nitrogen.

The EI-MS/MS daughter ion spectrum of the molecular ($M^{+\bullet}$, m/z 579) ion of OEMNP is shown in Figure 2-13. The most abundant daughter ions in the spectrum are listed in Table 2-3. The proposed origin of each of these ions will be discussed in turn. The ions at m/z 564, 562, 550, and 549 were discussed in the previous section.

An explanation for the origin of the ion at m/z 535 has not yet been published. It is not apparent in the EI-MS spectrum but has a relative intensity of 22% in the daughter ion spectrum of OEMNP. This difference may be due to the availability of higher energy fragmentation pathways under CID conditions in the collision cell. The presence of an ion at m/z 550 in the neutral loss of 15 spectrum (Figure 2-14a) and the presence of an

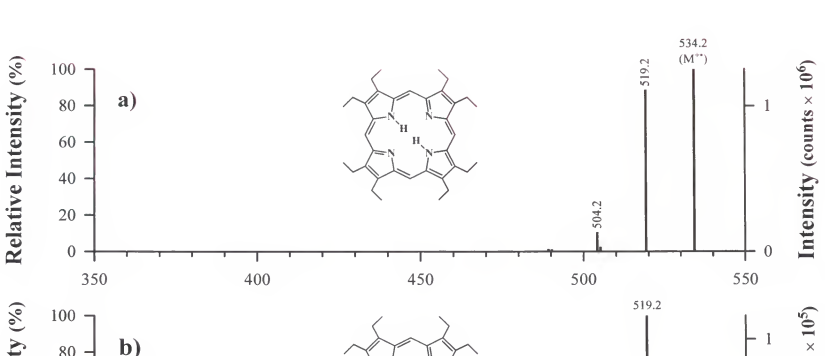


Figure 2-12. Daughter spectra of the $M^{+\bullet}$ ion of OEP at a) 12.5 eV collision energy and b) 20.0 eV collision energy.

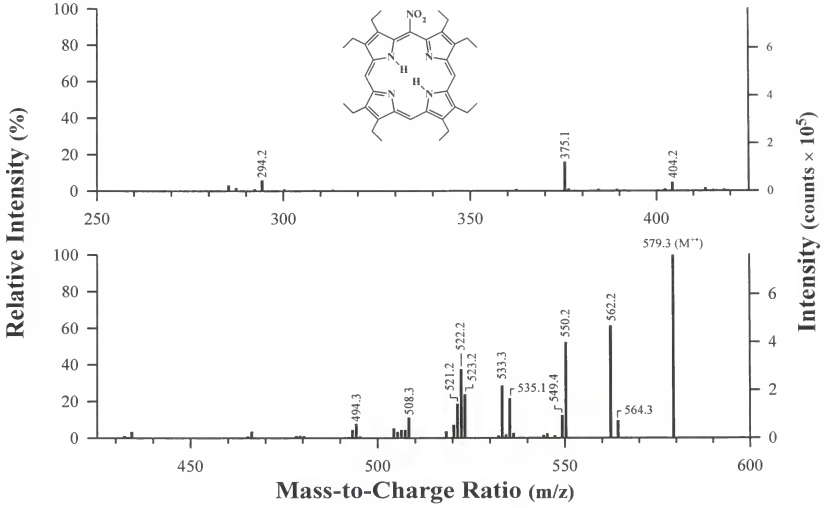


Figure 2-13. Daughter spectrum of the molecular ( $M^{+\bullet}$ ) ion of OEMNP.

Table 2-3. Selected Ions from the EI-MS/MS Daughter Spectrum of m/z 579 ($M^{+\bullet}$) of OEMNP.

| m/z | % Relative Abundance | Ion Formula | Neutral Loss Formula (radicals) | Comments |
|---|---|---|---|---|
| 579.3 | 100.00 | $C_{36}H_{45}N_5O_2$ | NA | Parent ion ($M^{+\bullet}$) |
| 564.3 | 9.55 | $C_{35}H_{42}N_5O_2$ | $CH_3$ | β-cleavage of methyl group |
| 562.2 | 61.28 | $C_{36}H_{44}N_5O$ | OH | Clezy *et al.*, 1974 |
| 550.2 | 24.17 | $C_{34}H_{40}N_5O_2$ | $C_2H_5$ | α-cleavage of ethyl group |
| 549.2 | 12.45 | $C_{36}H_{45}N_4O$ & $C_{35}H_{43}N_5O$ | NO & $CH_2O$ | Cannot distinguish using MS/MS |
| 535.1 | 21.65 | $C_{36}H_{45}N_5O_2$ | $CH_3$ & $C_2H_5$ | Neutral loss spectra confirm* |
| 533.3 | 28.57 | $C_{36}H_{45}N_4$ | $NO_2$ | Gas-phase loss of nitro group |
| 523.2 | 23.87 | $C_{33}H_{41}N_5O$? | $C_3H_4O$? | Relative abundance is too high to be $^{13}C$-isomer of the following ion |
| 522.2 | 37.56 | $C_{33}H_{40}N_5O$ | $C_3H_5O$ | Oxygen migration |
| 521.2 | 18.69 | $C_{33}H_{39}N_5O$ | $C_3H_6O$ | Oxygen migration |
| 520.2 | 7.28 | $C_{34}H_{40}N_4O$ | $C_2H_5$ & NO | Probably two steps: $C_2H_5$ and NO** |
| 508.3 | 11.35 | $C_{32}H_{38}N_5O$? | $C_4H_7O$? | Loss of nitro nitrogen is not indicated*** |
| 504.4 | 5.38 | $C_{34}H_{40}N_4$ | $C_2H_5$ & $NO_2$ | Two-step loss of ethyl and nitro groups |
| 494.3 | 7.87 | $C_{31}H_{36}N_5O$? | $C_5H_9O$? | Loss of nitro nitrogen is not indicated*** |
| 375.2 | 16.09 | $C_{24}H_{29}N_3O$ | $C_{12}H_{16}N_2O$ | ring scission with loss of one pyrrole |
| 294.1 | 4.97 | $C_{19}H_{24}N_3$ | $C_{17}H_{21}N_2O_2$ | ring scission with loss of two pyrroles |

* The presence of an ion at m/z 550 in the neutral loss of 15 spectrum and the presence of an ion at m/z 564 in the neutral loss of 29 spectrum confirm the loss of methyl and ethyl groups to form the m/z 535 ion.

** The presence of ions at m/z 520 and 504 in the daughter spectrum of m/z 580 ($M^{+\bullet}$) of the $^{15}NO_2$ labeled compound provides corroborates the loss of the nitro group nitrogen as postulated in this assignment.

*** Shift of these ions to m/z 509 and 495 in the $^{15}NO_2$ labeled compound indicate that the nitro group nitrogen is retained.

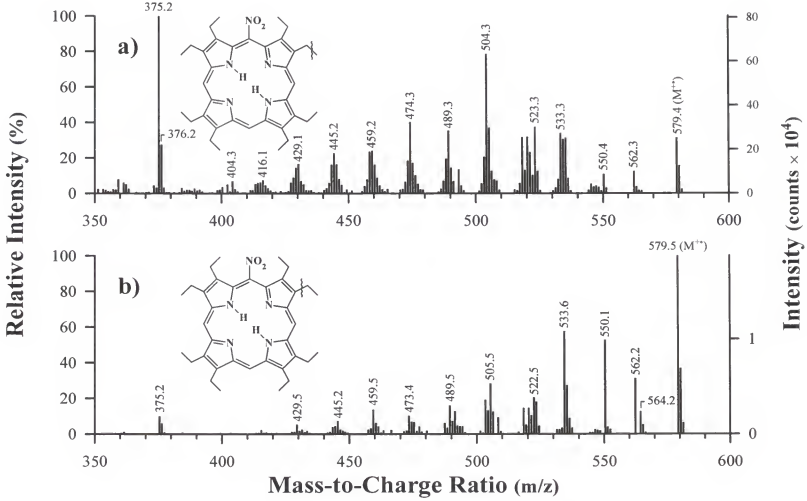


Figure 2-14. OEMNP neutral loss spectra: a) neutral loss of 15 (β-cleavage of a methyl group) and b) neutral loss of 29 (α-cleavage of an ethyl group).

ion at m/z 564 in the neutral loss of 29 spectrum (Figure 2-14b) provide strong evidence that the ion at m/z 535 is a result of the loss of both a methyl group and an ethyl group.

The ions at m/z 534, 489, 474, 459, and 444, which were present in the EI-MS spectrum, are absent from the EI-MS/MS spectrum. Their absence from the daughter spectrum confirms the hypothesis made in the previous section that they result from the surface-induced formation of OEP (m/z 534 ion). The other four ions are fragments of the $M^{+\bullet}$ ion of OEP and cannot form in the gas phase from the $M^{+\bullet}$ ion of OEMNP. The ion at m/z 533, however, is still present in the daughter spectrum (Figure 2-13), indicating that it does indeed result from a gas-phase fragmentation as postulated above.

Even with parent and neutral loss scans, and MS/MS studies on labeled compounds, the origins of the ions at m/z 523, $[M-56]^+$, 522, $[M-57]^+$, 521, $[M-58]^+$, 520 $[M-59]^+$, 508 $[M-71]^+$, 375 $[M-204]^+$ and 294 $[M-285]^+$ could not be assigned with absolute certainty using EI-MS and EI-MS/MS. Further discussion on the ions with mass-to-charge ratios above 510 amu will be postponed until the next section. The daughter spectra of the molecular ions of the three isotopically labeled OEMNP derivatives are shown in Figure 2-15. The OEMNP-$^{15}NO_2$ spectrum (Figure 2-15a) provides evidence that the nitro group nitrogen is not lost in the formation of the m/z 508 ion, since the ion is shifted from 508 in the unlabeled compound spectrum to 509 for the labeled one.

The m/z 375 ion is still present in the MS/MS spectrum, indicating that it is a product of gas-phase ionic decomposition. The parent spectrum of this ion is shown in Figure 2-16a. The molecular ion, at m/z 579, is the most abundant parent ion, as expected. In addition, m/z 522 is also a parent of m/z 375. Not readily apparent in Figure 2-16a, but visible in spectra taken on the TSQ45 [Laycock *et al.*, **1996**], are peaks at 390 and 404. These ions respectively represent β-cleavage of a methyl group and α-cleavage of an ethyl group from the ring and provide corroborating evidence for the idea that a pyrrolic ring, with its attached ethyl groups, is lost in the formation of the m/z 375 ion.

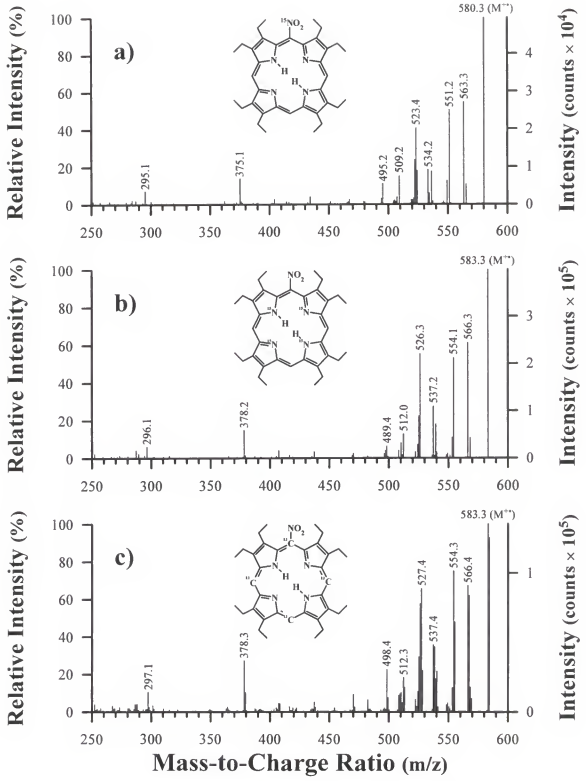


Figure 2-15. Daughter spectra of the molecular ions of ions of isotopically labeled OEMNP derivatives: a) OEMNP-$^{15}NO_2$, b) OEMNP-$(^{15}N_p)_4$, and c) OEMNP-$(^{13}C_m)_4$. (Larger structures are illustrated in Figure 2-11.)

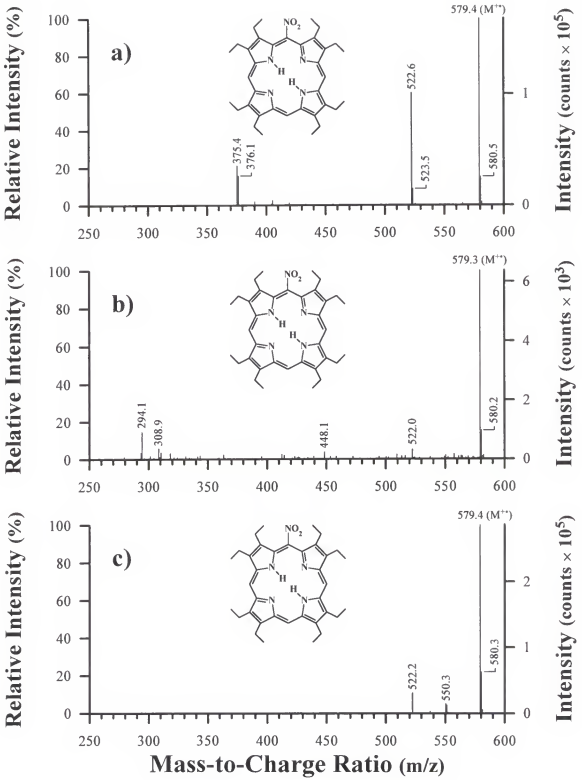


Figure 2-16. Parents spectra of selected OEMNP ions: a) parents of m/z 375, b) parents of m/z 294, c) parents of m/z 522.

The presence of the ion at m/z 375 in the daughter spectrum of the $M^{+\bullet}$ ion of OEMNP-$^{15}NO_2$ (Figure 2-15a) indicates that the nitro group nitrogen is not retained in the ion. The m/z 378 ions in the daughter spectra of the $M^{+\bullet}$ ions of OEMNP-$(^{15}N_p)_4$ and OEMNP-$(^{13}C_m)_4$ (Figure 2-15b and Figure 2-15c, respectively) indicate that three pyrrolic nitrogens and three *meso* carbons are retained in the ion. Construction of a complete fragmentation pattern for this ion at this point was still not possible because the composition of the m/z 522 ion was still not certain and required EI-HRMS for confirmation, as shown below.

The most important ion in the daughter spectrum of the molecular ($M^{+\bullet}$) ion of OEMNP (Figure 2-13) which is not apparent in the EI-MS spectrum and not reported in any previous work, is the m/z 294 ion. Its appearance in the EI daughter spectrum but not in the EI-MS spectrum is likely due to the higher signal-to-noise ratio provided by the second stage of mass spectrometry and may also be due to the availability of higher energy fragmentations due to CID. It has already been shown that loss of the nitro group produces an ion at m/z 533. If, in addition, all of the β-pyrrolic substituents were to be lost from the m/z 533 ion (involving the highly unlikely α-cleavages of all eight ethyl groups), the resulting ion would still have a mass-to-charge ratio of 301. Therefore any daughter ion with a lower m/z must result from a splitting apart of the porphyrin macrocycle and, furthermore, require the loss of two pyrrolic rings.

A parent spectrum of the m/z 294 ion is shown in Figure 2-16b. The presence of a parent ion at m/z 522 suggests a fragmentation pathway similar to that of m/z 375. In contrast to the m/z 375 ion pathway, the m/z 295 ion in the daughter spectrum of molecular ion of the $^{15}NO_2$-labeled compound (Figure 2-15a) indicates retention of the nitro group nitrogen in the ion. The presence of an m/z 296 ion in the daughter spectrum of the molecular ion of the $(^{15}N_p)_4$-labeled compound (Figure 2-15b) indicates the presence of two pyrrolic nitrogens in the ion. The m/z 297 ion in the daughter spectrum of the molecular ion of the $(^{13}C_m)_4$-labeled compound (Figure 2-15c) indicates the presence of three

*meso* carbons in the ion. The ambiguity over the composition of the m/z 522 ion, as mentioned in the discussion of the m/z 375 ion above, required further study using high resolution mass spectrometry, as presented next, for resolution.

High Resolution EI-MS

To help determine the fragmentations leading to the ions mentioned in the previous sections, a high resolution EI (EI-HRMS) spectrum of OEMNP was obtained. The significant ions in the EI-HRMS spectrum are listed in the first section of Table 2-4. Selected ions from the EI-HRMS spectra of the isotopically labeled OEMNPs are found in the remainder of the table. The molecular ion at m/z 579.3600 is only 2.7 millimass units (mmu) higher than the expected value of 579.3573. The elemental compositions of the m/z 564, 562, 533, and 504 fragment ions are all confirmed by the high resolution data. Unfortunately, because of the high observed Δ value (calculated m/z minus observed m/z), confirmation of the loss of an ethyl group to form the m/z 550 ion was not possible from this spectrum but was possible from the OEMNP-$^{15}NO_2$ spectrum (data in the second section of Table 2-4). Other possible losses of 29 include CHO and $CH_3N$. Loss of CHO would lead to an even higher Δ value of 27.6 mmu and loss of $CH_3N$, while it would result in a low Δ value of only 3.8 mmu, is highly unlikely from this ion. In the spectrum of the $^{15}NO_2$-labeled compound, the loss of an of ethyl group, resulting in the m/z 551.3191 ion, is only 3.9 mmu higher than the expected value of 551.3152 amu, indicating that loss of an ethyl group is the most likely explanation for loss of 29.

As mentioned in the EI-MS section above, the peak at m/z 549 (loss of 30) could be due to one or more of the following: 1) loss of NO, 2) loss of $CH_2O$, or 3) two β-cleavages of methyl groups. The likelihood of the third possibility is small considering the low relative abundance of the $[M-15]^+$ peak which results from one β-cleavage. In order to distinguish between the other two possibilities, the EI-HRMS spectrum of an OEMNP derivative with a $^{15}N$-labeled nitro group was obtained (OEMNP-$^{15}NO_2$). Infor-

Table 2-4. Selected Ions from the EI-HRMS Spectra of OEMNP and Isotopically Labeled Derivatives.*

| Compound | Accurate m/z | % Relative Abundance | Ion Formula | Δ (mmu) | Neutral Loss Formula (radicals) | Comments |
|---|---|---|---|---|---|---|
| OEMNP | 579.3600 | 100 | $C_{36}H_{45}N_3O_2$ | -2.7 | NA | Molecular ion ($M^{+\bullet}$): unlabeled compound |
| | 564.3384 | 1.9 | $C_{35}H_{42}N_3O_2$ | -4.5 | $CH_3$ | β-cleavage of methyl group |
| | 562.3505 | 6.3 | $C_{36}H_{44}N_3O$ | 4.1 | OH | [Clezy *et al.*, 1974] |
| | 550.3270 | 4.5 | $C_{34}H_{40}N_3O_2$ | -8.8 | $C_2H_5$ | α-cleavage of ethyl group |
| | 549.3505 | 4.5 | $C_{36}H_{45}N_4O$ | 8.8 | NO | Confirmed by $^{15}NO_2$ labeled OEMNP |
| | | | $C_{35}H_{43}N_4O$ | -3.7 | $CH_2O$ | (loss of 30 & 31 in High Res. spectrrum) |
| | 533.3621 | 15 | $C_{36}H_{45}N_4$ | 2.3 | $NO_2$ | Gas-phase loss of nitro group |
| | 523.3250 | 1.8 | $C_{33}H_{41}N_3O$ | 6.1 | $C_3H_4O$? | Too abundant to be 13C to 522 |
| | 522.3218 | 4.1 | $C_{33}H_{40}N_3O$ | 1.5 | $C_3H_5O$ | Oxygen migration |
| | 504.3222 | 4.0 | $C_{34}H_{40}N_4$ | 3.1 | $C_2H_5$ & $NO_2$ | Two-step loss of ethyl and nitro groups |
| | 375.2291 | 0.4 | $C_{24}H_{29}N_3O$ | 2.0 | $C_{12}H_{16}N_2O$ | Ring scission with loss of one pyrrole |
| OEMNP-$^{15}NO_2$ | 580.3554 | 100 | $C_{36}H_{45}N_4O_2{}^{15}N$ | -1.0 | NA | Molecular ion ($M^{+\bullet}$) with $^{15}N$-labeled nitro nitrogens |
| | 551.3191 | 5.0 | $C_{34}H_{40}N_4O_2{}^{15}N$ | -3.9 | $C_2H_5$ | α-cleavage of ethyl group |
| | 550.3463 | 2.8 | $C_{35}H_{43}N_4O^{15}N$ | -2.5 | $CH_2O$ | Indicates loss of $CH_2O$ contributes to unlabeled $[M\text{-}30]^+$ |
| | 549.3558 | 4.9 | $C_{36}H_{45}N_4O$ | 3.5 | $^{15}NO$ | Indicates loss of labeled N from Nitro group |
| | 533.3637 | 14 | $C_{36}H_{45}{}^{15}N_4$ | 0.7 | $^{15}NO_2$ | Indicates loss of labeled N from Nitro group |
| | 523.3134 | 6.0 | $C_{36}H_{40}N_4O^{15}N$ | 6.9 | $C_3H_5O$ | Oxygen migration |
| | 375.2320 | 1.1 | $C_{24}H_{29}N_3O$ | -0.9 | $C_{12}H_{16}NO^{15}N$ | Indicates loss of nitro nitrogen |
| OEMNP-($^{15}N_p$)$_4$ | 583.3412 | 100 | $C_{36}H_{45}NO_2{}^{15}N_4$ | 4.2 | NA | Molecular ion ($M^{+\bullet}$) with $^{15}N$-labeled pyrrolic nitrogens |
| | 553.3425 | 4.4 | $C_{36}H_{45}O^{15}N_4$ | 4.9 | NO | Loss of NO from Nitro group (unlabeled) |
| | 537.3467 | 15 | $C_{36}H_{45}{}^{15}N_4$ | 5.8 | $NO_2$ | Loss of Nitro group (unlabeled) |
| | 527.3188 | 3.1 | $C_{33}H_{41}NO^{15}N_4$ | 0.4 | $C_3H_4O$ | Oxygen migration |
| | 526.3117 | 5.0 | $C_{33}H_{40}NO^{15}N_4$ | -0.3 | $C_3H_5O$ | Oxygen migration |
| | 381.2210 | 1.0 | $C_{24}H_{29}O^{15}N_3$ | 1.1 | $C_{12}H_{16}NO^{15}N$ | Indicates loss of one pyrrolic nitrogen |
| OEMNP-($^{13}C_m$)$_4$ | 583.3716 | 100 | $C_{32}H_{45}N_3O_2{}^{13}C_4$ | -0.7 | NA | Molecular ion ($M^{+\bullet}$) with $^{13}C$-labeled *meso* carbons |
| | 527.3398 | 3.5 | $C_{29}H_{41}N_3O^{13}C_4$ | 4.9 | $C_3H_4O$ | Oxygen migration |
| | 526.3366 | 5.0 | $C_{29}H_{40}N_3O^{13}C_4$ | 0.3 | $C_3H_5O$ | Oxygen migration |
| | 378.2415 | 1.0 | $C_{21}H_{29}N_3O^{13}C_3$ | 0.2 | $C_{11}H_{16}N_2O^{13}C$ | Indicates loss of one *meso* carbon |

* The structures of the labeled compounds and a key to their abbreviations are found in Figure 2-11.

mation on significant ions in this spectrum is listed in the second section of Table 2-4. The molecular ion is at m/z 580.3554; one mmu higher than the expected 580.3544. Rather than eliminating one of the first two explanations for the m/z 549 ion, the spectrum of the $^{15}NO_2$-labeled compound has peaks at $[M-30]^+$ and at $[M-31]^+$ (loss of $CH_2O$ and $^{15}NO$, respectively) indicating that the loss of 30 observed in the unlabeled spectrum is probably due to a combination of loss of NO and loss of $CH_2O$. The $[M-30]^+$ peak at m/z 550.3463 is 2.5 mmu higher than the expected value of 550.3438 for loss of $CH_2O$. The calculated m/z for two β-cleavages of methyl groups is 550.3074. The difference between this figure and the observed value is 38.9 mmu, a difference so large that proposing two losses of methyl groups from the molecular ion as the origin of this ion strains credibility. It is important to note that an instrumental resolution ($m/\Delta m$) of 15,125 would be required for baseline resolution to of the loss of $C_2H_6$ from the loss of $CH_2O$. The instrument was operated at a resolution of only 7,000 for the collection of the high resolution data and, therefore, would not have resolved two ions so close in mass. However, if the loss of $C_2H_6$ were to have contributed to the loss of 30 from the molecular ion, the centroiding of the peaks from both losses would have produced a peak at some intermediate m/z depending on their relative abundances. Since the observed peak was 2.5 mmu higher than expected for the loss of $CH_2O$, any significant contribution from the loss of $C_2H_6$ which would have pulled the centroided value lower can reasonably be ruled out. The loss of NO in the $^{15}NO_2$-labeled compound becomes loss of $^{15}NO$ or loss of 31. In the spectrum of the labeled compound, the peak for loss of $^{15}NO$ is at m/z 549.3558 which is only 3.5 mmu lower than the calculated value of 549.3593. Based on the data from the spectrum of OEMNP-$^{15}NO_2$, the $[M-30]^+$ ion in the unlabeled OEMNP spectrum must be due to a combination of loss of NO and loss of $CH_2O$.

The composition of the ion at 522 ($C_{33}H_{40}N_5O$), could be confirmed by the low Δ value in the unlabeled spectrum. However, the composition of the ion at m/z 523 ($C_{33}H_{41}N_5O$) has too high a Δ value for confirmation. Data from the EI-HRMS spectra of

OEMNP-($^{15}N_p$)$_4$ and OEMNP-($^{13}C_m$)$_4$ are found in the third and fourth sections of Table 2-4, respectively. The m/z 522 and m/z 523 ions are shifted four amu higher in the labeled compound spectra since loss of either $C_3H_5O$ or $C_3H_4O$ would not be likely to involve any *meso* carbons and obviously does not include any nitrogens. The low $\Delta$ values for the m/z 526 and m/z 527 ions in the spectra of both labeled compounds helps confirm the composition of the m/z 522 and m/z 523 ions in the unlabeled spectrum as postulated in Tables 2-2 and 2-3. Unfortunately, the relative abundances of the m/z 521, 520, 508, and 294 ions were too low to obtain valid EI-HRMS data.

The composition of the ion at m/z 375 as listed in Tables 2-2, and 2-3 was also confirmed by the high resolution data. The losses to form the ion total up to $C_{12}H_{16}N_2O$. Because two nitrogens are lost in its formation, the m/z 375 ion must result from scission of the macrocycle and removal of at least one pyrrole unit. Fragmentations leading to macrocycle scission have only been observed previously as surface-induced processes in CI-MS of substituted porphyrins using methane, hydrogen, and ammonia as reagent gases [Shaw *et al.*, **1981**; Tolf *et al.*, **1986**; and Beato *et al.*, **1989a, b**]. The high resolution data from the isotopically labeled compounds also confirm the numbers of pyrrolic nitrogens and *meso* carbons lost in the formation of the m/z 375 ion as determined from EI-MS/MS (data in Figure 2-15).

Structures and Fragmentation Pathways for Selected Ions

To complete the elucidation of the fragmentation pathways in the interesting macrocycle scissions leading to the formation of the m/z 375 and 294 requires knowledge of the composition of their common parent ion at m/z 522 and its fragmentation pathway. The parent spectrum of the m/z 522 ion is shown in Figure 2-16c. The only two parents of this ion are the molecular ion and a relatively small (5%) contribution from the m/z 550 ion which is formed by $\alpha$-cleavage of an ethyl group from the $M^{+\bullet}$ ion as explained above. Armed with this information and the composition of the ion from the high resolu-

tion spectra, a workable scheme for the formation of the m/z 522 ion (Figure 2-17) can be proposed. The first step is migration of an oxygen from the nitro group to the β-pyrrolic carbon of an adjacent pyrrolic ring which is followed by removal of a $C_3H_5O$ radical. The resulting ion at m/z 522 then cyclizes and rearranges to form the ion with a nitrile group and carbocation shown. Another possible pathway (not illustrated) involves the loss of an ethyl group from a β-pyrrolic carbon adjacent to the nitro group to form the m/z 550 parent which then undergoes oxygen migration to the same β-pyrrolic carbon followed by elimination of CO and internal rearrangements to form the m/z 522 ion.

One possible fragmentation pathway to the m/z 375 ion which includes the intermediate m/z 522 ion, is illustrated in Figure 2-18. A number of elements are included in this pathway to be consistent with the data; these include: 1) from the high resolution data (Table 2-4), the composition of the ion must be $C_{24}H_{29}N_3O$ which requires losses totaling $C_{12}H_{16}N_2O$, 2) from its parent spectrum (Figure 2-16a), one of the parent ions is the m/z 522 ion which, based on the EI-HRMS data, has an elemental composition of $C_{33}H_{40}N_5O$, 3) based on the daughter spectrum of OEMNP-$^{15}NO_2$ (Figure 2-15a), the nitro group nitrogen must be lost, 4) its elemental composition, which includes an oxygen atom, and the loss of the nitro group nitrogen indicates that the remaining oxygen from the nitro group present in the m/z 522 ion is transferred to the macrocycle, 5) the m/z 378 ions in the daughter spectra of OEMNP-($^{15}N_p$)$_4$ and OEMNP-($^{13}C_m$)$_4$ indicate that the ion must include three pyrrolic nitrogens and three *meso* carbons. Loss of $C_9H_{11}N_2$ from the even-electron m/z 522 ion requires formation of an odd-electron, distonic ion. Such fragmentations rarely occur in the mass spectra of the majority of compounds but are not uncommon in the mass spectra of porphyrins. This is illustrated by the number of β-cleavages in the spectrum of OEP (see Figure 2-7) which must involve alternation between odd- and even-electron ions.

Rationalization of the formation of the m/z 294 ion (Figure 2-19) follows much the same arguments as put forth for the m/z 375 ion since they share a common parent,

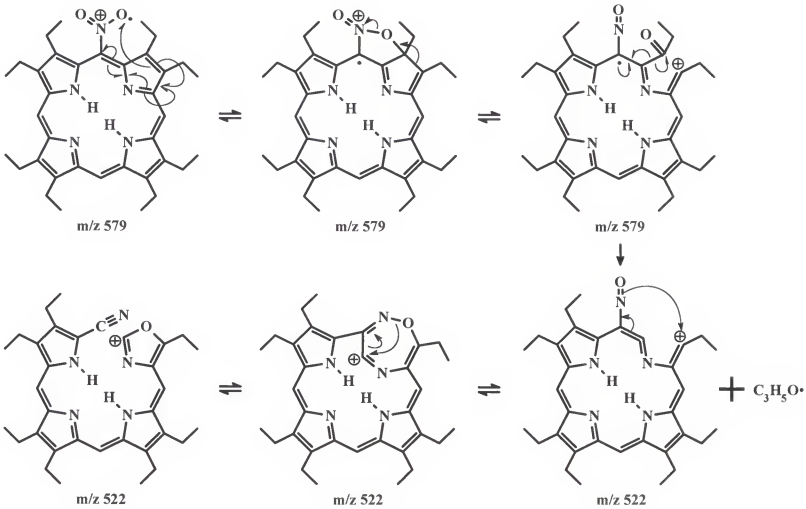


Figure 2-17. A plausible fragmentation pathway for the formation of the m/z 522 ion from the molecular (m/z 579) ion of OEMNP.

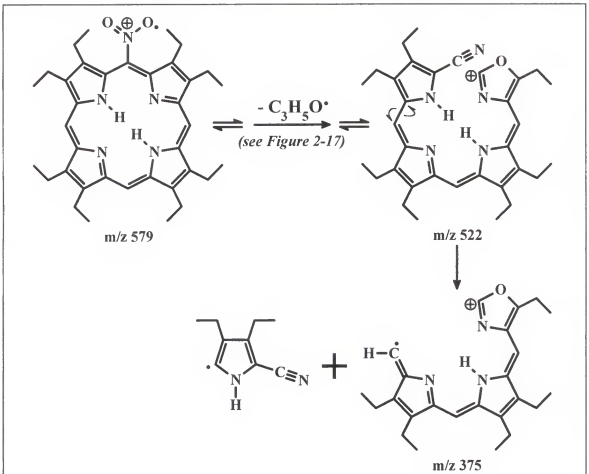


Figure 2-18. Completion of the fragmentation pathway from m/z 579 to m/z 375.

the m/z 522 ion. While high resolution data were not available to confirm elemental composition of the ion, the data from the daughter spectra of the molecular ions of the labeled compounds OEMNP-$^{15}NO_2$, OEMNP-$(^{15}N_p)_4$ and OEMNP-$(^{13}C_m)_4$ already discussed above provide important information about its make-up. A workable scheme for forming this ion which is consistent with the data requires retention of the nitro group nitrogen, two pyrrolic nitrogens, and three of the *meso* carbons. In order to get the proper elemental composition of the ion, transfer of the hydrogen attached to the nitrogen of pyrrolic ring C to ring D (first step shown in Figure 2-19) of the macrocycle must be invoked. NMR studies of the locations of the pyrrolic hydrogens in free base porphyrins have shown that they are free to move about among the four pyrrolic nitrogens [Storm

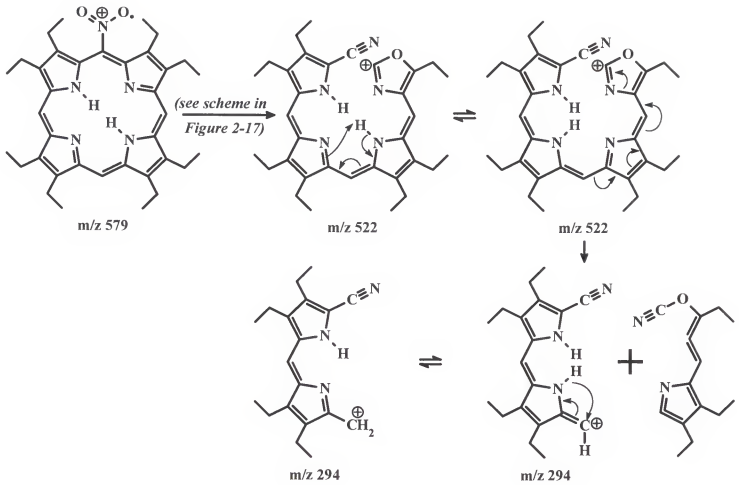


Figure 2-19. Proposed fragmentation pathway leading from the molecular (m/z 579) ion of OEMNP to the m/z 294 fragment ion.

and Teklu, **1972**, Storm et al, **1973**]. Thus, movement of the hydrogens among the core pyrrolic nitrogen positions to form a structure in a fragmentation pathway which leads to an ion of the requisite composition is reasonable in light of the fact that such shuffling about of these hydrogens is a common occurrence in porphyrins. The remainder of the fragmentation pathway shows reasonable processes for ring opening and ring scission.

Other NitroOEPs

Now that the fragmentation pathways of the simplest *meso*-nitroporphyrin, OEMNP, have been examined, it is possible to apply the knowledge gained in that process to the fragmentation pathways of the remaining nitroporphyrins.

EI-MS Spectra

Portions of the EI-MS spectra of the nitroporphyrins are illustrated in Figures 2-20 and 2-21. The spectrum of OEMNP is included in both figures as a benchmark. The spectra of the dinitroOEPs are broadly similar to the OEP spectrum. However the trinitroOEP and tetranitroOEP spectra are markedly different. The important features of the spectra to note are as follows.

OE5,10DNP The similarities to the OEMNP spectrum can first be noted: the loss of OH is, again, more pronounced than the β-cleavage of a methyl group; α-cleavage of an ethyl group is still a relatively favorable process, although less so than for OEMNP; and loss of a nitro group to form $[M-46]^+$ (m/z 578) is more favorable than the surface-induced thermal decomposition leading to formation of the $M^{+\bullet}$ ion of OEMNP at m/z 579. (More discussion on the thermal decomposition problem follows the discussion of the basic features of the spectra and fragmentations). Differences in the spectra include: no readily discernible ion at m/z 420 ($[M-204]^+$) analogous to the m/z 375 ion of OEMNP and a slightly different pattern in the intensities of the fragments. In the OEMNP spectrum, the ions follow a nearly linear decrease in intensity with mass, with loss of OH

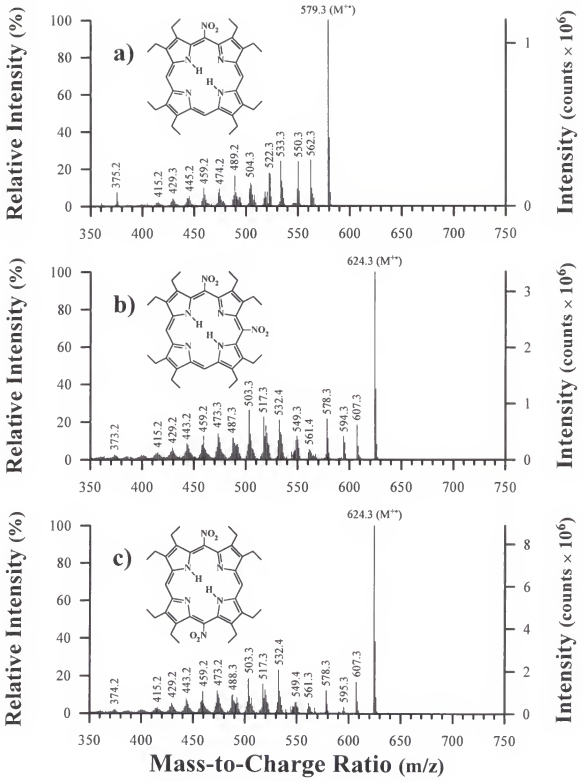


Figure 2-20. EI mass spectra of a) OEMNP, b) OE5,10DNP, and c) OE5,15DNP.

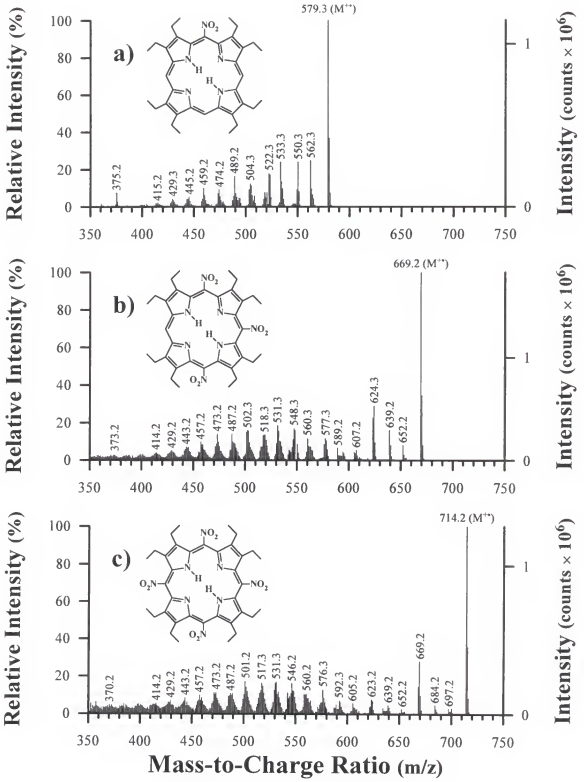


Figure 2-21. EI mass spectra of a) OEMNP, b) OETriNP, and c) OETNP.

being the most favored pathway. The OEMNP m/z 375 ion, formed by ring scission as discussed above, is seen after the fragment ion intensity nearly reaches baseline. In the OE5,10DNP spectrum, there are three easily discernible ions arising from losses of OH, $C_2H_5$, and $NO_2$, with the $NO_2$ loss now producing the most abundant fragment ion in this group. These initial fragments are followed by a dome-shaped distribution of ions which are mainly the result of β-cleavages, with the m/z 503 $[M-121]^+$ ion being the most abundant fragment overall. This distribution contains an ion at nearly every mass, making data interpretation very difficult. A possible reason for the differences in the β-cleavage patterns of the nitro compounds will be discussed in a later section of this chapter. Thermal decomposition of OEDNP to form OEMNP and OEP and their production of fragment ions may explain the large number of fragment ions at nearly every mass and may also help explain the intensity distribution.

OE5,15DNP This spectrum is essentially the same as the OE5,10DNP spectrum with the notable difference that the $[M-46]^+$ and $[M-29]^+$ ions are lower in intensity than in the OE5,10DNP spectrum. The $[M-30]^+$ ion, which was approximately 80% as intense as [M-29] ion in the OE5,10DNP spectrum, is a more favored fragment ion than the $[M-29]^+$ ion which is negligible in the OE5,15DNP spectrum.

OETriNP The trends first seen in the dinitro spectra are seen to be more pronounced in this spectrum. In the OETriNP spectrum, loss of OH is much less favored than loss of the nitro group. The $[M-30]^+$ ion is about twice as probable as α-cleavage to form $[M-29]^+$ in this spectrum. In addition, thermal decomposition to form OEDNP (either 5,10 or 5,15) with a $M^{+\bullet}$ ion at m/z 624, is now a more favored process than loss of $NO_2$ to form the ion at m/z 625 which has an intensity of approximately 80% that of the 624 ion. Again, we see the dome-shaped distribution with ions at every mass, complicating data interpretation. The ion-at-every-mass problem is exacerbated by the relatively high abundance (≈33% of the $M^{+\bullet}$ ion) of the thermal decomposition product which can then undergo its own ionic fragmentations and thermal decompositions.

OETNP In the spectrum of this most distorted of the nitroporphyrins, the most abundant "fragment" ion is the molecular ion of the thermal decomposition product, OETriNP, at m/z 669 which is now slightly more than twice as abundant as loss of $NO_2$. The ions resulting from the losses of OH and methyl and ethyl groups, and the $[M-30]^+$ ion have almost disappeared from the OETNP spectrum. The ion-at-every-mass problem is even worse now that OETNP, OETriNP, and presumably the OEDNPs, OEMNP, and OEP are all present in the source owing to successive thermal decompositions.

The highly complicated nature of the spectra make data interpretation extremely difficult. In order to increase the signal-to-noise ratio, and gather information on the sources of the various fragments, EI-MS/MS experiments were employed to help discover the origins of selected ions.

Selected EI-MS/MS Spectra and Fragmentation Pathways

The fragment ions of greatest interest in these spectra are those which result from breaking the porphyrin macrocycle. It is these ions on which the EI-MS/MS experiments were focused. An examination of the m/z 250 to m/z 350 portion of the daughter ion spectra of the $M^{+\bullet}$ ions of OE5,10DNP, OE5,15DNP, and OETriNP yields the spectra shown in Figure 2-24. This region of the spectrum was chosen because of the relatively low interference from the many fragments also found in the EI-MS spectra of these compounds. The OETNP spectrum proved to have too low of a signal-to-noise ratio in this region to merit further study on that compound. Ionic compositions and/or fragmentation pathways for ions at m/z 271 (OEDNPs only), 292, 294, 297 (OEDNPs only) and 308 will all be proposed based on the OEMNP fragmentations and the MS/MS data on the dinitro and trinitro compounds. Unfortunately, none of the ions appeared at a high enough intensity in the high resolution spectra of the $(^{15}N_p)_4$ and $(^{13}C_m)_4$ derivatives of the OEDNPs and OETriNP ($^{15}NO_2$-derivatives were not available) to provide corroboration for the fragmentation pathways.

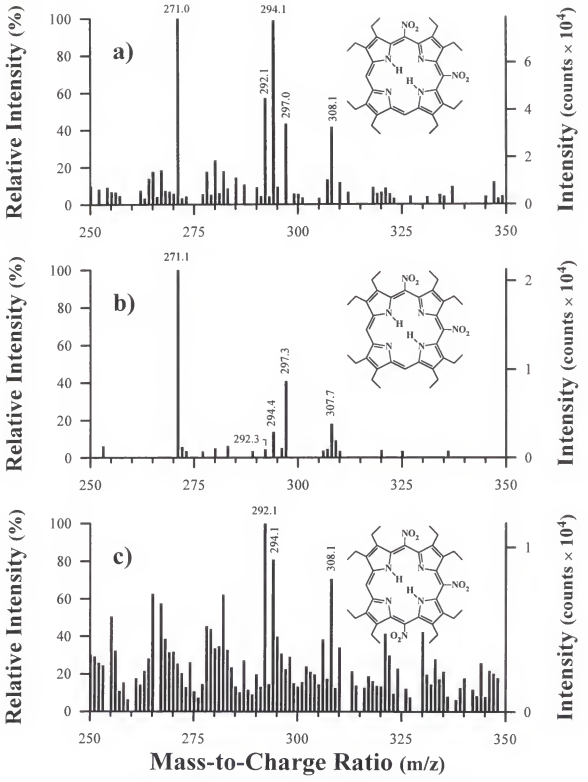


Figure 2-22. Daughter spectra of the molecular ions of a) OE5,10DNP, b) OE5,15DNP, and c) OETriNP in the m/z region between m/z 250 and m/z 350.

The scheme for the fragmentation leading to the m/z 294 ion in the OE5,10DNP spectrum can be produced by following much the same logic used to explain the formation of the m/z 294 ion from OEMNP and, therefore, will not be shown. The only difference between the two is that for formation of m/z 294 from OEDNP, the second nitro group must be part of the neutral fragment which is lost. Unfortunately, the parent spectrum of the m/z 294 ion of OE5,10DNP (Figure 2-23a) does not provide much useful information on the origins of the ion. Furthermore, the low relative abundance of the m/z 294 ion in the OE5,15DNP and OETriNP spectra made obtaining parent spectra of the impossible. The only two ions which can safely be deemed to be above the noise are at m/z 579 and m/z 624 ($M^{+\bullet}$). The m/z 579 ion is the surface-induced thermal decomposition product of OE5,10DNP and therefore cannot be a fragment ion intermediate between the $M^{+\bullet}$ ion and the m/z 294 ion. The fact that the m/z 294 ion is much less abundant in the OE5,15DNP daughter spectrum than in the OE5,10DNP daughter spectrum may be attributed to the attachment of the second nitro group to the *meso*-carbon on the opposite from the nitro group bearing the charge. The position of the nitro group will affect the stability of the bonds on either side of the *meso* carbon to which it is attached. The position of the nitro group may also affect either the thermodynamics or kinetics of any of the intra-ionic rearrangements or bond breaking processes in the fragmentation pathway, thereby rendering what had been a favorable fragmentation process for one OEDNP isomer, unfavorable for the other.

The daughter spectra of the molecular ions ($M^{+\bullet}$) of OE5,10DNP-$(^{15}N_p)_4$ and OE5,10DNP-$(^{13}C_m)_4$ provide corroboration for the supposition that the composition of the m/z 294 ion in the spectra of the OEDNPs (and probably OETriNP spectrum) is the same as was seen for OEMNP. The masses of the ions under discussion are listed in Table 2-5. The ion intensities in the OE5,10DNP-$(^{13}C_m)_4$ spectrum were somewhat low. However, ions at the same m/z ratios were found at higher intensities in the OE5,15DNP-$(^{13}C_m)_4$

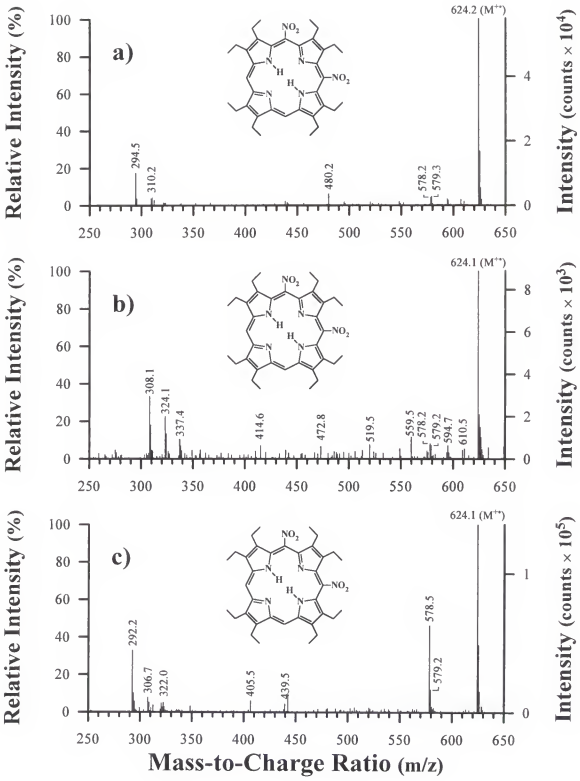


Figure 2-23. Parent spectra of the a) m/z 294, b) m/z 308, and c) m/z 292 ions of OE5,10DNP.

Table 2-5. Masses of selected ions (rounded to nearest whole amu) from isotopically labeled and unlabeled OE5,10DNP.

| Unlabeled OE5,10DNP | OE5,10DNP-$(^{15}N_p)_4$ | OE5,10DNP-$(^{13}C_m)_4$ | Comments |
|---|---|---|---|
| 271 | 273 | 272 | 2 pyrrolic nitrogens and 1 *meso* carbon |
| 292 | 294 | 295 | 2 pyrrolic nitrogens and 3 *meso* carbons |
| 294 | 296 | 297 | 2 pyrrolic nitrogens and 3 *meso* carbons |
| 297 | 299 | 299 | 2 pyrrolic nitrogens and 2 *meso* carbons |
| 308 | 310 | 311 | 2 pyrrolic nitrogens and 3 *meso* carbons |

spectrum. These data indicate that there are 2 pyrrolic nitrogens and three *meso* carbons in the m/z 294 ion just as in the m/z 294 ion arising from OEMNP.

The parent spectrum of the m/z 308 ion is found in Figure 2-23b and a proposed pathway for the formation of the ion from the molecular ion of OE5,10DNP is found in Figure 2-24. The m/z 308 fragment ion has as one of its parents, albeit not the most abundant one, the m/z 578 ion ($[M-46]^+$) which results from α-cleavage of one nitro group from the OEDNP molecule. The data from the labeled compounds (Table 2-5) indicate that the ion contains two pyrrolic nitrogens and three *meso* carbons. The fragmentation pathway begins with loss of $NO_2$ followed by transfer of one of the remaining nitro group oxygens to the macrocycle. Ring scission and formation of an ion with a nitrile group and a carbocation follow. Splitting two bonds produces a diradical which then rearranges and cyclizes. Rearrangement and opening of the ring results in the final fragment ion shown.

The parent ions of m/z 292 also include m/z 578 and 624 (Figure 2-23c). As was seen in the m/z 308 pathway, formation of m/z 578 occurs when one of the nitro groups of OEDNP is cleaved from the molecule. A scheme for the formation of m/z 292 from m/z 624 ($M^{+\bullet}$) is found in Figure 2-25. The difference of 16 amu between m/z 308 and m/z 292 suggests that the m/z 292 ion might have the same composition as the m/z 308 but without the oxygen. The scheme shows loss of $NO_2$ followed by oxygen migration

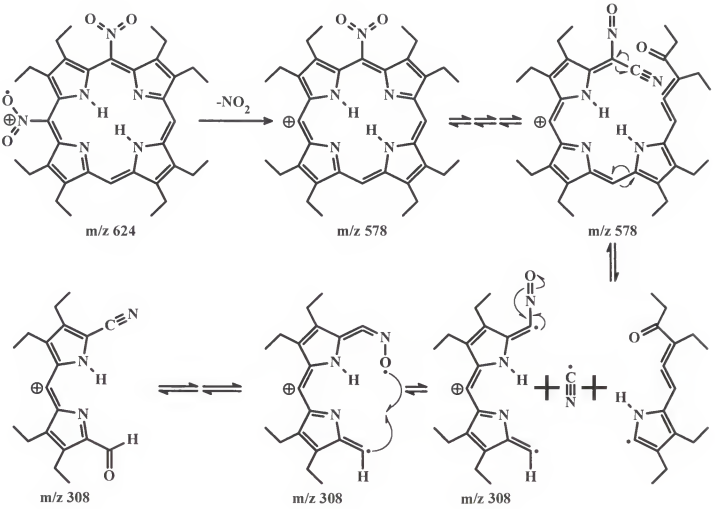


Figure 2-24. Fragmentation pathway for the formation of the m/z 308 fragment ion from the molecular (m/z 624) ion of OE5,10DNP.

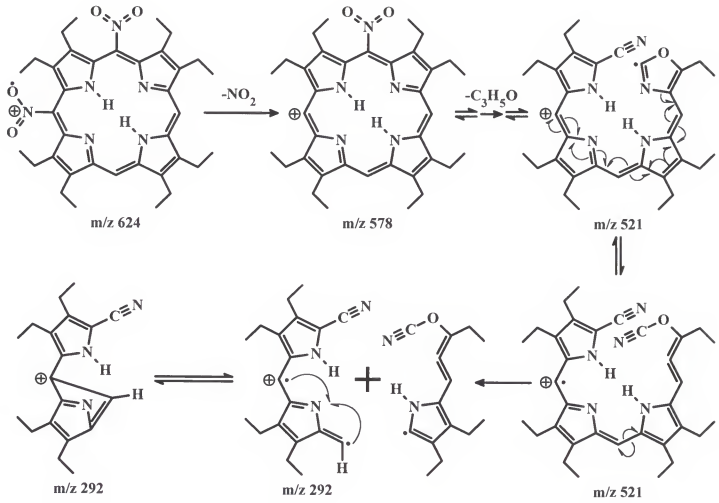


Figure 2-25. Fragmen pathway for the formation of the m/z 292 fragment ion from the molecular (m/z 624) ion of OE5,10DNP.

and $C_3H_5O$ elimination similar to the scheme for formation of m/z 522 (Figure 2-17) from the m/z 579 ( $M^{+\bullet}$ ) ion of OEMNP. Another oxygen transfer to the macrocycle with subsequent ring opening follows. Cleavage of the bond between carbon number 14 and carbon number 15 (the IUPAC porphyrin numbering system is illustrated in Figure 1-1) produces a diradical which can then cyclize to form the ion shown.

The fragmentation pathway to the ion at m/z 297 (not illustrated) in both dinitro spectra can be explained by examining the ion's parent spectrum (Figure 2-26a). One of the m/z 297 ion's parents is the m/z 312 ion. While the majority of the signal at m/z 312 in the EI-MS mode can be attributed to the $M^{2+}$ ion, it is unlikely that the doubly charged molecular ion would lose 30 amu to form an $[M-30]^{2+}$ ion at m/z 297. The m/z 312 ion can be formed from OEDNP by dividing the macrocycle into halves, each of which contains one of the nitro groups. A simple β-cleavage of a methyl group from the m/z 312 ion produces m/z 297. This is also consistent with the data from the labeled compounds (Table 2-5) which indicate the m/z 297 ion contains two pyrrolic nitrogens and two *meso* carbons.

A workable scheme for the formation of the m/z 271 ion remains elusive. Its parent spectrum (Figure 2-26b), as for other ions in this portion of the spectrum, does not provide much helpful information since the only significant parent is the molecular ion. It is interesting to note that adding 271 and 308 results in a total of 579 suggesting that the structure of the m/z 271 ion is likely to be complementary to that of the m/z 308 ion with an added hydrogen from somewhere in their common m/z 578 precursor. The labeled compound data indicate that the m/z 271 ion contains two pyrrolic nitrogens and one *meso* carbon which is what would be left after removal of the two pyrrolic nitrogens and three *meso* carbons for the formation of the m/z 308 ion. Taken together, these data indicate a probable composition of $C_{17}H_{23}N_2O$ for the m/z 271 ion.

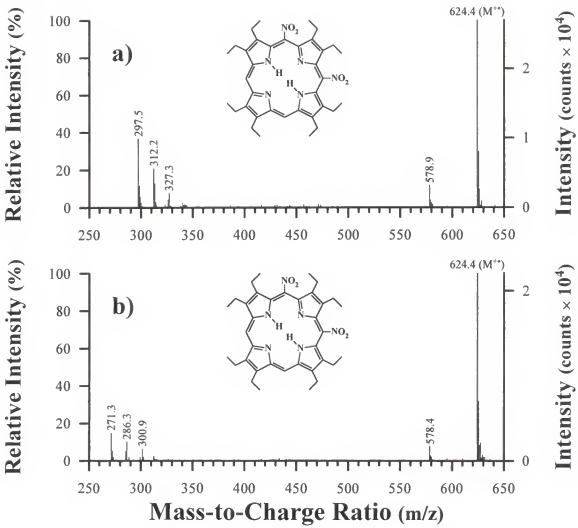


Figure 2-26. Parent spectra of the a) m/z 297 and b) m/z 271 ions of OE5,10DNP.

Surface-Induced Thermal Decomposition

As was seen in the OEMNP spectrum, the surface-induced thermal elimination of the nitro groups with subsequent hydrogen abstraction to form OEP, as first reported by Clezy [Clezy *et al.*, **1974**] (Figure 2-8), is a common problem in the analysis of nitro-substituted porphyrins. This phenomenon was observed in these studies for all of the nitroOEPs. A diagram illustrating the effect of the thermal decomposition on the spectra of the more nitrosubstituted OEP derivatives is shown in Figure 2-27. The figure shows that although only OETNP is placed on the DEP filament, all of the nitroOEPs might be available for ionization owing to surface-induced dissociation on the surface of the ion volume and subsequent volatilization of the decomposition products.

The percent relative abundances (%RA) of the $[M-45]^+$ (thermal decomposition) and $[M-46]^+$ (gas-phase loss) ions for the entire series, along with the intensity ratio of thermal decomposition ($I_{TD}$) to gas-phase loss of $NO_2$ ($I_{G-P}$) for each compound, are listed in Table 2-6. It is interesting to note that the ratio is lowest for OE5,15DNP. The data indicate that the trend toward greater thermal instability with increased substitution (and therefore increased distortion of the macrocycle) does not follow a monotonic increase. This is most likely because of the large number of other factors which may affect the stability of the ions, as was discussed earlier in this chapter.

Table 2-6. The nitroOEPs with relative intensities of the ions resulting from surface-induced thermal decomposition ($[M-45]^+$) and gas-phase loss of $NO_2$ ($[M-46]^+$) along with the ratio of the intensities.

| Compound | %RA of the $[M-45]^+$ ion | %RA of the $[M-46]^+$ ion | $I_{TD} / I_{G-P}$ |
|---|---|---|---|
| OEMNP | 13.7 | 24.2 | 0.56 |
| OE5,10DNP | 11.6 | 21.7 | 0.53 |
| OE5,15DNP | 5.22 | 12.3 | 0.42 |
| OETriNP | 28.8 | 22.8 | 1.3 |
| OETNP | 28.1 | 14.7 | 1.9 |

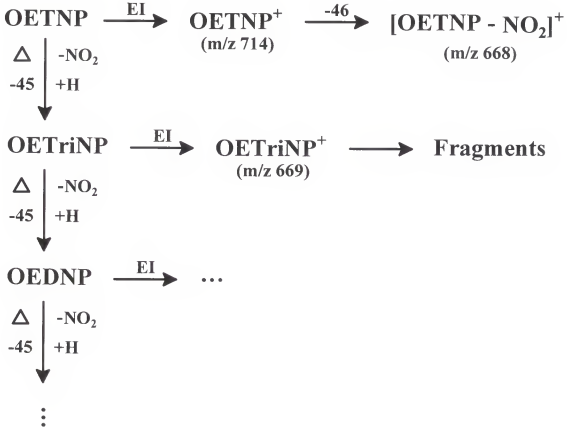


Figure 2-27. The effect of surface-induced dissociation on the mass spectrum of OETNP.

There are several possible means of minimizing (but not, unfortunately, eliminating) the impact of thermal decomposition on the data. Volatilization of samples off of a DEP filament is analogous to gas chromatography in that the more volatile components enter the gas phase before the less volatile components. A plot of the reconstructed ion current (total current from all ions in a given mass scan) versus scan number (time) produces a mass thermogram analogous to the mass chromatogram familiar from GC/MS and LC/MS. A mass thermogram of OETNP off the DEP is shown as the solid curve (y-axis on the left) in Figure 2-28. In order to smooth the data somewhat, a running average of every two spectra in the mass thermogram (*e.g.*, average of scans 71 and 72, average of 72 and 73, ...) is plotted at the x-value corresponding to the average of the two scan numbers. The dashed curves are traces of the indicated ion intensity ratios. The data have a skip between scan numbers 109 and 110 owing to bad centroiding of the 668 and 669 peaks by the TSQ70's centroiding algorithm. Note that the 678/714 ratio (squares) remains relatively constant over the entire peak, increasing only slightly at the very end. This suggests that the formation of the m/z 678 ion is indeed a gas-phase process, dependent on the amount of m/z 714 ion. The ratios of 679/714 (circles) and 679/678 (diamonds), however, increase rapidly as the mass thermogram peak tails off. This would seem to indicate that surface-induced thermal decomposition products are being voltatilized from the ion volume surface later in the thermogram, at higher temperatures owing to radiative heating from the DEP filament.

One means of minimizing the effects of thermal decomposition would be heating the sample so rapidly that it would not have time to decompose. A difficulty arising from this approach is that heating too fast produces a mass thermogram which is only a few scans wide, making data averaging difficult. Furthermore, if there were any impurities in the sample they could desorb at the same time, ionize, and complicate the spectra. Taking data only from spectra early in the mass thermogram is another way to work around the inevitable thermal decomposition problem.

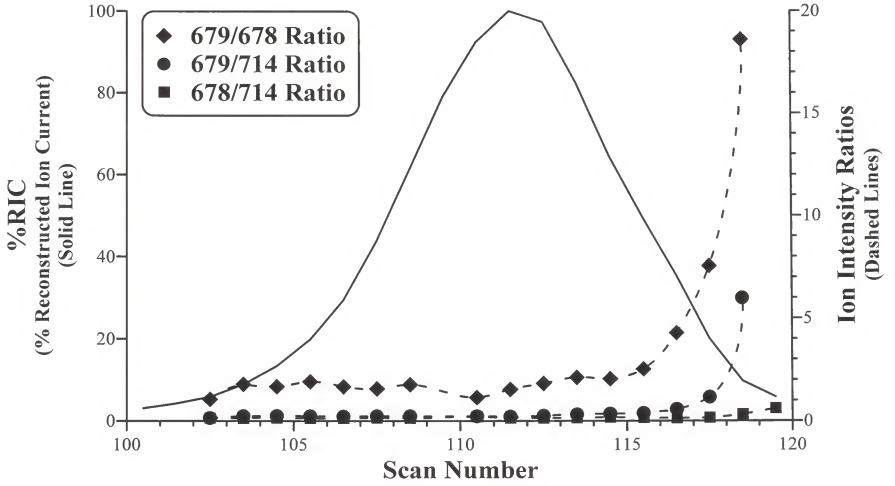


Figure 2-28. Reconstructed mass themogram (definition in text) for the desorption of OETNP from the DEP (solid curve, left y-axis). Using the right y-axis: ratios of the intensities of m/z 678 (gas-phase loss of $NO_2$) and the m/z 679 (thermal decomposition product) to the molecular (m/z 714) ion and to each other.

Suppression of β-Cleavage of Methyl Groups

The neutral loss (NL) of 15 spectra (β-cleavage of methyl groups) for OEMNP and OETNP are shown in Figure 2-29. The NL spectrum for OEMNP shows nearly typical behavior for a substituted porphyrin. The NL spectrum of OETNP, however, is quite unusual and illustrates most dramatically the β-cleavage suppression seen to some extent in all of the nitrosubstituted OEPs. The typical β-cleavage of methyl groups, characteristic of OEP, does not occur to any appreciable extent from ions which have an m/z greater than 600. (There is a minor amount of β-cleavage from the molecular ion indicated by its low intensity in the spectrum.) This means that approximately 100 amu of fragments must be lost from the OETNP macrocycle before it becomes stable enough for β-cleavage to be competitive with other losses. The fragmentations in the 100 amu of losses most likely correspond to cleavages of the bulky nitro groups which sterically induce the distortion of the macrocycle. By eliminating the bulky nitro groups, the porphyrin macrocycle can become more planar and therefore more aromatic. The greater the aromatic character of the macrocycle, the more stable it will be and the more favorable the conditions for β-cleavage relative to other fragmentation pathways.

## Conclusions

Novel fragmentations for the entire suite of nitroporphyrins have been proposed based on the EI-MS, EI-MS/MS, and EI-HRMS data presented. The fragmentation leading to the m/z 294 ion, resulting in elimination of two pyrrolic subunits, along with fragmentations of the more substituted nitroporphyrins are reported for the first time. The data indicate that increasing the number of nitro substituents increases suppression of β-cleavage fragmentations in favor of other fragmentation pathways. Also, in general, the more substituted the nitroporphyrin, the more likely it is that it will undergo surface-induced thermal decomposition.

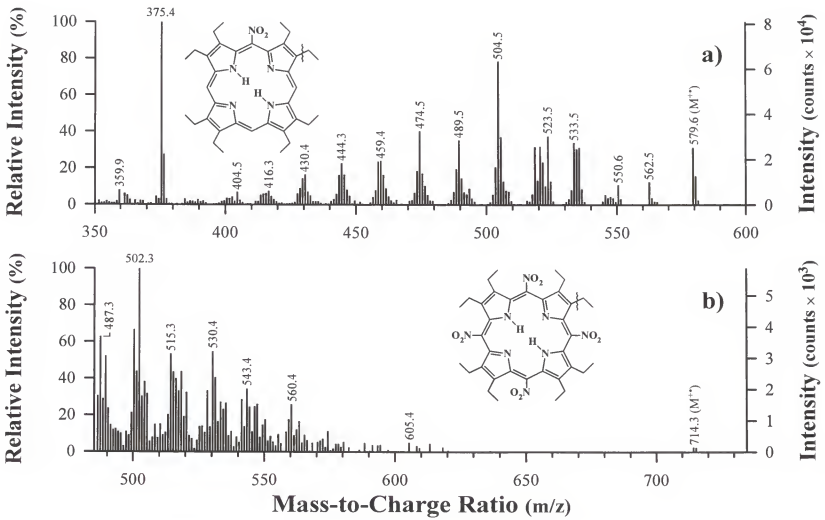


Figure 2-29. Neutral loss spectra of a) OEMNP and b) OETNP, showing neutral loss of 15 (β-cleavage of methyl groups.)

One way to explain the differences in the fragmentation pathways of the nitroOEPs and OEP would be to say the nitro group is a more labile substituent than the alkyl groups. However, this reasoning only explains the suppression of the β-cleavage pathways and cannot account for the increased α-cleavages of alkyls or the macrocycle scissions. Another explanation is that the electron withdrawing character of the nitro group lowers the electron density in the aromatic porphyrin macrocycle, with resulting changes in fragmentation. As mentioned in Chapter 1, the porphyrinogen (non-aromatic hexahydroporphyrin) macrocycle is readily cleaved in EI-MS. This phenomenon is also observed for the tetraoxoporphyrins [Boylan, **1970**; Budzikiewicz and Pesch, **1976**]. The lowered electron density explanation might provide a rationale for the macrocyclic cleavages but would not be a good explanation for the suppression of β-cleavage of methyl groups.

A third proposal makes use of the distortions known to exist in the these porphyrins in their crystal forms (see Figure 1-8). The porphyrins are likely to remain distorted as in the gas phase and as ions. The distortions lead to weakening of the π-bonds which have greatest orbital overlap and, therefore, strength when the bond angles are kept to 90 degrees [Pine *et al.*, **1980**; Streitweiser and Heathcock, **1981**]. Distortion will also decrease the aromaticity of the porphyrin for the same reason. While the data presented here provide more evidence, useful for solving the problem, they are not adequate to answer the question as to whether the electron withdrawing effect of the nitro group or the distortions it induces play a greater role. The experiments needed to help answer this question will be discussed in Chapter 4.

CHAPTER 3

# IONIZATION ENERGY DETERMINATIONS

## Background

### Thermodynamics

The first adiabatic ionization energy ($IE_a$) of a cation ($AB^{+\bullet}$) is the energy required to remove an electron from the neutral molecule ($AB$) and produce the ion [Lias *et al.*, **1988**]:

$$AB \xrightarrow{IE_a} AB^{+\bullet} + e^- \qquad (3\text{-}1$$

The second ionization energy ($IE_2$) of a dication ($AB^{2+}$) is the energy required to remove two electrons from the neutral molecule ($AB$) and produce the ion:

$$AB \xrightarrow{IE_2} AB^{2+} + 2e^- \qquad (3\text{-}2$$

The adiabatic ionization energy is related to the heat of formation of the ion at a given temperature ($\Delta H_f(M^+)_T$) and the heat of formation of the neutral precursor at that temperature ($\Delta H_f^\circ(M)_T$) as shown here:

$$\Delta H_f(M^+)_T = \Delta H_f^\circ(M)_T + IE_a \qquad (3\text{-}3$$

The relationship between the enthalpy parameters and the ionization energy is discussed in greater detail in the Ionization and Appearance Energy section of Chapter 1. The definition of appearance energy is found there as well.

IE Determination using EI-MS: Problems and Solutions

Several methods for determining ionization energies, including optical spectroscopy, ion/molecule equilibrium constant determinations, photoelectron spectroscopy (PES), and photoelectron-photoion coincidence (PEPICO), have their appropriate applications discussed in detail in Chapter 1. The ionization method chosen for this research was electron ionization (EI).

In EI, formation of the singly charged molecular ion ($M^{+\bullet}$) involves bombarding the neutral sample molecule with electrons which cause the loss of a valence electron and formation of a cation. The EI ionization process can be written:

$$M + e^- \rightarrow M^{+\bullet} + 2e^- \qquad (3\text{-}4$$

In EI determinations of ionization energies, the electrons striking the neutral molecules have known energies which are varied over a range including the ionization energy of the ion. The bombarding electrons are produced at a filament which produces electrons with a Maxwellian distribution of energies as shown in Figure 3-1 [Field and Franklin, **1957**].

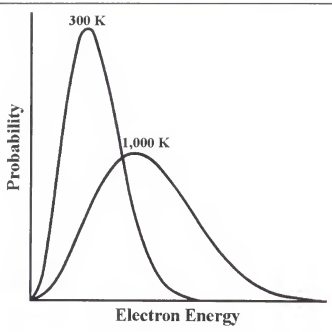


Figure 3-1. Maxwellian energy distributions at two different temperatures. Total probability under each curve is 1.

One of the difficulties of using EI to determine ionization energies is producing monoenergetic electrons or compensating for an energetically inhomogeneous electron beam. The effects of an energetically inhomogeneous electron beam on the determination of IEs were discussed in Chapter 1 and illustrated in Figure 1-15.

There are several methods available for extracting ionization energies from ionization efficiency curves which do not have the ideal shape. They include the vanishing current method, also known as initial onset or threshold method, the linear extrapolation method, the critical slope method, and the extrapolated difference method [Field and Franklin, **1957**].

The extrapolated difference method [Field and Franklin, **1957**] requires the use of a calibration compound of known ionization energy (IE) along with the sample of interest. The ionization efficiency curves of the two compounds are plotted on separate y-axes which are adjusted so that the straight portions of the curves, after the initial onset, are parallel. The differences in the electron energies ($\Delta V$) at several values of the ion current (I) are measured and a graph of $\Delta V$ *vs*. I is plotted and extrapolated to zero current. The extrapolated value of $\Delta V$ is taken as the difference between the ionization energies of the two compounds. The reasoning behind this method is rather arbitrary. It does not work well for appearance energies (AEs), and is not useful for low intensity ions.

The critical slope method [Field and Franklin, **1957**] was devised to avoid the difficulties which arise in the linear extrapolation and threshold methods which are discussed below. In this method, the ion current is assumed to be proportional to the square of the electron energy. Using this assumption, the number of ions produced per second $N_i(V)$ can be written:

$$N_i(V) = 2C_1 kT^3[(V_C - V) + 3kT]exp[-\frac{\phi + V_c - V}{kT}] \qquad (3\text{-}5$$

where $C_1$ is an arbitrary integration constant, $k$ is Boltzmann's constant, T is the temperature (K) of the EI filament, $V_C$ is the ionization energy (eV), V is the actual energy of the

electron (eV), $\phi$ is the work function of the filament, and T is the temperature (K) of the EI filament.

Taking the logarithm of both sides of equation 3-5 produces:

$$ln\,N_i(V) = ln[(V_C - V) + 3kT] - \frac{\phi + V_C - V}{kT} + C_2 \qquad (3\text{-}6$$

where $C_2$ is another arbitrary constant. A plot of the logarithm of the ion current versus the electron voltage is a curve which approximates a straight line for small values of $(V_C - V)$. The slope of the line is:

$$\frac{dln\,N_i(V)}{dV} = \frac{-1}{V_C - V + 3kT} + \frac{1}{kT} \qquad (3\text{-}7$$

At the ionization energy, the slope becomes:

$$\frac{dln\,N_i(V)}{dV} = \frac{2}{3kT} \qquad (3\text{-}8$$

This method also requires the use of a calibrant for the electron energy. The assumption that the ion current is proportional to the square of the electron energy is open to debate. This method is not commonly employed in the determination of appearance energies so its suitability for that purpose is unknown. However, since the mathematical relationship between an ionization probability and electron energy is even more complex for appearance energies than for ionization energies, the likelihood that this method would provide useful AE information is small.

The linear extrapolation method [Field and Franklin, **1957**] applied to a determination of the first ionization energy of nitrogen is illustrated in Figure 3-2. In this method, the ionization efficiency curve is determined over a range well below the ionization energy and well into the linear portion of the curve. The average baseline is determined and extended past the initial onset region. The linear portion of the curve is then subjected to linear regression. The regression line is extrapolated back to the baseline. The intersection of the two lines is taken as the ionization energy. The two curves on

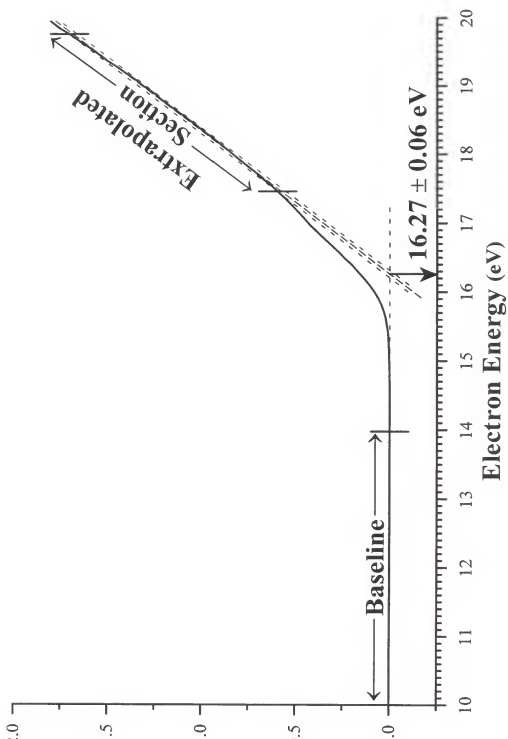


Figure 3-2. Extrapolation method for determining ionization energies. Determination of the first ionization energy of $N_2$.

either side of the extrapolation line represent the 95% confidence interval. The result of 16.26 ± 0.06 eV shown in the figure is based on one determination and reflects the 95% confidence interval on the extrapolated lines. (The 95% confidence interval on the baseline was so small that it is not shown in the figure.) The literature value for the first ionization energy of $N_2$ is 15.58 eV [Lias *et al.*, **1988**]. This method can also be applied graphically but with less accuracy. It has the advantages of using well-behaved portions of the ionization efficiency curve and ease of application. The values from linear extrapolation, however, tend to overestimate the ionization energy. Use of a standard of known IE might possibly compensate for the overestimation. Another consideration is the shape of the ionization efficiency curve. No ionization efficiency curve taken on apparatus employing non-monoenergetic electron beams is truly linear at any point after the onset of ionization. Additionally, the ionization efficiency curves for some ions which can be formed by more than one process, exhibit "fine structure" as illustrated in Figure 3-3. The curve shown is for the formation of the $CH_2^+$ ion from $CH_4$. The ionization process starting at about 14 eV is believed to be $CH_4 + e^- \rightleftharpoons CH_2^+ + H_2 + 2e^-$. The change in slope at *ca.* 19 eV is thought to be due to the onset of production of $CH_2^+$ by the process $CH_4 + e^- \rightleftharpoons CH_2^+ + 2H + 2e^-$. The postulated processes are based on the fact that the difference between their onsets closely corresponds to the bond dissociation energy of the $H_2$ molecule of 4.5 eV. Finally, the method does not work for determining appearance energies of fragment ions because of the complicated shape of their ionization efficiency curves resulting from reasons discussed in the previous paragraph.

In the threshold method [Field and Franklin, **1957**], a calibrant is introduced into the instrument and the ionization efficiency curves for both compounds are obtained simultaneously. The threshold method for determining the ionization energy of nitrogen (without calibrant) is illustrated in Figure 3-4. An average baseline (long dashed line) of the curve is calculated for electron energies below the compound's IE and the standard deviation is also obtained. For the work presented here, a cutoff point of three standard

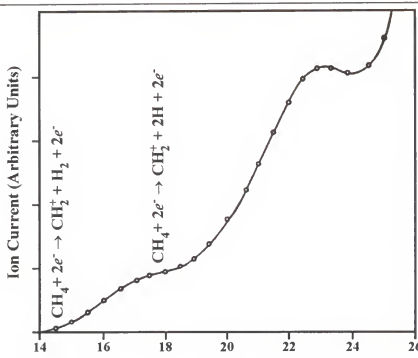


Figure 3-3. Ionization efficiency curve for the production of $CH_2^+$ ions from $CH_4$ [adapted from McDowell and Warren, **1951**].

deviations above the mean was chosen as the threshold value (short dashed line). The first point in the curve at which this threshold was exceeded and the curve continued to exceed the threshold was taken as the ionization energy (indicated by a diamond).

The uncorrected result for this determination of the first IE of $N_2$ was $12.71 \pm 0.10$ eV. The error in this result is given as the value of the smallest possible step in the electron energy values allowed by the instrument. This method, although it produced a result which is farther from the accepted value (15.58 eV) than the extrapolation method, does produce the low value for the ionization energy expected in a system where the electrons are not monoenergetic (see Figure 1-15, where all of the curves in which the beam is not monoenergetic produce a low result irrespective of the method used to extract the IE from the data). Simultaneous determination of the IE of the standard compound allows correction for the low value which results from the determination of only one compound. Additionally, since only a small portion of the ionization efficiency curve (a base-

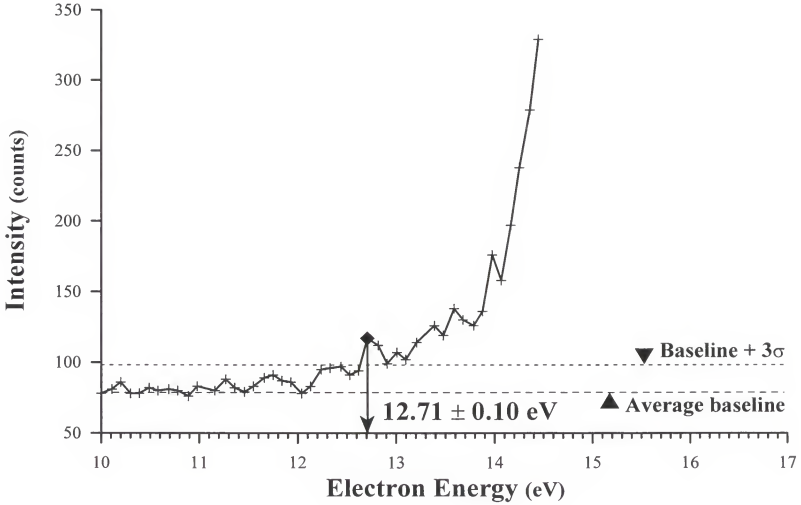


Figure 3-4. Threshold method for determining ionization energies. Determination of the first ionization energy of $N_2$.

line and the onset portion) needs to be generated, data can be acquired more rapidly than any of the other methods mentioned. For these reasons and the fact that it is both simple and applicable to appearance energies, this method was chosen for use in determining the ionization energies presented here.

For determination of IEs on an actual sample, the difference between the literature value of the standard compound's IE ($IE_{SL}$) and the standard's experimentally determined IE ($IE_{SE}$) is added to the simultaneously determined ionization energy for the unknown ($IE_{UE}$) to obtain the corrected IE of the unknown ($IE_{UC}$):

$$IE_{UC} = IE_{UE} + (IE_{SL} - IE_{SE}) \quad (3\text{-}9$$

It is important to have the relative intensities of the calibrant and sample approximately the same because the shapes of the ionization efficiency curves change with the amount of sample in the source. The effect of sample concentration on the shape of the ionization efficiency curve is illustrated in Figure 3-5. Additionally, if the standard were present at a concentration of, for example, an order of magnitude higher than the sample, then its onset would be that much easier to see than that of the unknown. In this case the experimental IE of the standard would appear to be lower, resulting in higher value for the sample after the correction for the standard value had been made.

## Experimental

### Samples

The first ionization energies of octaethylporphyrin (OEP) and tetraphenylporphyrin, several divalent metal/OEP complexes (Ag, Co, Cu, Ni, Pd, Pt, TiO, VO, and Zn) and the Ni(II) complexes of the entire suite of meso-nitroOEPs were determined using several strategies. The second ionization energies and the appearance energies for the fragment ions resulting from the β-cleavages of one and two methyl groups from OEP,

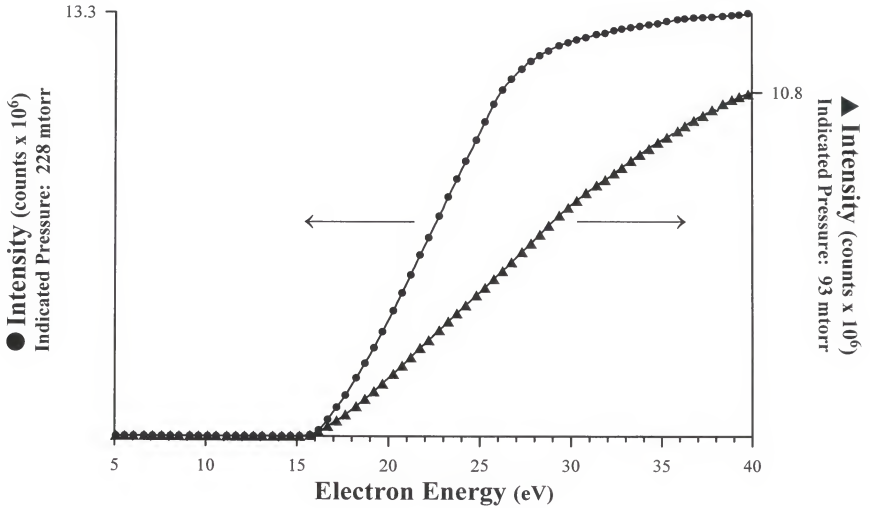


Figure 3-5. Effect of ion intensity (sample concentration in the source) on the shape of the ionization efficiency curves. Determination of the first ionization energy of $N_2$ at two different indicated pressures of $N_2$ in the ion source.

Ni(II) OEP, and VO(II)OEP were also determined. In addition, $N_2$ and Ar gases were used to help determine the best method of determining ionization energies using the TSQ70. All porphyrin samples were obtained from Dr. J. Martin E. Quirke, Chemistry Department, Florida International University. Gas samples were obtained as standard compressed gases from Bitec, Ocala, Florida. The calibrant, *N,N*-dimethylaniline was obtained from Chem Service, West Chester, Pennsylvania. Reagent grade solvents were obtained from Fisher Scientific, Atlanta, Georgia.

Sample Preparation

Each individual sample was dissolved in methylene chloride and the resulting solutions stored in either amber glass vials with Teflon-lined caps or in clear glass vials wrapped in aluminum foil and topped with the same caps. The porphyrin solution (in 3 μL aliquots) was transferred by syringe to the bottom portion of an aluminum direct insertion probe (DIP) vial. The vial was then covered loosely with a cap from a screw-cap vial and the methylene chloride allowed to evaporate. The transfer and evaporation steps were repeated anywhere between ten and twenty times until sufficient sample was deposited on the walls of the vial for the sample to last for several hours (subjective determination). The amount of sample in the vial was not quantitated.

MS Operating Conditions

The ion source region of the Finnigan MAT TSQ70 was illustrated in Figure 2-1. In order to minimize the amount of sample condensing on the ion volume, the source region was operated at 225°C while the manifold was maintained at the usual operating temperature of 70°C. The scan rate was set to 4 amu/s and the instrument was operated in the Q3MS mode to increase the signal-to-noise ratio (S/N). For some samples the scan rate was slowed to 2 amu/s to increase S/N. Samples were introduced into the ion vol-

ume from capped aluminum vials using the DIP which was operated isothermally at 225°C throughout the experiment. In order to allow time for the temperature of the probe to stabilize, it was raised to 225°C and held there for 1 min. before data acquisition was started.

The parameter which controls the electron energy on the TSQ70 (ELEN) was varied in 0.1 eV increments (the smallest allowed by the instrument) under automated instrument control using Finnigan's instrument control language (ICL) version E1.5. A listing of the ICL programs with explanatory comments is found in Table 3-1. The actual ELEN increments were not always 0.1 eV, but usually varied usually between 0.09 and 0.11 eV. However, every so often, the increment would be 0.20 eV. These 0.20 eV jumps are due to a quirk of the digital-to-analog converter responsible for producing the ELEN voltage. Since the actual voltage on the filament could not be read by the instrument, a digital voltmeter was used to read the voltage drop between the filament and instrumental ground using the test points provided on the Source Interface board of the instrument. Initially the voltage was recorded for each sample run. After collecting the data on the actual voltage versus ELEN many times, it was noticed that the values for the voltage remained essentially constant (± 0.01 eV) for a given EI filament. Since the 0.01 eV difference is only one tenth of the average increment, for the greater proportion of the experiments, only one recording of the ELEN parameter versus actual voltage was obtained each time the filament was replaced.

In its normal operating mode, the TSQ70 automatically varies the emission current on the EI filament (ECURR) as the ELEN parameter is changed. The Maxwellian energy distribution of the electrons is a function of the temperature of the filament and, therefore, of the emission current. In order for the experiments with internal standards to work properly, the electron energy distribution must remain constant over the entire range of ELEN values during data acquisition. In order to insure that the energy distribution remains constant, the ICL programs (see the fourth line of first program in Table 3-1)

Table 3-1. ICL Programs used to determine IEs (with explanatory comments). Note: semicolons are used to separate commands in ICL programs.

| F960717J.ICL - For Data Acquisition under Automated Instrument Control | |
|---|---|
| **Program Listing** | **Explanatory Comments** |
| ELEN=70;ECURR=200;EMULT 1800;CENT;Q3MS;COLL=0;MINAREA=0 | Turns on El filament (ELEN) at 70 V and 200 μA (ECURR); turns the multiplier on at -1800 V; puts the instrument in the centroid and Q3MS modes; sets the collector (COLL) to 0 V; and the minimum peak count to 0 |
| INITG;UCLR;DOZE 5;ELEN=4;SPHTR=225;DOZE 30;ZERO=-18 | Initializes the graphing program; clears the entire user list (ULIST); waits 5 s; sets theEl filament at 4 V and solids probe at 225°C; waits 30 seconds; sets electrometer zero to -18 |
| FELEN=4.0;LELEN=10;DELEN=0.1 | Sets the values for the first and last ELEN voltages and the amount ELEN is incremented |
| ELEN=FELEN;ECURR=18;FHOLDIE | Sets ELEN at the FELEN value (4.0 V); sets the El emission current to 18 μA; and calls the program FHOLDIE |
| SN=0;ASTART | Sets scan number to 0 and starts data acquisition |
| UNTIL ELEN > LELEN | Sets up a loop which will end when ELEN is greater than LELEN |
| ..#Electron Energy =;..ELEN;..#Current -;.ECURR | Prints a message at the bottom of the screen with the ELEN and ECURR values |
| UCLR(1);UCLR(2);Doze 1;REPEAT 10 | Clears ULIST 1 and ULIST 2; waits 1 s; starts a loop which will run 10 times |
| GO(120.1,122.1;0.5);GO(679.3,681.3,0.5);STOP | Acquires 1 scan between m/z 120.1 and 122.1 in 0.5 s and 679.3 and 681.3 in another 0.5 s and writes it to disk (since ASTART is still active). This line is altered to include the appropriate masses for the compound of interest. |
| UAPP(AREA(121.1),1);UAPP(AREA(680.3),2) | Writes the areas of the two peaks into the ULIST 1 and ULIST 2 |
| END | Ends the REPEAT loop |
| PLOT(ELEN,UMEAN(1),1,1);PLOT(ELEN,UMEAN(2),2,2) | Plots the average areas of the peaks versus the ELEN value using the built-in GRAPH program. The third argument in the PLOT command is the trace to which the point is added and the fourth argument is the color of the trace |
| UAPP(UMEAN(1),3);UAPP(UMEAN(2),4) | Adds the average areas for each ELEN value to ULISTs 3 and 4 |
| ELEN+=DELEN | Increments the ELEN value by the value stored in the DELEN parameter |
| END;ASTOP;ELEN=70;ECURR=200;OFF;SPHTR=25;BEEP;.#1 AM DONE | Ends the UNTIL loop; stops data acquisition; returns the El filament voltage and current to their normal settings and then turns them off along with the multiplier; returns the solids probe to room temp; and lets the operator know the program is done |
| FHOLDIE.ICL - Allows the Instrument to Equilibrate at the Settings Used for Data Collection | |
| SN=100 | Sets scan number to 100 |
| UNTIL SN > 130 | Starts a loop which will run until the scan number exceeds 130 (30 seconds of equilibration) |
| GO(120.1,122.1,0.5);GO(679.3,681.3,0.5);STOP | Acquires 1 scan between m/z 120.1 and 122.1 in 0.5 s and 679.3 and 681.3 in another 0.5 s. Does not write to disk because ASTART is not active. This line is changed to agree with the GO;STOP parameters used in the program which calls this one (*e.g.*, F960717J) |
| END | Ends the UNTIL loop |
| RETURN | Returns instrument control to the program which called it (*e.g.*, F960717J) |

were written so that the ECURR parameter was maintained at a fixed value throughout the experiment.

The instrument was operated in the selected ion monitoring mode and set to scan one amu above and below the ion(s) of interest. For OEP complexes with divalent metals which have a number of isotopes, the two or three most abundant isotopic peaks were monitored and the results were added together for one pooled intensity. Ten scans were obtained at each ELEN value for each ion under study. The data were then averaged and printed out using the LIST program of Finnigan's Interactive Chemical Information System (ICIS) version 6.20. The data were then entered into either a Quattro Pro or an Excel spreadsheet, an appropriate baseline range was chosen, and the first point above the threshold was determined.

In some experiments, the collector and the first extraction lens, L11, were set to instrumental ground to minimize the effect of fringing fields on the results. One effect of this unusual tuning was to lower the sensitivity of the instrument by approximately an order of magnitude. This tuning was used for the initial experiments on instrument stability and those in which mixed samples of porphyrins were employed. Unfortunately, for the higher molecular weight porphyrins, this produced conditions under which the signal-to-noise ratio was too low for accurate IE determinations. In most experiments, the calibration standard was being run simultaneously with the sample, thereby providing a correction factor for any extra inhomogeneity in the electron energies produced by the fields from the collector and/or L11. For this reason, while the collector was still set at instrumental ground, L11 was "tuned flat" (*i.e.*, independent of m/z) at a value which provided the best sensitivity for the porphyrin. L11 is commonly tuned flat when any Q3MS mode is used, therefore, the flat tuning of L11 did not greatly affect the signal strength of the calibrant ion which was at m/z 121.2. This more typical tuning was used for the experiments in which the *N,N*-dimethylaniline standard was bled into the source through an adjustable leak valve.

Sample Handling

Three different means of dealing with sample preparation were tried. Descriptions of the three sample handling protocols follow below. The results and relative merits of each sample handling technique will be presented in the Results and Discussion section which follows.

Single Compounds

Initial experiments included plumbing in the gases $N_2$ and Ar through the TSQ70's CI reagent gas line. Several compounds with known ionization energies, including anthraquinone, *p*-nitrobenzoic acid, and acetamide, and individual porphyrins, were also examined using the direct insertion probe for sample introduction. Unfortunately the results of these experiments showed that the instrument tended to drift over time and were not as reproducible as desired.

Porphyrin Mixtures

In order to avoid the problems of instrumental drift encountered in the initial experiments, it was decided to employ mixed standards of porphyrins in which OEP would serve as an uncalibrated internal standard to provide an IE value against which the others could be compared on a run-to-run basis. The greatest difficulty with this approach was preparation of the sample. Preparation of samples in which the intensities of all of the components were within about 10-15% of each other at appropriate points in their ionization efficiency curves was very difficult and time-consuming. Each change in the amount of one component required starting over with a new sample vial and then depositing enough sample into the vial for several determinations. This process alone takes about two to three hours per sample. An additional difficulty with using the mixed sample approach was that the porphyrins appeared to have different volatilities and a sample which had approximately equal intensities for all components in the first two or three runs did not usually continue to produce ions with the same relative intensities. One or more of

the components tended to deplete more rapidly than the others. This meant that several sample vials of each mixed standard had to be prepared in order to have a sufficient number of sample runs for data averaging.

Internal Standard and Compound Experiments

Owing to the difficulties of preparing mixed porphyrin samples in which the relative intensities of all the components were within 10% as discussed above, experiments were performed in which a variable leak valve (Model 203, Granville-Phillips, Boulder Colorado) was attached to the GC transfer line of the TSQ70. The Granville-Phillips valve allowed careful control of the amount of calibrant reaching the ion volume and, therefore, the intensity of the calibrant. It still took some time to adjust the leak valve to the appropriate setting, as between a quarter and a half an hour was required for equilibration whenever the setting was increased and about an hour was required to pump out the excess and start over again if the appropriate setting was overshot. Still, despite the time required to set up the experiment, this method produced much better results than the mixed standard method. As long as the sample did not run out, the sample signal stayed relatively constant and it was possible to collect enough sample runs for statistical analysis. Most samples were run so that there were data from separate sample runs on different days rather than relying on data from one day's sample run.

## Results and Discussion

Results from initial experiments showed the need for an internal standard. Secondary experiments using mixed porphyrin samples showed that reproducible results using a reference compound could be obtained. Finally, results from the variable leak valve experiments which provided a calibrant of known IE produced reproducible, calibrated results. The relative merits of the data from the latter two types of samples will be discussed.

Single Compound Results

Samples were initially run singly to see if it were possible to get reproducible results. Unfortunately the results had a high variability. For example, three determinations of the first IE of argon produced the following results: 12.71, 13.10, and 14.37 eV. The standard deviation of these three results is 0.87 eV. Taking into account that the average step in the electron energy in these experiments is approximately 0.1 eV, this standard deviation shows that there are sources of variation other than determining the onset voltage. If the major source of error were in determining the onset voltage, the standard deviation should reasonably be expected to be close to the 0.1 eV step in the electron energy. The variability in the results can be attributed to instrumental drift with time and to a considerable variation in the baseline and the noise on the baseline from one run to the next. The average baselines and standard deviations (in counts) for the three determinations were: $\bar{x}_1 = 72$, $\sigma_1 = 4$; $\bar{x}_2 = 87$, $\sigma_2 = 13$; and $\bar{x}_3 = 75$, $\sigma_3 = 4$. The intensities of the $Ar^+$ ion at 14.97 eV during the three determinations were 184, 172, and 2776 respectively. This shows that the baseline and noise levels are apparently not a function of the sample concentration in the source, but arise from random fluctuations in the instrument. Because of these difficulties it was decided to abandon any attempt at determining IEs without some sort of internal standard which could be used to compensate for instrumental fluctuations.

Mixed Sample Results

The next step in investigating the best method for determining IEs was to use samples containing mixtures of porphyrins. From these samples, it was determined that good relative values for the porphyrins could be obtained. IE results from repeated determinations on mixture #1 are reported in Table 3-2. Results from three mixed samples

for determinations of the first and second IEs and AEs for the loss of one and two methyl groups are reported in Table 3-3.

Table 3-2. IE Results from Porphyrin Mixture #1

| Observation Number | First IE OEP (eV) | First IE Ni(II)OEP (eV) | First IE V=O(II)OEP (eV) | Ni(II)OEP minus OEP (eV) | V=O(II)OEP minus OEP (eV) |
|---|---|---|---|---|---|
| 1 | 5.65 | 5.65 | 5.65 | 0.00 | 0.00 |
| 2 | 6.04 | 6.33 | 6.14 | 0.29 | 0.10 |
| 3 | 5.65 | 5.85 | 5.94 | 0.20 | 0.29 |
| 4 | 5.74 | 5.74 | 6.04 | 0.00 | 0.30 |
| 5 | 6.04 | 5.94 | 6.04 | -0.10 | 0.00 |
| 6 | 6.43 | 6.33 | 6.63 | -0.10 | 0.20 |
| 7 | 5.94 | 5.94 | 6.24 | 0.00 | 0.30 |
| 8 | 6.14 | 6.14 | 6.14 | 0.00 | 0.00 |
| Mean | 5.95 | 5.99 | 6.10 | 0.04 | 0.15 |
| Std. Dev. | 0.25 | 0.24 | 0.26 | 0.13 | 0.13 |

Table 3-3. IE Results from Samples Containing Porphyrin Mixtures.

| | Porphyrin | First IE Run #1 (eV) | Run #2 (eV) | Second IE (eV) | AE Loss of $CH_3$ (eV) | AE Loss of 2 $CH_3$ (eV) |
|---|---|---|---|---|---|---|
| Mix #1 | OEP | 5.85 | 6.04 | 19.59 | 13.10 | 14.46 |
| | Ni(II)OEP | 6.04 | 6.04 | 19.30 | 13.21 | 14.07 |
| | V=O(II)OEP | 6.33 | 5.93 | 18.82 | 13.21 | 14.46 |
| Mix #2 | OEP | 6.04 | 5.93 | Intensity too low | Not a significant fragment ion | Not a significant fragment ion |
| | OEMNP | 6.13 | 6.04 | | | |
| | Mg(II)OEMNP | 6.43 | 6.62 | | | |
| | Ni(II)OEMNP | 6.24 | 6.13 | | | |
| | Zn(II)OEMNP | 6.43 | 6.43 | | | |
| Mix #3 | OEP | 5.46 | 5.64 | Intensity too low | Not a significant fragment ion | Not a significant fragment ion |
| | TPP | 6.71 | 6.81 | | | |
| | OETNP | 8.45 | 8.45 | | | |
| | Ni(II)OETNP | 8.17 | 8.17 | | | |

From the results in Table 3-2 and Table 3-3, it is apparent that absolute determination of IEs without a reference point does not give results as reproducibly as expected. Just as for the single compound experiments, the standard deviations of the data on the first IE results for OEP, Ni(II)OEP, and V=O(II)OEP in Table 3-3 are greater than the 0.1 eV expected if the major source of variability were the determination of the onset. However, the standard deviations of the differences between the metallated OEPs and OEP are about half the amount seen for the absolute determination and are on the expected order of 0.1 eV, showing that determinations relative to a standard compound have much better reproducibility.

The values reported in Table 3-3 are based on OEP as a reference point, and therefore provide information about relative values for the determinations shown. While a value of 6.39 eV for the first IE of OEP (from photoelectron spectroscopy) has been reported in the literature [Kitagawa *et al.*, **1979**], the values for the second IE and the AEs have not yet been published. Having no standardized value to compare against, these results, while providing values relative to those for OEP, still do not provide absolute values. In order to provide a recognized standard against which to compare the results and avoid the difficulties of sample preparation encountered in the mixed sample determinations, it was decided to try bleeding volatile standards into the ion volume through the GC transfer line of the instrument.

Variable Leak Valve Results

Results from the variable leak valve experiments using *N,N*-dimethylaniline as the calibrant (first IE = 7.12 eV [Lias *et al.*, **1988**]) are found in Table 3-4. In addition to the experimental data, the metal-to pyrrolic nitrogen distance and, when available, IE values from photoelectron spectroscopy (PES) are also tabulated. The small variability, as seen in the 95% confidence intervals, indicates that, except in the case of Cu(II)OEP, the major

Table 3-4. First IE Determinations for OEP and Selected Divalent Metal Complexes.

| "Metal" | First IE[1] (EI-This Work) (eV) | First IE[2] (PES) (eV) | Number of Determinations | $M\text{-}N_p$[3] Distance (Å) |
|---|---|---|---|---|
| (none) | 6.27 ± 0.05 | 6.39 | 12 | Not Applic. |
| Ni(II) | 6.26 ± 0.06 | 6.38 | 15 | 1.929 |
| Co(II) | 6.16 ± 0.08 | 6.09 | 7 | 1.949 |
| Cu(II) | 6.23 ± 0.20 | 6.31 | 9 | 2.000 |
| Pt(II) | 6.36 ± 0.08 | Not Avail. | 12 | 2.012 |
| Pd(II) | 6.36 ± 0.07 | 6.37 | 18 | 2.013 |
| Zn(II) | 6.34 ± 0.08 | 6.29 | 9 | 2.036 |
| Ag(II) | 6.31 ± 0.11 | Not Avail. | 6 | 2.092 |
| Ti=O(II) | 6.36 ± 0.06 | Not Avail. | 18 | Not Avail. |
| V=O(II) | 6.37 ± 0.07 | Not Avail. | 8 | Not Avail. |

[1] 95% confidence interval shown
[2] Kitagawa *et al.*, **1979**
[3] Metal to pyrrolic nitrogen distance [Stanley *et al.*, **1993**].

source of error is in determining the onset. No reasonable explanation for the higher variability in the Cu(II)OEP data is apparent. Comparison with the PES data is also good. The average of the absolute values of the differences between the EI results (this work) and the PES results is 0.08 eV with a maximum difference of 0.12 eV. The metal-pyrrolic nitrogen ($M\text{-}N_p$) distance is tabulated in order provide a measure of the distortion of the porphyrin macrocycle by complexation with the metal. The higher the $M\text{-}N_p$ distance, the more distorted the porphyrin [Stanley *et al.*, **1993**]. From the tabulated results, there is no apparent correlation between the $M\text{-}N_p$ distance and the first IE of the molecule. However, the differences between $M\text{-}N_p$ distances may not be large enough to produce a noticeable change in the first IE.

The results of the determinations of the first IEs of the Ni(II) complexes of the entire suite of *meso*-nitroOEPs, using the same techniques used for the divalent metal complexes reported above, are found in Table 3-5. The root-mean-square out-of-plane (RMS OOP) distortion of the porphyrin macrocycle is measured from the plane com-

Table 3-5. First IE Determinations for Ni(II) complexes of OEP and *meso*-nitroOEPs.

| Ni(II) Complex of | First IE[1] (eV) | Number of Determinations | RMS OOP[2] Distortion (Å) |
|---|---|---|---|
| OEP | 6.26 ± 0.06 | 15 | 0.015 |
| OEMNP | 6.54 ± 0.11 | 9 | 0.081 |
| OE5,15DNP | 6.65 ± 0.06 | 10 | 0.164 |
| OE5,10DNP | 6.70 ± 0.03 | 20 | 0.199 |
| OETriNP | 7.11 ± 0.09 | 6 | 0.384 |
| OETNP | 7.22 ± 0.06 | 20 | 0.685 |

[1] 95% confidence interval shown

[2] Root-mean-square out-of-plane distortion values from Hobbs *et al.*, **1994**. (see Figure 1-8).

prised of the $C_\alpha$, $C_\beta$, $C_m$ and pyrrolic nitrogen as illustrated in Figure 3-6. The values reported were calculated using the molecular mechanical calculation program POLYGRAF (Molecular Simulation, Inc.) using potential energy functions and force constants based on normal coordinate analysis of Ni(II)OEP [Li *et al.*, **1989**, **1990**; Shelnutt *et al.*, **1991**].

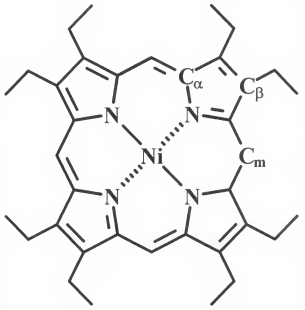


Figure 3-6. Structure of Ni(II)OEP showing the four atoms comprising the plane from which the RMS OOP distortion of the porphyrin is measured.

In order to ascertain whether the distortion of the macrocycle had any effect on the ionization energy, the first IE of the molecules versus their RMS OOP distortions is graphed in Figure 3-7. The graph indicates that as the distortion increases, the ionization energy does as well. The effect is not linear and may also be a product of the decreased electron density in the

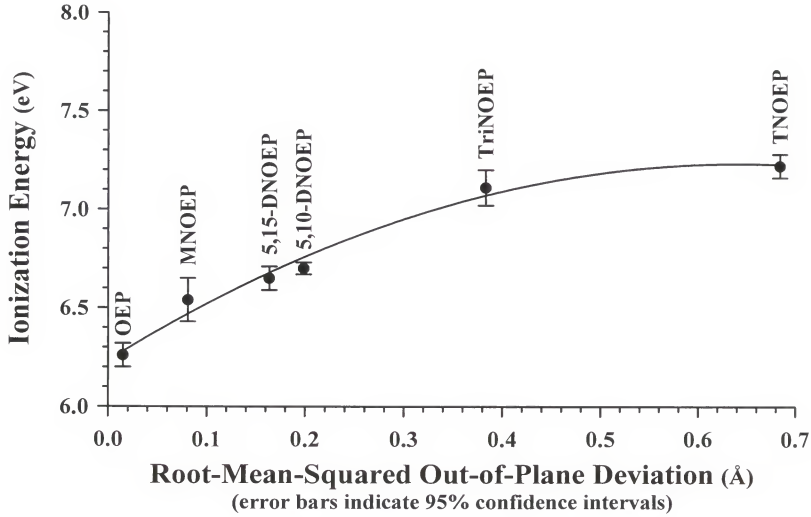


Figure 3-7. First IE of Ni(II) complexes of the indicated OEP and meso-nitroOEP compounds versus the root-mean-squared out-of-plane distortion of the porphyrin macrocycle. Distortion data from Hobbs *et al.*, **1994**.

conjugated macrocycle owing to the electron withdrawing character of the nitro groups. For example, an examination of the effect of nitrating benzene shows a similar trend. The first ionization energies of benzene and five nitrobenzenes are found in Table 3-6. As can be seen from these data, increased nitration of benzene also increases the ionization energy. Perhaps more importantly, the trend in the ionization energies of the three dinitro isomers seems to indicate that increased distortion (steric crowding and, therefore, distortion increases as the second number in the IUPAC name of the isomer decreases) does lead to higher ionization energies for the nitrobenzenes.

Table 3-6. First Ionization Energies of Nitrobenzenes [Lias *et al.*, **1988**].

| Compound | First IE (eV) |
|---|---|
| Benzene | 9.3 |
| Nitrobenzene | 9.9 |
| 1,4-Dinitrobenzene | 10.3 |
| 1,3-Dinitrobenzene | 10.4 |
| 1,2-Dinitrobenzene | 10.7 |
| 1,3,5-Trinitrobenzene | 11.0 |

## Conclusions

Three methods of determining the IEs by EI-MS under automated instrument control on the TSQ70 have been presented and the advantages and disadvantages of each discussed. Using a variable leak valve to introduce a calibrant into the ion source *via* the GC transfer line coupled with the "threshold technique" for data reduction produced the quickest and least variable results. The data handling process could be speeded considerably if the data system on the instrument were PC-based or at least PC-compatible. Most of the time spent in data reduction involved typing values from hard copy generated by the TSQ70's antiquated RSX-11 data system into software packages on a PC.

The first ionization energy data for metallated OEPs determined here by electron ionization are in reasonable agreement with literature values produced by PES, as discussed above. The results for the first ionization energies of the Ni(II) complexes of the

complete suite of *meso*-nitrosubstitued OEPs are reported here for the first time. The plot of the first IE versus ring distortion clearly indicates a correlation between ionization energy and distortion. This correlation suggests that ring distortion may play a role in increasing the ionization energy of porphyrins. In order to experimentally determine whether the increased ionization energies are due solely to distortion, solely to nitration, or a combination of the two, it will be necessary for future analysts to examine additional compounds which have varying degrees of distortion and substituents with electron withdrawing and electron donating character. The compounds to be examined and the reasons behind their selection will be discussed in detail in the Future Work section of Chapter 4. Calculations of the IEs of these molecules using sophisticated quantum mechanical models and programs could also be used to answer the distortion versus electron density question.

# CHAPTER 4

## CONCLUSIONS AND FUTURE WORK

The purpose of this research was to determine the fragmentation patterns of distorted porphyrins and ascertain the feasibility of determining ionization and appearance energies using the TSQ70 triple quadrupole mass spectrometer. The impetus for this was curiosity over why the porphyrins in many biological systems are distorted from planarity by their environments. The most well known example of this distortion is the heme unit in cytochrome *c*. Heme is essentially planar when not in the protein; however, in cytochrome *c*, it is substantially distorted due to covalent linkages between the heme periphery and cysteine residues in the protein [Anderson *et al.*, **1993**; Hobbs *et al.*, **1994**]. A greater understanding of how distortion affects the fundamental properties of the molecule such as bond strengths and heats of formation may be useful information for modeling the photosynthetic process or designing biomimetic molecules such as catalysts and molecules for transporting oxygen or electrons. The experimental data also can be used to confirm quantum mechanical predictions.

Natural selection places several demands on any porphyrin found in a biological system. It must be stable in both its ground state and in its ionized or excited state; *i.e.*, it must not undergo ring scission in its ionized form. The porphyrin must also have appropriate redox properties if it is to function in an electron transport or photosynthetic role. The organism with a biological system employing a porphyrin which does not meet these criteria, will probably not live long enough to pass on its genetic information.

The porphyrin fragmentation pathway studies provide information on the stability of the molecules in the excited state. The ionization energy measurements offer informa-

tion on the redox properties of the molecule in addition to the thermodynamic heat of formation.

Fragmentation Pathways

As discussed in Chapter 1, the normal fragmentations of porphyrins with peripheral substitutents are β-cleavages (β to the macrocycle) with the macrocycle remaining intact. Novel ring scission fragmentations of the entire suite of nitroporphyrins along with pathways explaining the fragmentation process were presented in Chapter 2. The fragmentation leading to the m/z 294 ion of 5-mononitroOEP is reported for the first time along with selected fragmentations of the dinitro and trinitro OEPs. It was difficult to obtain much useful information on tetranitroOEP due to the facility with which it undergoes surface-induced thermal degradation reactions in the ion source. In addition to the fragmentation pathways, the data indicate that the greater the nitro substitution, the more likely it is that fragmentation by β-cleavage will be suppressed in favor of other fragmentation pathways. Additionally, the greater the nitro substitution, the more likely it is that the porphyrin will undergo surface-induced thermal degradation.

The novel fragmentations may be explained in several ways: 1) the nitro group is more labile than alkyl substituents, 2) the electron withdrawing character of the nitro group reduces the aromaticity of the porphyrin, or 3) the distortions from planarity induced by the steric crowding introduced by the nitro substitutions weaken the bonds of the porphyrin and thereby affect the aromaticity. The first explanation, while it explains the observed suppression of the β-cleavage pathways, does not provide information on why α-cleavage of alkyls is increased with respect to α-cleavage fragmentation observed in OEP. Neither does it explain the macrocycle scissions. The second and third explanations might provide the reasons for the cleavages of the macrocycles. There is circumstantial support for the macrocylic distortion argument from other studies; cycloalkano

geoporphyrins having 5-, 6- and 7-membered exocyclic rings that cause some macrocyclic distortion are known to generate some unusual daughter ions in EI-MS/MS [Laycock *et al.*, **1995**]. While the data presented here provide more evidence useful for solving the problem, they are not adequate to answer the question as to whether the electron withdrawing effect or the distortions plays a greater role. A proposal for studies to resolve the electron-withdrawing versus distortion issue is presented in the future work section which follows.

Ionization/Appearance Energies

The first ionization energy data for metallated OEPs, determined here by electron ionization, are in reasonable agreement with literature values produced by PES, as discussed in Chapter 3. The first ionization energies of the Ni(II) complexes of the complete suite of *meso*-nitrosubstitued OEPs, determined by the same technique used for the metallated OEPs, are reported here for the first time. The plot of the first IE versus macrocycle distortion indicates that increased distortion may play some role in increasing the ionization energy. As in the fragmentation pattern discussion, the electron withdrawing character of the nitro group may also play a role in the observed increase in the ionization energies. Studies designed to help resolve the electron withdrawing versus distortion question are presented in the following section

Future Work

Proposals for experiments to answer the question of whether the electron withdrawing character of the nitro group or the distortions its presence induce in the macrocycle lead to the observed effects on the fragmentations and first ionization energies of the nitroOEPs will be discussed in the first subsection below. Reasons for extending these experiments to other biologically active tetrapyrroles will be presented under the

next subheading. The third subsection will deal with the preference of nature for cyclization of certain porphyrin type isomers. A proposal for answering the question, posed in Chapter 1, of why nature chose porphyrin, as opposed to one of its isomers, as its workhorse tetrapyrrolic macrocycle follows. The concluding section contains a proposal for experiments to improve the reliability of the information from EI ionization energy determinations on the TSQ70.

Distortion versus Electron Withdrawing Question

Examination of a wide range of substituted porphyrins will be required to explain fully several facets of the chemistry of the distorted porphyrin systems. The porphyrins to be examined in order to answer the distortion vs. electron withdrawing character question and the rationale for their selection are discussed below.

*Meso*-nitromethyloctaethylporphyrins and their divalent metal complexes: in this series of compounds, the nitro group is removed one step from the porphyrin ring by an intervening methylene group. The first compound in the series, 5-nitromethylOEP, is illustrated in Figure 4-1. These compounds are likely to be at least as distorted at their nitroOEP analogs due to steric crowding. However, the influence of the electron-withdrawing character of the nitro substituent will be lessened by the intermediate methylene group. These porphyrins can be prepared by a modification of the method of Fanning [Fanning *et al.* **1979**].

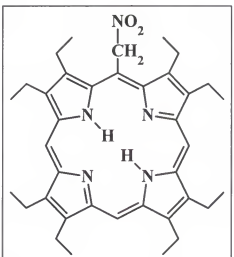

Figure 4-1. 5-nitromethylOEP.

*meso*-Halooctaethylporphyrins: the *meso*-chloro and *meso*-fluoro compounds will provide an interesting contrast with their *meso*-nitro analogs. The halogens have strong

electron withdrawing inductive effects, but are relatively small atoms and will therefore induce much less distortion in the macrocycle. The chlorinated compounds may be prepared by the methods of Bonnett [Bonnett *et al.*, **1966**]. Because of the danger inherent in handling fluorine and the expense required to set up a laboratory with appropriate safety features, the fluoro compounds will need to be prepared at a facility equipped to do the synthesis such as the University of Durham (U.K.). Additionally the *meso*-haloOEPs will not be able to fragment by the oxygen migration pathways available to the *meso*-nitrosubstituted compounds.

Octaethyl-tetraphenylporphyrin: this commercially available, distorted compound was the centerpiece of the elegant work of the Smith group on dodecasubstituted porphyrins [Evans *et al.* **1977**], and as such it merits attention.

Other Biologically Active Tetrapyrroles

Extension of these studies to other biologically active cyclic tetrapyrroles such as the chlorins is an obvious next step. The differences in ionization energies and fragmentation pathways between the metallated (especially Ni(II) and Co(II) complexes common in nature) and the metal-free forms will be useful. Studies on the biologically important Fe(III) complexes may follow at a later date, but are to be avoided at first due to possible complications arising from the axial ligands present in porphyrin complexes with metals other than the divalents. More detailed information on the dihydroporphyrin system will be especially valuable in view of its importance in photosynthesis and potential as new drug candidates for use in photodynamic therapy [Boyle and Dolphin, **1996**]. Octaethylchlorin can be prepared from octaethylporphyrin [Fuhrhop and Smith, **1975**].

Porphyrin Type Isomers

Nature goes to great trouble in the first steps of the biosynthesis of cyclic tetrapyrroles such as heme, chlorophyll, and vitamin $B_{12}$ to make the asymmetric macrocyclic ring compound uroporphyrinogen-III [Rawn, **1983**]. The biosynthetic pathway to the hemes from their basic starting materials, glycine and succinyl-CoA, is shown in Figure 4-2. The details of the biosynthesis of uroporphyrinogen III from porphobilinogin are illustrated in Figure 4-3. The cyclization leading to the formation of uroporphyrinogen III requires the catalyst uroporphyrinogen III cosynthetase. Without this enzyme, the symmetrical molecule, uroporphyrinogen I is formed. (The structure of uroporphyrinogen I can be obtained by reversing the positions of the A and P groups on ring D of uroporphyrinogen III). Uroporphyrinogen I is not a precursor to the important biomolecules mentioned above. Congenital erythropoietic porphyria, (the porphyrias were discussed in Chapter 1) arises as a result of an insufficient amount of cosynthetase, which leads to the accumulation of large amounts of the useless type I isomer and its derivatives. These lead to symptoms including red urine, teeth which show a red fluorescence under UV light, and skin which is extremely sensitive to light since the photoexcited porphyrins are very reactive.

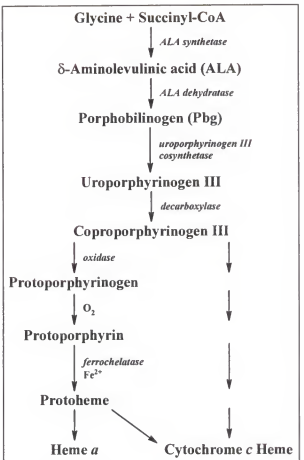


Figure 4-2. The biosynthesis of hemes. Adapted from Lemberg and Barrett, **1973**.

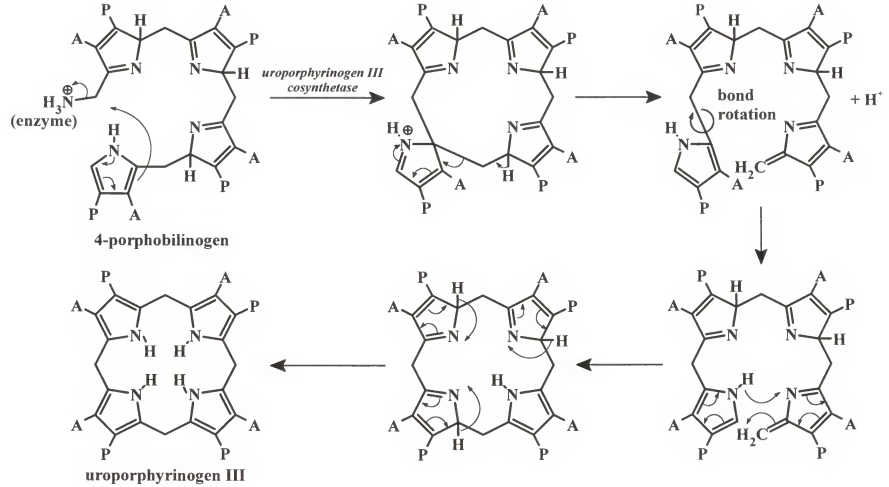


Figure 4-3. Biosynthetic pathway from 4-porphobilinogen to uroporphyrinogen III. Abbreviations: A, acetate; P, proprionate [adapted from Rawn, **1983**].

The cyclization leading to the type III isomer is unique and the reason for it is not readily apparent. There may be a preference for cyclization of compounds containing certain substitution patterns such as type-III (*e.g.*, uroporphyrinogen-III) or type-IX (*e.g.*, heme). There are four possible type isomers for porphyrins with two different substituents (acetyl and proprionyl in the case of uroporphyrins) arranged with one of each substituent on each pyrrolic ring. The four uroporphyrin type isomers are shown in the middle portion of Figure 4-4, the key to which is found at the top of the figure. Porphyrins with three different substituents (A, B, and C) can be arranged into fifteen type isomers having one A substituent on each pyrrole, one B substituent on two of the pyrroles, and one C substituent on the other two. (A=methyl, B=vinyl and C=proprionyl in the case of protoporphyrins which are precursors to the hemes.) The fifteen type isomers of protoporphyrin are shown in the bottom portion of Figure 4-4. It would be interesting to investigate the fragmentation pathways and ionization energies of suites of porphyrin type isomers, in which what are seemingly very small changes in the molecular structure have great effects on the properties of the molecule. These studies combined with spectroscopic data and information on other physical properties of the molecules might lead to an understanding of the preference for certain substitution types.

Porphyrin Structural Isomers

Until recently, no stable isomers of porphine, the unsubstituted parent compound of the porphyrins which has four one-carbon bridges (*meso* carbons) between the pyrroles, had been observed in nature or synthesized in the laboratory. However, in the last few years, several novel porphyrin isomers in which the linkages between the pyrrole groups differ (Figure 4-5) have been synthesized [Borman **1995**; Sessler **1994**; Sessler *et al.*, **1994**; Vogel, **1989**; Vogel *et al.*, **1986**, **1987**]. A total of twelve fully conjugated isomers of porphine having different *meso* carbon arrangements are possible. However,

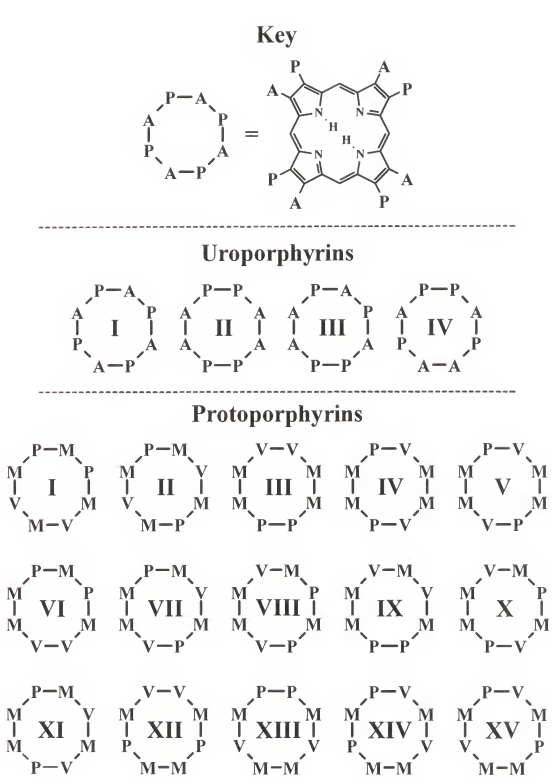


Figure 4-4. Porphyrin type isomers. Abbreviations: A, acetyl; E, ethyl; M, methyl; P, proprionyl; and V, vinyl [adapted from Bonnett, **1978**].

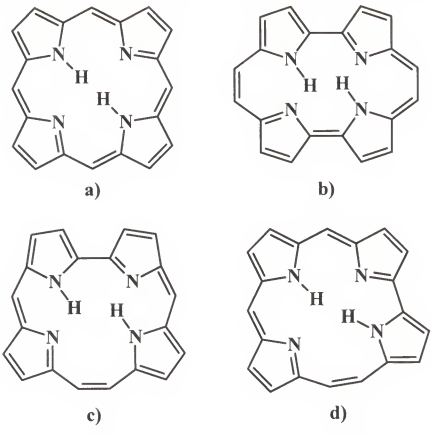


Figure 4-5. Porphine and three isomers with differing meso carbon arrangements: a) porphine, b) porphycene, c) corrphycene, and d) hemiporphycene.

only the ones illustrated in Figure 4-5 have been synthesized to date. These isomers have been found to be stable and, although they have core shapes which differ significantly from those of porphyrins, also chelate the full range of biologically important metals. The change in core shapes may significantly alter the ligating properties and allow for chelation with metals in oxidation states which are not stable in porphyrins. Mass spectrometric studies of the ionization and appearance energies and tandem mass spectrometry of these molecules may be able to add significant information on bond strengths and macrocycle stability to help answer the question about nature choosing porphyrin over these isomers.

Another recently developed class of porphyrin isomers, in which the carbon at position 7 and the nitrogen at position 22 switch places, has been synthesized by groups

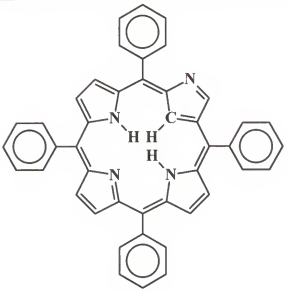


Figure 4-6. N-confused tetraphenylporphyrin.

from Poland and Japan [Chmielewski *et al.*, **1994**; Furuta *et al.*, **1994**]. The porphryins in this class are called the N-confused porphyrins. N-confused tetraphenylporphyrin is illustrated in Figure 4-6. While these compounds have no apparent biological application, their novelty would make them interesting to study.

Additional Experiments to Improve the Reliability of IE Determinations

Greater reliability in the ionization energy data obtainable from the TSQ70 could be obtained by modifying the instrument slightly to allow finer control of the electron energy. Better knowledge of the true ionization energy could also be obtained by increasing the number of calibrants employed.

One of the difficulties encountered in determining the ionization energies was the manner in which the TSQ70 generates the voltage on the EI filament. Since the TSQ70 works under automated control, a digital-to-analog converter (DAC) is used to convert the digital signal produced by the computer to the analog one required by the instrument. The DAC in the TSQ70 used to gather the data presented here produces voltage increments in the ELEN (filament voltage) of slightly less than 0.1 eV most of the time, but

every so often, at regular intervals, the increment is 0.2 eV. Owing to the random noise and other ion statistical considerations, the threshold voltage for the ionization of either the calibrant or the sample sometimes fell at or near one of these 0.2 eV skips. Replacement of the built-in circuit which controls the voltage and current on the EI filament with one which produces a smoother voltage ramp or modifications to the existing circuit would provide an obvious advantage and still allow automated instrument control using existing instrument control language (ICL) programs. Alternatively, the built-in circuit could be disabled and an external circuit could be designed. There are two user output voltages (UO1 and UO2) available on the TSQ70. UO1 and UO2 both have a range of -10.00 to +10.00 V, which can be controlled in 0.01 V increments. Ideally, the external circuit would be designed to produce voltage and current based on the voltages present at UO1 and UO2, which can be controlled along with all the other experimental parameters under ICL.

A second possible instrumental improvement might be achieved by use of a circuit which allows smaller steps in the ELEN parameter. The degree of improvement in the accuracy of the determinations which the smaller increments would produce would have to be determined experimentally. It is not clear at present whether other instrumental parameters would have a greater effect on the variability of the data than the size of the ELEN increment. The fact that the variability of the data is on the order of 0.1 eV, however, provides some indication that the increment size may be the limiting factor. Again, this circuit would ideally be controlled by one of the user output voltages.

The data presented here are all based on a one-point calibration using *N,N*-dimethylaniline as the compound of known IE. This is based on the assumption that controlling the emission current (and, thereby, the temperature) of the filament produces the same electron energy distribution independent of voltage. This assumption is more likely to be valid over a small voltage range than over a larger range. Repeat experiments with one or more other calibrants with IEs bracketing the sample IE would give an idea of

the validity of the energy distribution assumption. Use of judiciously chosen standards might also help to avoid the 0.2 eV skips in the filament voltage. Simultaneous introduction of two calibrants using two leak valves would probably not save much time as a great deal of the experimentalist's time is spent in adjusting the amount of calibrant bled into the source so that it is of comparable intensity to the sample. The prospect of adjusting the levels of two standards simultaneously would be quite daunting.

## REFERENCES


Addison, A. W.; Cullen, W. R.; Dolphin, D.; Jones, B. R. *Biological Aspects of Inorganic Chemistry*, Wiley, New York, NY **1977**.

Alden, R. G.; Crawford, B. A.; Doolen, R.; Ondrias, M. R.; Shelnutt, J. A. *J. Am. Chem. Soc.* **1989**, *111*, 2070-2072.

Alden, R. G.; Ondrias, M. R.; Shelnutt, J. A. *J. Am. Chem. Soc.* **1990**, *112*, 691-697.

Anderson, K. K.; Hobbs, J. D.; Luo, L.; Stanley, K. D.; Quirke, J. M. E.; Shelnutt, J. A. *J. Am. Chem. Soc.* **1993**, *115*, 12346-12352.

Angnes, L.; Azevedo, C. M. N.; Araki, K.; Toma, H. E. *Anal. Chim. Acta* **1996**, *329*, 91-96.

Annachino, A. P. *Associative Ion-Molecule Reactions and Ion Trapping with a Triple Quadrupole Mass Spectrometer*, Ph.D. Dissertation, University of Florida, **1993**.

Arpino, P. *Mass Spectrom. Rev.* **1992**, *11*, 3-40.

Aston, F. W. *Phil. Mag.* **1919**, *38*, 707-714.

Badr, I. H. A.; Meyerhoff, M. E.; Hassan, S. S. M. *Anal. Chim. Acta* **1996**, *321*, 11-19.

Baker, E. W. *J. Am. Chem. Soc.* **1966**, *88*, 2311-2315.

Baker, E. W.; Corwin, A. H.; Klesper, E.; Wei, P. E.; *J. Org. Chem.* **1968**, *33*, 3144-3148.

Baker, E. W.; Smith, G. D. *Adv. Org. Geochem., Proc. Int. Meet.* **1973**, 649-660.

Baker, E. W.; Yen, T. F.; Dickie, J. P.; Rhodes, R. E.; Clark, L. F. *J. Am. Chem. Soc.* **1967**, *89*, 3631-3639.

Barkigia, K. M.; Berber, M. D.; Fajer, J.; Medforth, C. J.; Renner, M. W. ; Smith, K. W. *J. Am. Chem. Soc.* **1990**, *112*, 8851-8857.

Bauder, C.; Ocampo, R.; Callot, H. J. *Tetrahedron* **1992**, *48*, 5135-5150.

Beato, B. D. *Structure Elucidation of Porphyrins by Tandem Mass Spectrometry: Fundamental Studies, New Strategies, and Geochemical Applications*, Ph.D. Dissertation, University of Florida, **1989**.

Beato, B. D.; Yost, R. A.; Quirke, J. M. E. in *Novel Techniques in Fossil Fuel Mass Spectrometry*, Ashe, T. R.; Wood, K. V., Eds, ASTM STP 1019, Philadelphia, PA **1989a**, pp. 84-93.

Beato, B. D.; Yost, R. A.; Quirke, J. M. E. *Org. Mass Spectrom.* **1989b**, *24*, 875-884.

Beato, B. D.; Yost, R. A.; Van Berkel, G. J.; Filby, R. H.; Quirke, J. M. E. *Org. Geochem.* **1991**, *17*, 93-105.

Bennett, A. *The Madness of King George*, Random House, New York, NY **1995**.

Bernard, C.; Gisselbrecht, J. P.; Gross, M.; Vogel, E.; Lausmann, M. *Inorg. Chem.* **1994**, *33*, 2393-2401.

Belova, V. S.; Khenkin, A. M.; Shilov, A. E. *Kinet. Catal. Engl. Transl.* **1987**, *28*, 1016-1017.

Bernier, U. R. *Mass Spectrometric Investigation of Mosquito Attraction to Human Skin Emanations*, Ph.D. Dissertation, University of Florida, **1995**.

Bhugun, I.; Lexa, D.; Saveant, J.-M., *J. Am. Chem. Soc.* **1994**, *116*, 5015-5016.

Biemann, K. *Mass Spectrometry: Organic Chemical Applications*, McGraw Hill, New York, NY **1962**.

Blum, H. F. *Photodynamic Action and Diseases Caused by Light*, Van Nostrand-Reinhold, Princeton, NJ **1941**.

Bonnett, R. in *The Porphyrins*, Dolphin, D., Ed., Academic Press, New York, NY **1978**, Vol. I, pp. 1-27.

Bonnett, R.; Burke, P. J.; Dewey, C. R.; Fairbrother, A. C.; Major, H. A. *Energy Fuels* **1991**, *70*, 1227-1229.

Bonnett, R.; Gale, I. A. D.; Stephenson, G. F. *J. Chem. Soc., Perkin Trans.* I **1966**, 1600-1604.

Bonnett, R.; Stephenson, G. F. *J. Org. Chem.* **1965**, *30*, 2791-2798.

Borman, S. *Chem. Eng. News* **1995**, *73* (June 26), 30-31.

Boyd, R. K.; Harris, F. M.; Beynon, J. H. *Int. J. Mass Spectrom. Ion Processes* **1985**, *66*, 185-194.

Boylan, D. B. *Org. Mass Spectrom.* **1970**, *3*, 339-351.

Boyle, R. W.; Dolphin, D. *Photochem. Photobiol.*, **1996**, *64*, 469-485.

Brennan, T. D.; Scheidt, W. R.; Shelnutt, J. A. *J. Am. Chem. Soc.* **1988**, *110*, 3919-3924.

Britton, E. D. *Analysis of High Carbon Number Geoporphyrins in Boscan Oil by Tandem Mass Spectrometry*, M. S. Thesis, University of Florida, **1985**.

Brundle, C. R.; Baker, A. D. *Electron Spectroscopy: Theory, Techniques and Applications*, Academic Press, New York, NY **1977**.

Buchler, J. W., in *Porphyrins and Metalloporphyrins*, Smith, K. M., Ed., Elsevier, Amsterdam **1975**, pp. 157-231.

Buchler, J. W. in *The Porphyrins*, Dolphin, D., Ed., Academic Press, New York, NY **1978**, Vol. I, pp. 389-483.

Budzikiewicz, H.;Pesch, R. *Org. Mass Spectrom.* **1976**, *11*, 821-830.

Budzikiewicz, H.; Taraz, K.; Münster, H.; Wasgestian, F.; Heucher, R. *Monatsh. Chem.* **1985**, *116*, 525-536.

Callot, H. J.; Louati, A.; Gross, M. *Bull. Soc. Chim. France* **1983**, *10*, II-317-II-320.

Callot, H. J.; Roher, A.; Tschamber, T.; Metz, B. *New J. Chem.* **1995**, *19*, 155-159.

Chakraborty, S.; Clezy, P. S.; Sternhill, S.; Van Thuk, K. *Austr. J. Chem.* **1982**, *35*, 2315-2323.

Chase, M. W.; Davies, C. A.; Downey, J. R.; Frurip, D. J.; McDonald, R. A.; Syverud, A. N.; *J. Phys. Chem. Ref. Data* **1985**, *14 (Suppl. 1)*.

Chicarelli, M. I.; Kaur, S.; Maxwell, J. R. in *Metal Complexes in Fossil Fuels*, Filby, R. H., Branthaver, J. F., Eds, ACS Symposium Series 344, American Chemical Society, Washington, DC **1987**, pp. 40-67.

Chillier, X. F. D.; Monnier, A.; Bill, H.; Gülaçar, F. O.; Buchs, A.; McLuckey, S. A.; Van Berkel, G. J. *Rapid Commun. Mass Spectrom.* **1996**, *10*, 299-304.

Chmielewski, P. J.; Latos-Grazynski, L.; Rachlewicz, K.; Glowiak, T. *Angew. Chem. Int. Ed. Engl.* **1994**, *33*, 779-781.

Clarke, E. M. *Can. J. Phys.* **1954**, *32*, 764-774.

Clezy, P. S.; Lim, C. L; Shannon, J. S. *Austr. J. Chem.* **1974**, *27*, 1103-1120.

Corwin, A. H. *Proc. Fifth World Pet. Congr.* **1960**, 119-129.

Crossley, M. J.; Burn, P. L. *J. Chem. Soc. Chem. Commun.* **1991**, *21*, 1569-1571.

Cullen, D. L.; Meyer, E. F., Jr. *J. Am. Chem. Soc.* **1974**, *96*, 2095-2102.

Dannacher, J. *Org. Mass Spectrom.* **1984**, *19*, 253-275.

Dawson, P. H.; Douglas, D. J. in *Tandem Mass Spectrometry* McLafferty, F. W., Ed., Wiley Interscience, New York, **1983**, pp. 125-148.

Dawson, P. H.; Sun, W.-F. *Int. J. Mass Spectrom. Ion Phys.* **1982**, *44*, 51-59.

Deisenhofer, J.; Michel, H. *Science*, **1989**, *245*, 1463-1473.

de Poorter, B.; Ricci, M.; Bortolini, O.; Muenier, B.; *J. Mol. Catal.* **1985**, *31*, 221-224.

Dolphin. D., Ed. *The Porphyrins*, Academic Press, New York, NY **1978**.

Donne, J. in *The Variorum Edition of the Poetry of John Donne, Volume 6, The Anniversaries and the Epicedes and Obsequies*, Stringer, G. A., Ed., Indiana University Press, Bloomington, IN **1995**.

Downey, D. *Med. Hypotheses* **1992**, *39*, 185-190.

Downey, D. *Med. Hypotheses* **1994** *42*, 285-290.

Downey, D. *Med. Hypotheses* **1996**, *46*, 378-382.

Drabkin, D. L. in *The Porphyrins*, Dolphin, D., Ed., Academic Press, New York, NY **1978**, Vol. I, pp. 29-83.

Duckworth, H. E.; Barber, R. C.; Venkatasubramanian, V. S. *Mass Spectrometry*, Cambridge University Press, Cambridge, **1986**.

Edwards, W. D.; Head, J. D.; Zerner, M. C. *J. Am. Chem. Soc.* **1982**, *104*, 5833-5834.

Edwards, W. D.; Weiner, B.; Zerner, M. C. *J. Am. Chem. Soc.* **1986**, *108*, 2196-2204.

Edwards, W. D.; Zerner, M. C. *Int. J. Quant. Chem.* **1983**, *23*, 1407-1432.

Eglinton, G.; Calvin, E. *Sci. Am.* **1967**, *216*, *(January)* 32-43.

Eglinton, G.; Hajlbrahim, S. K.; Maxwell, J. R.; Quirke, J. M. E.; Shaw, G. J.; Volkmann, J. K.; Wardroper, A. M. K. *Philos. Trans. R Soc. Lond. A* **1979**, *293*, 69-91.

Evans, B.; Smith, K. N.; Fuhrhop, J. H. *Tetrahedron Lett.* **1977**, 443-446.

Fajer, J. J. *Chem. Ind.* **1991**, *23*, 869-873.

Falk, J. E. *Porphyrins and Metalloporphyrins*, Elsevier, Amsterdam, **1964**.

Fanning, J. C.; Mandel, F. S.; Gray, T. L.; Datta-Gupta, N. *Tetrahedron* **1979**, *35*, 1251-1255.

Feher, G.; Allen, J. P.; Okamura, M. Y.; Rees, D. C. *Nature* **1989**, *339*, 111-116.

Ferguson, E. E. in *Ion Molecule Reactions* Franklin, J. L., Ed., Plenum Press, New York, NY **1972**, Vol.2, pp. 363-393.

Field, F. H.; Franklin, J. L. *Electron Impact Phenomena,* Academic Press, New York, NY, **1957**.

Filby, R. H.; Van Berkel, G. J. in *Metal Complexes in Fossil Fuels*, Filby, R. H., Branthaver, J. F., Eds, ACS Symposium Series 344, American Chemical Society, Washington, DC **1987**, pp. 2-39.

Finnigan MAT *TSQ70 Operator's Manual*, San Jose, CA **1984**.

Fischer, H.; Orth, H. *Die Chimie des Pyrrols*, Akademische Verlagsgesellschaft, Leipzig **1937a**, Vol. I.

Fischer, H.; Orth, H. *Die Chimie des Pyrrols*, Akademische Verlagsgesellschaft, Leipzig **1937b**, Vol. II(i).

Fischer, H.; Stern, H. *Die Chimie des Pyrrols*, Akademische Verlagsgesellschaft, Leipzig **1940**, Vol. II(ii).

Fox, R. E.; Hickham, W. M.; Kjeldass, T., Jr.; Grove, D. J. *Phys. Rev.* **1951**, *84*, 859-860

Franck, B.; Nonn, A.; *Angew. Chem. Int. Ed. Engl.* **1995**, *34*, 1795-1811.

Freeman, J. A.; Johnson, J. V.; Hail, M. E.; Yost, R. A; Kuehl, D. W.; *J. Am. Soc. Mass Spectrom.* **1990**, *1*, 110-115.

Fuhrhop, J. H.; Smith, K. M. *Laboratory Methods in Porphyrin and Metalloporphyrin Research*, Elsevier, Amsterdam, **1975**.

Furuta, H.; Asano, T.; Ogawa, T.; *J. Am. Chem. Soc.* **1994**, *116*, 767-768.

*The Gainesville Sun*, December 3, **1996**, 121, 9A.

Goldstein, E. *Sitzengsber. K. Preuss. Akad. Wiss.* **1886,** *39*, 691-699.

Gomer, C. J., Ed. *Future Directions and Applications in Photodynamic Therapy*, SPIE Optical Engineering Press, Bellingham, WA **1990**.

Gong, L.-C.; Dolphin, D. *Can. J. Chem.* **1985**, *63*, 401-405.

Gouterman, M. in *The Porphyrins*, Dolphin, D., Ed., Academic Press, New York, NY **1978**, Vol. III, pp. 1-165.

Griffiths, I. W.; Mukhtar, E. S.; March, R. E.; Harris, F. M.; Beynon, J. H. *Int. J. Mass Spectrom. Ion Phys.* **1981**, *39*, 125-132.

Harden, G. J.; Coombs, M. M. *J. Chem. Soc. Perkin Trans 1* **1995**, 3037-3042.

Hobbs, J. D.; Majumder, S. A.; Luo, L.; Sickelsmith, G. A.; Quirke, J. M. E.; Medforth, C. J.; Smith, K. M.; Shelnutt, J. A. *J. Am. Chem. Soc.* **1994**, *116*, 3261-3270.

Jackson, A. H.; Kenner, G. W.; Smith, K. M.; Aplin, R. T.; Budzikiewicz, H.; Djerassi, C. *Tetrahedron* **1965**, *21*, 2913-2924.

James, L. K. *Nobel Laureates in Chemistry*, American Chemical Society, Washington, DC **1993**.

Johnson, J. V.; Britton, E. D.; Yost, R. A.; Quirke, J. M. E.; Cuesta, L. L. *Anal. Chem.* **1986**, *58*, 1325-1329.

Johnson, J. V.; Yost, R. A. *Anal. Chem.* **1985**, *57*, 758A-768A.

Kebarle, P. *Ann. Rev. Phys. Chem.* **1977**, *28*, 445-476.

Kebarle, P.; Tang, L. *Anal. Chem.* **1993**, *65*, 972A-986A.

Kitagawa, S.; Morishima, I.; Yonezawa, T.; Sato, N. *Inorg. Chem.* **1979**, *18*, 1345-1349.

Kuroki, M.; Watanabe, T.; Aida, T.; Inoue, S. *J. Am. Chem. Soc.* **1991**, *113*, 5903-5904.

Laycock, J. D. *Tandem Mass Spectrometric Studies of Porphyrins: Structural and Photochemical Studies*, Ph.D. Dissertation, University of Florida, **1994**.

Laycock, J. D.; Ferguson, J. A.; Yost, R. A.; Quirke, J. M. E; Callot, H. J.; Ocampo, R. *J. Mass Spectrom.* submitted, **1996**.

Laycock, J. D.; Yost, R. A.; Quirke, J. M. E. *Energy Fuels* **1995**, *9*, 1079-1085.

Lemberg, R.; Barrett, J. *Cytochromes*, Academic Press, London **1973**.

Le Nouën, D.; Marko, J.; Vermeersch, G. Febvay-Garot, N.; Lablache-Combier, A.; Peree-Fuavet, M.; Guademer, A. *Photochem. Photobiol.* **1989**, *49*, 7-18.

Li, X.-Y.; Czerniszewicz, R. S.; Kincaid, J. R.; Stein, P.; Spiro, T, G. *J. Am. Chem. Soc.* **1989**, *111*, 7012-7023.

Li, X.-Y.; Czerniszewicz, R. S.; Kincaid, J. R.; Stein, P.; Spiro, T, G. *J. Phys. Chem.* **1990**, *94*, 47-61.

Lias, S. G.; Bartmess, J. E.; Liebman, J. F.; Holmes, J. L.; Levin, R. D.; Mallard, W. G. *J. Phys. Chem. Ref. Data* **1988** *17 (Suppl. 1)*, 5-18.

Lias, S. G.; Ausloos, P. *J. Am. Chem. Soc.* **1978**, *100*, 6027-6034.

Liu, C.; Hasty, T.; Bard, A. J. *J. Electrochem. Soc.* **1996**, *143*, 1914-1918.

Lyons, J. E.; Ellis, P. E., Jr, Myers, H. K. *J. Catal.* **1995**, *155*, 59-73.

Macalpine, I; Hunter, R. *George III and the Mad-Business*, Pantheon Books, New York, NY, **1969**.

Maeda, K. Semeluk, G. P.; Lossing, F. P. *Int. J. Mass Spectrom. Ion. Phys.* **1968**, *1*, 395-407.

Marks, G. S. *Heme and Chlorophyll, Chemical, Biological and Medical Aspects*, D van Nostrand, London **1969**.

Marmet, P.; Kerwin, L. *Can. J. Phys.* **1960**, *38*, 787-796.

McDowell, C. A; Warren, J. W. *Disc. Faraday Soc.*, **1951**, *10*, 53-65.

McLafferty, F. W. in *Mass Spectrometry of Organic Ions*, McLafferty, F. W., Ed., Academic Press, New York, NY **1963**, pp. 309-342.

McLafferty, F. W. *Chem. Commun.* **1968**, 956-958.

McLafferty, F. W. *Interpretation of Mass Spectra*, University Science Books, Sausalito, CA **1980**.

Merchat, M.; Bertolini, G.; Giacomini, P.; Villanueva, A.; Jori, G. *J. Photochem. Photobiol. B.* **1996**, *32*, 153-157.

Meyer, E. F., Jr. *Acta Crystallogr., Sect. B: Struct. Cystallogr. Cryst. Chem.* **1972**, *B28*, 2162-2167.

Minnock, A.; Vernon, D. I.; Schofield, J.; Griffiths, J.; Parish, J. H.; Brown, S. B. *J. Photochem. Photobiol. B.* **1996**, *32*, 159-164.

Moore, C. E. *Nat. Stand. Ref. Data Ser. Nat. Bur. Stand. (U. S.)* **1970**, *34*.

Moylan, C. R.; Brauman, J. I. *Ann. Rev. Phys. Chem.* **1983**, *34*, 187-215.

Murashima, T.; Uchihara, Y.; Wakamori, N.; Uno, H.; Ogawa, T.; Ono, N. *Tetrahedron Lett.* **1996**, *37*, 3133-3136.

Nauta, J. M.; van Leengoed, H. L. L. M.; Star, W. M.; Roodenburg, J. L. N.; Witjes, M. J. H.; Vermey, A. *Eur. J. Oral Sci.* **1996**, *104*, 69-81.

Norris, J. R.; Schiffer, M. *Chem. Eng. News* **1990**, *68 (July 30)*, 22-37.

Ocampo, R.; Callot, H. J.; Albrecht, P. in *Metal Complexes in Fossil Fuels*, Filby, R. H., Branthaver, J. F., Eds, ACS Symposium Series 344, American Chemical Society, Washington, DC **1987**, pp. 68-73.

Orenstein, A.; Kostenich, G.; Roitman, L.; Shechtman, Y.; Kopolovic, Y.; Ehrenberg, B.; Malik, Z. *Br. J. Cancer* **1996**, *73*, 937-944.

Ortiz de Montellano, P. R. *Cytochrome P450 Structure, Mechanism and Biochemistry*, Plenum Press, New York, NY **1995**.

Pasternak, R. F.; Gibbs, E. J.; Villafranca, J. J. *Biochem.* **1983**, *22*, 5409-5417.

Pine, S. H.; Hendrickson, J. B.; Cram, D. J.; Hammond, G. S. *Organic Chemistry*, McGraw-Hill, New York, NY **1980**, pp. 68-88.

Priyantha, N. Weerabahu, D. *Anal. Chim. Acta* **1996**, *320*, 263-268.

Quirke, J. M. E.; Cuesta, L. L.; Yost, R. A.; Johnson, J. V.; Britton, E. D. *Org. Geochem.* **1989**, *14*, 43-50.

Quirke , J. M. E.; Perez, M.; Britton, E. D.; Yost, R. A. in *Geochemical Biomarkers*, Yen, T. F.; Moldowan, J. M., Eds., Harwood Academic Publishers, Chur, **1988**, pp. 355-371.

Rabalais, J. W. *Principles of Ultraviolet Photoelectron Spectroscopy*, Wiley-Interscience, New York, NY **1977**.

Rawn, J. D. *Biochemistry*, Harper & Row, New York, **1983**, pp 861-928.

Reimers, J. R.; Lü, T. X.; Crossley, M. J.; Hush, N. S. *Chem. Phys. Lett.* **1996**, *256*, 353-359.

Richards, R. A.; Hammons, K.; Joe, M.; Miskelly, G. M. *Inorg. Chem.* **1996**, *35*, 1940-1944.

Rosenstock, H. M. *Int. J. Mass Spectrom. Ion. Phys.* **1976**, *20*, 139-190.

Rosenstock, H. M.; Draxl, K. Steiner, B. W.; Herron, J. T. *J. Phys. Chem. Ref. Data* **1977**, *6 (Suppl. 1)*.

Rosenstock, H. M.; Krauss, M. in *Mass Spectrometry of Organic Ions*, McLafferty, F. W., Ed., Academic Press, New York, NY **1963**, pp. 1-64.

Rosenstock. H. M., Wallenstein, M. B.; Wahrhaftig, A. L.; Eyring, H. *Proc. Natl. Acad. Sci. U. S.* **1952**, *38*, 667-678.

Scheidt, W. R. in *The Porphyrins*, Dolphin, D., Ed., Academic Press, New York, NY **1978**, Vol. III, pp. 463-511.

Schuitmaker, J. J.; Bass, P.; van Leengoed, H. L. L. M.; van der Meulen, F. W.; Star, W. M.; van Zandwijk, N. *J. Photochem. Photobiol. B.* **1996**, *34*, 3-12.

Seibl, J. *Adv. Mass. Spectrom.* **1968**, *4*, 317-321.

Sessler, J. L. *Angew. Chem. Int. Ed. Engl.* **1994**, *33*, 1348-1350.

Sessler, J. L.; Brucker, E. A.; Weghorn, S. J.; Kisters, M.; Schäfer, M.; Lex, J.; Vogel, E. *Angew. Chem. Int. Ed. Engl.* **1994**, *33*, 2308-2312.

Seto, J.; Tamura, S.; Asai, N.; Kishii, N.; Kijima, Y.; Matsuzawa, N. *Pure Appl. Chem.* **1996**, *68*, 1429-1434.

Shaw, G. J.; Quirke, J. M. E.; Eglinton, G. *Anal. Chem.* **1981**, *53*, 2014-2020.

Shelnutt, J. A.; Medforth, C. J.; Berber, M. D.; Barkigia, K. M.; Smith, K. M. *J. Am. Chem. Soc.* **1991**, *113*, 4077-4087

Shimidzu, T.; Segawa, H.; Wu, F. P.; Nakayama, N. *J. Photochem. Photobiol. A* **1995**, *92*, 121-127.

Sigma Chemical Company *1996 Catalog*, Saint Louis, MO, **1996**.

Smith, K. M. in *Comprehensive Heterocyclic Chemistry*, Katritzky, A. R.; Rees, C. W., Eds., Pergamon Press, Oxford **1984**, pp. 377-442.

Sparks, L. D.; Medforth, C. J.; Park M.-S.; Chamberlain, J. R.; Ondrias, M. R.; Senge, M. O.; Smith, K. M.; Shellnut, J. A. *J. Am. Chem. Soc.* **1993**, *115*, 581-592.

Stanley, K. D.; Luo, L.; Lopez de la Vega, R.; Quirke, J. M. E. *Inorg. Chem.* **1993**, *32*, 1233-1236.

Stern, A.; Wenderlein, H. *Z. Phys. Chem. Abt. A* **1936**, *A176*, 81-124.

Stevenson, D. P. *Disc. Faraday Soc.* **1951**, *10*, 35-45.

Storm, C. B.; Teklu, Y. *J. Am. Chem. Soc.*, **1972**, *94*, 1745-1747.

Storm, C. B.; Teklu, Y.; Sokolski, E. A. *Ann. NY Acad. Sci.* **1973**, *206*, 631-640.

Streitwieser, A.; Heathcock, C. H. *Introduction to Organic Chemistry*, MacMillan, New York, NY **1981**, pp. 277-281.

Tanaka, K. ; Igarashi, C.; Tagliatesta, P.; Boschi, T.; Sadaoka, Y. *J. Mater. Chem.* **1996**, *6*, 953-956.

Thomson, J. J. *Phil. Mag.* **1897**, *44*, 293-314.

Thomson, J. J. *Phil. Mag.* **1912a**, *24*, 209-253.

Thomson, J. J. *Phil. Mag.* **1912b**, *24*, 668-672.

Tolf, B.-R.; Jiang, X.-Y.; Wegmann-Szente, A.; Kehres, L. A.; Bunnenberg, A.; Djerassi, C. *J. Am. Chem. Soc.* **1986**, *108*, 1363-1374.

Treibs, A. *Liebigs Ann. Chem.* **1934**, *510*, 42-62.

Treibs, A. *Angew. Chem.* **1936**, *49*, 682-686.

Trévin, S.; Bedioui, F.; Devynck, J. *J. Electroanal. Chem.* **1996**, *408*, 261-265.

Tronrud, D. E.; Schmid, M. F.; Matthews, B. W. *J. Mol. Biol.* **1986**, *188*, 443-454.

Van Berkel, G. J.; Glish, G. J.; McLuckey, S. A. *Org. Geochem.* **1989a**, *14*, 203-212

Van Berkel, G. J.; Glish, G. J.; McLuckey, S. A.; Tuinman, A. A. *J. Am. Chem. Soc.* **1989b**, *111*, 6027-6035

Van Berkel, G. J.; Zhou, F. *Anal. Chem.* **1995**, *67*, 3958-3964.

Vestal, M. L. Science **1984**, 226, 275-281.

Vogel, E. *Pure Appl. Chem.* **1996**, *68*, 1355-1360.

Vogel, E.; Balci, M.; Pramod, K.; Koch, P.; Lex, J.; Ermer, O. *Angew. Chem. Int. Ed. Engl.* **1987**, *26*, 928-931.

Vogel, E.; Köcher, M.; Schmickler, H.; Lex. J. *Angew. Chem. Int. Ed. Engl.* **1986**, *25*, 257-259.

Wachs, T.; McLafferty, F. W. *J. Am. Chem. Soc.* **1967**, *89*, 5044-5045.

Wagman, D. D.; Evans, W. H.; Parker, V. B.; Schumm, R. H.; Halow, I.; Bailey, S. M.; Churney, K. L. ; Nuttall, R. L. *J. Phys. Chem. Ref. Data* **1982**, *11 (Suppl. 2)*.

Wagner, R. W.; Lindsey, J. S.; *J. Am. Chem. Soc.* **1994**, *116*, 9759-9760.

Wagner, R. W.; Lindsey, J. S.; Seth, J.; Palaniappan, V.; Bocian, D. F. *J. Am. Chem. Soc.* **1996**, *118*, 3996-3997.

Waluk, J.; Müller, M.; Swiderek, P.; Köcher, M.; Ermer, O.; Vogel, E.; Hohlneicher, G.; Michl, J. *J. Am. Chem. Soc.* **1991**, *113*, 5511-5527.

Watson, J. T. *Introduction to Mass Spectometry*, Raven Press, New York, NY **1985**.

Wayland, B. B.; Del Rossi, K. J. *J. Organomet. Chem.* **1984**, *276*, C27-C30.

Wien, W. *Verh. Phys. Ges. Berlin* **1898**, *17*, 10-12.

Wien, W. *Ann. Phys. Chem. Leipzig* **1902**, *8*, 244-266.

Williams, R. J. P.; Moore, G. R.; Wright, P. E in *Biological Aspects of Inorganic Chemistry*, Addison, A. W.; Cullen, W. R.; Dolphin, D.; Jones, B. R., Eds., Wiley, New York, NY **1977**, pp. 369-401.

Woods, J. S. *Can. J. Physiol. Pharmacol.* **1996**, *74*, 210-215.

Xiao, J.; Meyerhoff, M. E. *J. Chromatogr. A* **1995**, *715*, 19-29.

Yost, R. A.; Enke, C. G. *Anal. Chem.* **1979**, *51*, 1251A-1264A.

Yost, R. A.; Fetterolf, D. D. *Mass Spectrom. Rev.*. **1983**, *2*, 1-45.

Zenkevich, E.; Sagun, E.; Knyukshto, V.; Shulga, A.; Mironov, A.; Efremova, O.; Bonnett, R.; Songca, S. P.; Kassem, M. *J. Photochem. Photobiol. B* **1996**, *33*, 171-180.

## BIOGRAPHICAL SKETCH

James Allen Ferguson, the first-born son of James H. Ferguson and Martha W. Ferguson, was born November 22, 1959. Sister Beth, brother Tod, and sister Julia joined the family in succession. Jim grew up in the Town of Newfane, New York, attending Wrights Corners Elementary School, Trinity Lutheran School in Lockport and Newfane Junior and Senior High Schools. He took music (piano and organ) lessons, was active in Cub Scouts and Boy Scouts, and enjoyed both drama club and math club in high school. Family (both nuclear and a large extended family) and church (just across the street) were also important parts of his upbringing. He earned his B.S. degree in chemistry at the University of Rochester, where he was a Bausch & Lomb Scholar and did undergraduate research under Dr. George McLendon. His M.S. in analytical chemisty was earned at Texas A&M University where he did thermochemistry research with Dr. Marvin Rowe. At Texas A&M, he was inducted into Phi Lambda Upsilon, an honorary chemistry fraternity. After earning his M.S., Jim worked for four years in the Office of the Texas State Chemist where he supervised a staff of five to six people in the analysis of feeds and fertilizers. He then accepted the post of Assistant Bureau Chief in the Feed Laboratory of the Florida Department of Agriculture in Tallahassee, Florida, where he supervised a staff of eleven. After working for the State of Florida for two years, Jim decided to do what he had wanted to do for a long time and get his doctorate. This led to his enrollment at the University of Florida where he was a Grinter Fellow and performed mass spectrometry research with Dr. Richard Yost. Upon completion of his Ph.D., Jim will be moving south to Riviera Beach, Florida, where he has accepted a position with ThermoQuest Corporation.

I certify that I have read this study and that in my opinion it conforms to acceptable standards of scholarly presentation and is fully adequate, in scope and quality, as a dissertation for the degree of Doctor of Philosophy.

Richard A. Yost, Chair
Professor of Chemistry

I certify that I have read this study and that in my opinion it conforms to acceptable standards of scholarly presentation and is fully adequate, in scope and quality, as a dissertation for the degree of Doctor of Philosophy.

Willard W. Harrison
Professor of Chemistry

I certify that I have read this study and that in my opinion it conforms to acceptable standards of scholarly presentation and is fully adequate, in scope and quality, as a dissertation for the degree of Doctor of Philosophy.

John R. Eyler
Professor of Chemistry

I certify that I have read this study and that in my opinion it conforms to acceptable standards of scholarly presentation and is fully adequate, in scope and quality, as a dissertation for the degree of Doctor of Philosophy.

Robert T. Kennedy
Associate Professor of Chemistry

I certify that I have read this study and that in my opinion it conforms to acceptable standards of scholarly presentation and is fully adequate, in scope and quality, as a dissertation for the degree of Doctor of Philosophy.

Peggy R. Borum
Professor of Human Nutrition

This dissertation was submitted to the Graduate Faculty of the Department of Chemistry in the College of Liberal Arts and Sciences and to the Graduate School and was accepted as partial fulfillment of the requirements for the degree of Doctor of Philosophy.

May, 1997

_____

Dean, Graduate School